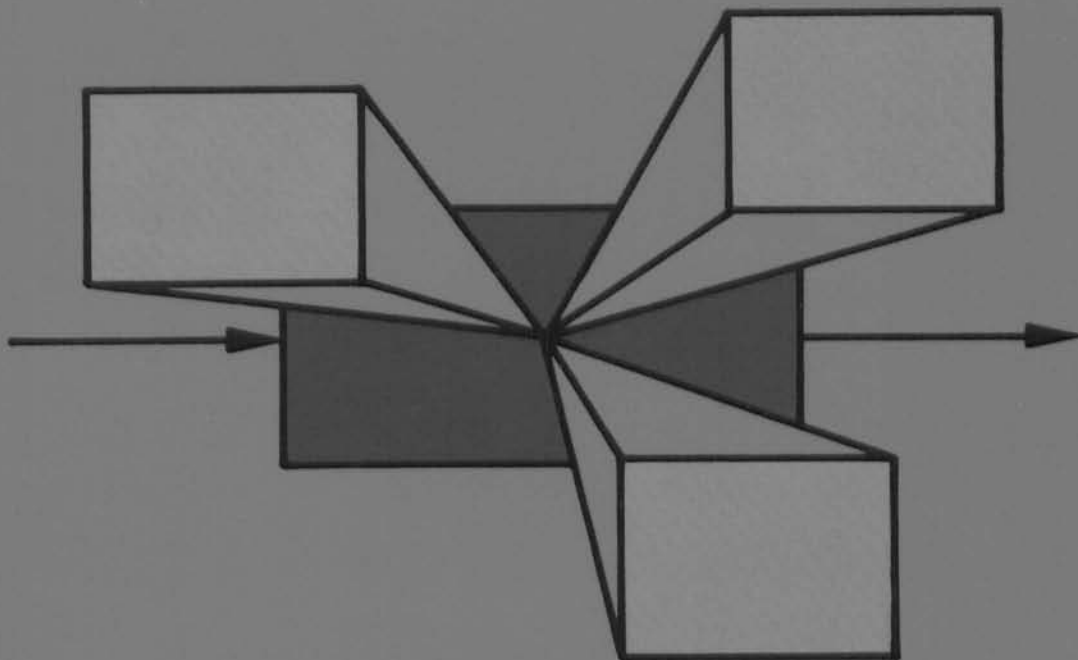


SELECTED  
TOPICS  
IN

# Identification Modelling and Control

Volume 4, 1992

Edited by O.H. Bosgra and P.M.J. Van den Hof



Delft University Press

684



# IDENTIFICATION, MODELLING AND CONTROL

## MODELLING AND CONTROL

Progress Report on Research Activities in the  
Mechanical Engineering Systems and Control Group

541514  
3059194  
TR 2995684

Edited by O.H. Bosgra and P.M.J. Van den Hof

Volume 4, March 1992



Mechanical Engineering Systems and Control Group  
Delft University of Technology

Delft University Press 1992

1000.00 RPA, 500.00 RPA, 1000.00 RPA

Contents

# SELECTED TOPICS IN IDENTIFICATION, MODELLING AND CONTROL

## Progress Report on Research Activities in the Mechanical Engineering Systems and Control Group

Edited by O.H. Bosgra and P.M.J. Van den Hof

Volume 4, March 1992

Mechanical Engineering Systems and Control Group  
Delft University of Technology

Delft University Press/1992



Copyright Delft University Press. All rights reserved. No part of this journal may be reproduced in any form or by any means without written permission from the publisher.

Published and Distributed by

Delft University Press  
Stevinweg 1  
2628 CN Delft  
The Netherlands  
Tel.: (0)15 - 783254  
Telefax: (0)15 - 781661

By order of

Mechanical Engineering Systems and Control Group  
Delft University of Technology  
Mekelweg 2, 2628 CD Delft  
The Netherlands  
Tel.: +31-15-786400; Telefax: +31-15-784717



CIP-GEGEVENS KONINKLIJKE BIBLIOTHEEK, DEN HAAG

Selected

Selected topics in identification, modelling and control:  
progress report on research activities in the mechanical engineering  
systems and control group. - Delft: Mechanical Engineering Systems and Control Group,  
Delft University of Technology, Vol. 4-ed. by O.H. Bosgra and  
P.M.J. Van den Hof.-ill. Met lit.opg.  
ISBN 90-6275-761-8  
SISO 656 UDC 531.7 + 681.5 NUGI 841

Cover design by Ruud Schrama

© 1992 Copyright Delft University Press. All rights reserved. No part of this journal may be reproduced,  
in any form or by any means, without written permission from the publisher.

# Quantification of model uncertainty from experimental data.

## Contents

Editorial

### Volume 4, March 1992

|  |    |
|--|----|
| Quantification of model uncertainty from data<br><i>D.K. de Vries and P.M.J. Van den Hof</i>                                     | 1  |
| Accurate identification for control: the necessity of an iterative scheme.<br><i>R.J.P. Schrama</i>                              | 11 |
| An indirect method for transfer function estimation from closed loop data.<br><i>P.M.J. Van den Hof and R.J.P. Schrama</i>       | 17 |
| Control of wind turbine systems for load reduction<br><i>P.M.M. Bongers, T. van Holten and S. Dijkstra</i>                       | 23 |
| Robust control using coprime factorizations, application to a flexible wind turbine<br><i>P.M.M. Bongers</i>                     | 29 |
| $H_{\infty}$ control of an experimental inverted pendulum with dry friction<br><i>G.W. van der Linden and P.F. Lambrechts</i>    | 37 |
| Observability and controllability aspects of continuous industrial crystallisers<br><i>R.A. Eek, A. Bozman and S.J. Dijkstra</i> | 47 |

Recently, several approaches to the identification problem have been presented, considering the identification in view of the control design. By far the most attention is paid to the construction of so-called hard error models, often related to an  $H_{\infty}$  identification, see e.g. Sjöstrand et al. (1986), Helmicki et al. (1988a), De and Chaperot (1991), Lallain et al. (1991), and Wallberg and

We are happy to present the fourth issue of our progress report Journal of Intelligent and Robotic Systems. We have selected a number of papers pointing on different parts of the research that is presently being done within our group. With this special issue, we hope to provide a forum for the presentation of research results in the area of intelligent and robotic systems. The Journal of Intelligent and Robotic Systems is a peer-reviewed journal, and we are pleased to announce that it is now published by Kluwer Academic Publishers. We believe that a high-quality journal in this area is essential for the progress of research in this field. We are pleased to announce that the Journal of Intelligent and Robotic Systems is now published by Kluwer Academic Publishers. We believe that a high-quality journal in this area is essential for the progress of research in this field.

## Editorial

We are happy to present the fourth issue of our progress report *Selected Topics in Identification, Modelling and Control*, published by Delft University Press. We have selected a number of papers reporting on different parts of the research that is presently taking place within our group.

With three ongoing Ph.D.-projects in the area of system identification and its relation to robust control design (Ruud Schrama, Douwe de Vries and Richard Hakvoort) we attempt to contribute to the stimulating developments that are being made in this field. We believe that a synergetic approach to identification and control problems (and solutions) can provide valuable insights and tools for high performance control of (industrial) processes. The first Ph.D.-thesis out of this "synergetic world" is currently in its final stage of construction; Ruud will defend his thesis in the course of May. A slight flavour of his point of view is presented in his paper incorporated in this issue, motivating an iterative scheme of identification for high performance control design. On the interplay between identification and robust control, model uncertainty plays an essential role. In a paper authored by Douwe de Vries and Paul Van den Hof, a method is presented for identification of model uncertainty for a prespecified nominal model. It refers to the situation that nominal model and model uncertainty do not necessarily have to be identified in one single procedure, but that it may be advantageous to have separate identification procedures. Paul Van den Hof and Ruud Schrama present a new method for closed loop system identification, very much relying on classical results, creating the possibility of approximately identifying the (open loop) plant

with an explicit approximation criterion, as is possible in the open loop case.

Identification, modelling and control of wind turbines has already for several years been subject of research within our group. Currently two Ph.D.-students are working towards their thesis, i.e. Peter Bongers and Gregor van Baars. Peter combines his work on modelling and control of wind turbines with an intensive research on robust control with coprime factor perturbations. Both types of work are reported on in this issue, the first type in a paper with Theo van Holten (Stork Product Engineering) and Sjoerd Dijkstra; the second type in a paper showing the control of a nonlinear system through a robust linear control design scheme employing coprime factor uncertainty.

In the final part of this issue two papers are incorporated of Ph.D.-students who started their project more recently. Gert-Wim van der Linden, in a paper with Paul Lambrechts, reports on his M.Sc.-project, in which he has designed and experimentally validated an  $H_\infty$  controller on an inverted pendulum containing (nonlinear) dry friction. We hope to see more of Gert-Wim's work in the future when he is able to report on results in his Ph.D.-project. Rob Eek with co-authors Arthur Boxman (Department of Chemical Process Engineering) and Sjoerd Dijkstra report on control aspects of a newly designed continuous industrial crystallizer, which, as an experimental setup, is available at Delft University, and which is subject of Rob's Ph.D.-project.

We hope you enjoy this *Selected Topics*.

Okko Bosgra  
Paul Van den Hof  
*Editors*

## Quantification of model uncertainty from experimental data.

Douwe K. de Vries, Paul M.J. Van den Hof

*Mechanical Engineering, Systems and Control Group,  
Delft University of Technology, Mekelweg 2, 2628 CD Delft, The Netherlands.*

**Abstract.** Identification of linear models in view of robust control design requires the identification of a control-relevant nominal model, and a quantification of model uncertainty. In this paper a procedure is presented to quantify the model uncertainty of any prespecified nominal model, from a sequence of measurement data of input and output signals from a plant. By employing a non-parametric empirical transfer function estimate (ETFE), we are able to split the model uncertainty into three parts: the inherent uncertainty in the data due to data-imperfections, the unmodelled dynamics in the nominal model, and the uncertainty due to interpolation. A frequency-dependent hard error bound is constructed, and results are given for tightening the bound through appropriate input design. When the upper bound on the model uncertainty is too conservative, in view of the control design specifications, information is provided as to which additional experiments have to be performed in order to improve the bound.

**Keywords.** Identification, frequency domain, model uncertainty, robust control.

### 1 Introduction

In the systems and control community there is a growing interest in merging the problems of system identification and (robust) control system design. This interest is based on the conviction that, in many situations, models obtained from process experiments will be used as a basis for control system design. On the other hand, in model-based robust control design, models and model uncertainties have to be available that are essentially provided by, or at least validated by, measurement data from the process.

Recently several approaches to the identification problem have been presented, considering the identification in view of the control design. By far the most attention is paid to the construction of so-called hard error bounds, often referred to as  $H_\infty$ -identification, see e.g. Helmicki *et al.* (1990a), Helmicki *et al.* (1990b), Gu and Khargonekar (1991), LaMaire *et al.* (1991), and Wahlberg and

Ljung (1991). In Goodwin and Ninness (1991) an identification procedure is presented that provides probabilistic (soft) error bounds.

In the references mentioned, there is a strong connection between the identification of nominal models and the quantification of model uncertainty. This has two serious drawbacks. Firstly, only identification methods for nominal models are selected for which ( $H_\infty$ ) error bounds can be derived. This seems to exclude many methods and model structures that could be useful but are rather intractable when it comes to deriving error bounds. When discussing the suitability of models as a basis for control system design, the availability of reliable error bounds certainly is important in order to obtain robust stability, and possibly also robust performance. However the nominal model that is used as a basis for the design, will determine the nominal performance of the control system, and one will definitely not be willing to implement a control system when the nominal performance does not meet

the specifications. As a result, the identification of nominal models, apart from the quantification of model uncertainty, is an important issue in identification for control design, see e.g. Bitmead and Zang (1991), Hakvoort (1990), and Schrama (1991).

The second drawback is that one is not able to further tighten the error bound by performing additional experiments, without simultaneously changing the nominal model. E.g. when the error bound is not tight enough and needs improvement in a specific frequency region, new experiments could be performed to reduce the uncertainty. However, when designing a new input signal it is not possible to restrict attention to the specific frequency region of interest, since this would essentially also affect the nominal model and the error bound outside this frequency region, and data sets from the different experiments cannot directly be combined to reduce the model uncertainty.

In addition to this reasoning, in this paper we will deal with the following problem: given a prespecified nominal model  $G_{nom}$  for an unknown linear plant  $G_0$ , can we construct an error bound for

$$|G_0(e^{j\omega}) - G_{nom}(e^{j\omega})| \quad (1)$$

based on noise corrupted measurements from input and output samples of the plant? Note that the nominal model may be available from any (control-relevant) identification procedure.

The problem is going to be tackled, through the construction of an intermediate data representation in the frequency domain, leading to the inequality:

$$|G_0(e^{j\omega_k}) - G_{nom}(e^{j\omega_k})| \leq |G_0(e^{j\omega_k}) - \hat{G}(e^{j\omega_k})| + |\hat{G}(e^{j\omega_k}) - G_{nom}(e^{j\omega_k})| \quad (2)$$

with  $\hat{G}(e^{j\omega_k})$  an -intermediate- representation of the measurement data in the frequency domain. This means that  $\hat{G}(e^{j\omega_k})$  basically is a finite number of (complex) points on the unit circle, obtained from the Discrete Fourier Transformation (DFT) of the time-domain data. The first term on the right hand side of (2) can be considered to reflect inherent uncertainty in the data, whereas the second term is related to the quality of the nominal model, e.g. determined by unmodelled dynamics. Having constructed a data representation  $\hat{G}(e^{j\omega_k})$ , the second term can be calculated exactly. Hence, to give an upper bound on the model error  $|G_0(e^{j\omega_k}) - G_{nom}(e^{j\omega_k})|$ , the problem is to construct an upper bound for the error  $|G_0(e^{j\omega_k}) - \hat{G}(e^{j\omega_k})|$ . Note however that inequality (2) is only defined at the finite number of frequency points  $\omega_k$ , while our aim is to bound the model error for all  $\omega \in [0, 2\pi)$ .

The fact that the data does not contain information for frequencies  $\omega \neq \omega_k$  gives rise to the uncertainty due to interpolation. The second problem therefore is to bound the model error for all  $\omega \in [0, 2\pi)$  using the error bounds at  $\omega_k$ . These two problems will be the main topics of this paper.

Related work has been published in LaMaire *et al.* (1991) and Helmicki *et al.* (1990b) where error bounds for  $|G_0(e^{j\omega_k}) - \hat{G}(e^{j\omega_k})|$  have been obtained at a finite number of frequency points. In LaMaire *et al.* (1991) this has been done by employing the Empirical Transfer Function Estimate (ETFE, see Ljung (1987)), and in Helmicki *et al.* (1990b) through sinewave excitation and actually measuring the frequency response in a finite number of points. In Gu and Khargonekar (1991) and Helmicki *et al.* (1990a) the frequency domain estimate and discrete error bound are used to obtain a model in  $H_\infty$  and a continuous error bound (valid on the whole unit circle). It is tried to keep the  $H_\infty$  error small by using an intermediate high order  $L_\infty$  model and Nehari approximation, obtaining a Finite Impulse Response (FIR) model.

In section 3 of this paper also the ETFE is used to obtain a nonparametric frequency domain estimate  $\hat{G}(e^{j\omega_k})$ , and a discrete error bound. In contrast with Gu and Khargonekar (1991), Helmicki *et al.* (1990a) and Helmicki *et al.* (1990b) this error bound is frequency-dependent, which makes it more informative than a simple  $H_\infty$ -bound. Moreover it does not require the frequency points of the discrete estimate to be equidistantly distributed over the unit circle. This paves the way for designing specific input signals in order to improve the estimates, and tightening the bound. Additionally a continuous error bound is constructed in section 4 by interpolation of the discrete bound, using smoothness properties of the system. In section 5 it is shown how robust control design specifications can advocate new experiments in order to reduce model uncertainty in specific (frequency) ranges. Finally, in section 6, a simulation example is given to illustrate the merits of the procedure proposed.

## 2 Preliminaries

It is assumed that the plant, and the measurement data that is obtained from this plant, allow a description:

$$y(t) = G_0(q)u(t) + v(t) \quad (3)$$

with  $y(t)$  the output signal,  $u(t)$  the input signal,  $v(t)$  an additive output noise,  $q^{-1}$  the delay operator, and  $G_0$  a proper transfer function that is time-

invariant and exponentially stable. The transfer function can be written in its Laurent expansion around  $z = \infty$ , as

$$G_0(z) = \sum_{k=0}^{\infty} g_0(k)z^{-k} \quad (4)$$

with  $g_0(k)$  the impulse response of the plant. Throughout the paper we will consider discrete time intervals for input and output signals denoted by  $T^N := [0, N-1]$ ,  $T_{N_s}^N := [N_s, N+N_s-1]$  with  $N$  and  $N_s$  appropriate integers. We will denote

$$\sup_{t \in T^{N+N_s}} |u(t)| = \bar{u}$$

For a signal  $x(t)$ , defined on  $T^N$ , we will denote the  $N$ -point Discrete Fourier Transform (DFT) and its inverse by:

$$X\left(\frac{2\pi k}{N}\right) = \sum_{t=0}^{N-1} x(t)e^{-j\frac{2\pi k}{N}t} \text{ for } k \in T^N \quad (5)$$

$$x(t) = \frac{1}{N} \sum_{k=0}^{N-1} X\left(\frac{2\pi k}{N}\right)e^{j\frac{2\pi k}{N}t} \text{ for } t \in T^N \quad (6)$$

When a signal  $x(t)$  is defined on the interval  $T_{N_s}^N$ ,  $N_s > 0$ , then we will denote the  $N$ -point DFT of a shifted version of the signal  $x$ , shifted over  $N_s$  time instants, by

$$X^s\left(\frac{2\pi k}{N}\right) = \sum_{t=0}^{N-1} x(t+N_s)e^{-j\frac{2\pi k}{N}t} \text{ for } k \in T^N \quad (7)$$

$$x(t) = \frac{1}{N} \sum_{k=0}^{N-1} X^s\left(\frac{2\pi k}{N}\right)e^{j\frac{2\pi k}{N}(t-N_s)} \text{ for } t \in T_{N_s}^N \quad (8)$$

Note that this reflects the  $N$ -point DFT of a signal, of which the first  $N_s$  time instants are discarded. Throughout this paper we will adopt a number of additional assumptions on the system and the generated data.

**Assumption 2.1** *There exists a finite*

- i.  $\bar{u}^p$ , such that  $|u(t)| \leq \bar{u}^p$  for  $t < 0$ ;
- ii. pair of reals  $M, \rho \in \mathbb{R}$ ,  $\rho > 1$ , such that  $|g_0(k)| \leq M\rho^{-k}$ , for  $k \in \mathbb{Z}_+$ ;
- iii. upper bound on the DFT of the output noise:  $|V^s(\frac{2\pi k}{N})| \leq \bar{V}^s(\frac{2\pi k}{N})$ , for  $k \in T^N$ .

### 3 Discrete error bound.

#### 3.1 Motivation.

The motivation to consider the ETFE is that we want  $\hat{G}(e^{j\omega_k})$  to be an intermediate data representation in the frequency domain. The ETFE is the quotient of the DFT of the output signal and the DFT of the input signal. In discrete Fourier transforming a signal no information is lost or added, the mapping from time to frequency domain is one to one. Also, the system is assumed to be linear. Therefore the ETFE can indeed be regarded as a representation of the data in the frequency domain.

The motivation to look at input design is that the ETFE for an arbitrary input signal is in general not satisfactory. We will try to improve the quality of the frequency domain data by input design.

#### 3.2 Results.

A nonparametric frequency domain discrete upper bound on the additive error for the ETFE will be presented in this section. Errors due to unknown initial and final conditions of the system and additive noise on the output are taken into account. We will use a partly periodic input signal for excitation, and we will discard the first part of the signals in the estimation.

**Definition 3.1** *A partly periodic signal  $x$  is a signal having the first part equal to the last part:  $x = [x_1 \ x_2 \ x_1]$ .*

The length of  $x_1$  will be denoted by  $N_s$ . Only the part  $[x_2 \ x_1]$  will be used in the identification and has length  $N$ . The total length of the signal  $x$  now is  $N_s+N$ . We will show that the value of  $N_s$  influences the error due to initial and final conditions in the estimate. Note that the largest possible value of  $N_s$  is  $N$ .

**Theorem 3.2** *Consider a SISO system, satisfying the assumptions stated in section 2. Using a partly periodic input signal,  $N_s \in T^{N+1}$ , and the estimate*

$$\hat{G}^s\left(\frac{2\pi \ell}{N}\right) = \frac{Y^s\left(\frac{2\pi \ell}{N}\right)}{U^s\left(\frac{2\pi \ell}{N}\right)} \text{ for } \ell = \{\ell \in T^N | U^s\left(\frac{2\pi \ell}{N}\right) \neq 0\}$$

*the following error bound is satisfied*

$$|G_0\left(\frac{2\pi \ell}{N}\right) - \hat{G}^s\left(\frac{2\pi \ell}{N}\right)| \leq \alpha\left(\frac{2\pi \ell}{N}\right)$$

*with*

$$\alpha\left(\frac{2\pi \ell}{N}\right) = \frac{\bar{u}^p + \bar{u}}{|U^s\left(\frac{2\pi \ell}{N}\right)|} \frac{M\rho(1-\rho^{-N})}{(\rho-1)^2} \rho^{-N_s} + \frac{\bar{V}^s\left(\frac{2\pi \ell}{N}\right)}{|U^s\left(\frac{2\pi \ell}{N}\right)|}$$

Proof: See appendix A.  $\square$

The first term on the right hand side of the error bound given in the theorem is the error due to the effects of initial and final conditions of the system, i.e. the effects of the unknown signals outside the measurement interval. This error converges exponentially with  $N_s$  (convergence as  $\rho^{-N_s}$ ). The properties of  $|U^s(\frac{2\pi\ell}{N})|$  of course depend on the specific choice of the input signal  $u(t)$  for  $t \in T_{N_s}^N$ . For a random signal the magnitude of the  $N$  point DFT, as defined in (5) and (7), is proportional to  $\sqrt{N}$ , see Ljung (1987) lemma 6.2. Hence, if the input is random for  $t \in T_{N_s}^N$ , the error due to the effects of initial and final conditions converges as  $\rho^{-N_s}/\sqrt{N}$ . The second term on the right hand side is the error due to the additive noise on the output. This error does not converge at all, it is just the noise to signal ratio in the frequency domain. By designing an appropriate input signal, one can of course shape the error due to noise. An input signal having a DFT with desired magnitude can be designed easily using the inverse DFT of the desired spectrum, see e.g. Schoukens *et al.* (1991).

We will now focus on the error due to the noise, the second term on the right hand side of the error bound given in theorem 3.2. It is possible to obtain convergence for this error by choosing the input signal to be periodic. The highest rate of convergence is obtained by an input signal having an integer number of periods in the interval  $T_{N_s}^N$ . Let  $N_0$  denote the length of one period of the input signal and let the interval  $T_{N_s}^N$  contain exactly  $k_0$  periods, so that  $N = k_0 N_0$ . In this case  $U^s(\frac{2\pi k}{N}) = 0$  if  $k/k_0$  is not an integer, only  $U^s(\frac{2\pi k}{N_0})$  is not identically equal to zero, see Ljung (1987) example 2.2. It is now straightforward to show that the DFT over  $k_0$  periods of a periodic signal is exactly  $k_0$  times as large as the DFT over one period. In conclusion,  $|U^s(\frac{2\pi k}{N_0})|$  is exactly proportional to  $N$  if  $N = k_0 N_0$  with  $k_0 \in \mathbb{Z}$ .

**Corollary 3.3** Consider a SISO system, satisfying the assumptions stated in section 2. Using a partly periodic input signal having an integer number of periods in the interval  $T_{N_s}^N$ ,  $N_s \in T^{N+1}$ , and the estimate

$$\hat{G}^s(\frac{2\pi\ell}{N_0}) = \frac{Y^s(\frac{2\pi\ell}{N_0})}{U^s(\frac{2\pi\ell}{N_0})} \text{ for } \ell = \{\ell \in T^{N_0} | U^s(\frac{2\pi\ell}{N_0}) \neq 0\}$$

the following error bound is satisfied

$$|G_0(\frac{2\pi\ell}{N_0}) - \hat{G}^s(\frac{2\pi\ell}{N_0})| \leq \alpha(\frac{2\pi\ell}{N})$$

with

$$\alpha(\frac{2\pi\ell}{N}) = \frac{\bar{u}^p + \bar{u}}{|U^s(\frac{2\pi\ell}{N_0})|} \frac{M\rho(1 - \rho^{-N})}{(\rho - 1)^2} \rho^{-N_s} + \frac{\bar{V}^s(\frac{2\pi\ell}{N_0})}{|U^s(\frac{2\pi\ell}{N_0})|}$$

The error bound given in the corollary goes to zero if  $N_s$  and  $N$  are going to infinity,  $N_0$  is constant, and the noise  $v(t)$  does not contain a periodic component. The error due to the effects of initial and final conditions converges as  $\rho^{-N_s}/N$ . The error due to the additive noise on the output converges as  $1/\sqrt{N}$  if  $v(t)$  is a random signal, because the magnitude of the  $N$  point DFT of a random signal is proportional to  $\sqrt{N}$ , see Ljung (1987) lemma 6.2, while the magnitude of the DFT of the periodic input is exactly proportional to  $N$ . The price for this convergence is that less points of the transfer function are estimated ( $N_0$  instead of  $N = k_0 N_0$ ).

### 3.3 Remarks.

A partly periodic signal can be seen as a generalization of a sinewave input. This generalization is useful because sinewave testing (sinewave excitation and actually measuring the frequency response in a finite number of frequency points) is time consuming. For each new sinewave input one must wait until the system has reached its steady state response. A partly periodic signal can consist of  $N$  sinewaves, but one has to wait only one time for the effects of initial and final conditions to vanish.

For  $N_s = 0$  the ETFE as defined in Ljung (1987) arises. In this case the error due to initial and final conditions converges as  $1/\sqrt{N}$  if  $u(t)$  is a random signal for  $t \in T^N$ , as was also shown in Ljung (1987). Note that for  $N_s = 0$  the input signal is completely free. The choice for  $N_s > 0$  hence is a choice to restrict the input signal in order to be able to obtain a tight error bound for the nominal model.

Finally we note that the extension to the MIMO case of theorem 3.2 has been made by the authors. To be able to do this, the Fourier transforms of the different input signals have to satisfy an orthogonality condition.

## 4 Continuous error bound.

### 4.1 Motivation.

We now have an upper bound  $\alpha(\omega_k)$  on the error  $|G_0(e^{j\omega_k}) - \hat{G}(e^{j\omega_k})|$ . This error bound is only defined in a finite number of frequency points  $\omega_k \in \Omega$ , with  $\Omega := \{\omega_k \in \mathbb{R} \cap [0, 2\pi) \mid |U^s(e^{j\omega_k})| \neq 0\}$ . This is due to the fact that  $\hat{G}(e^{j\omega_k})$  is only defined at a finite number of frequency points when  $N$ , the

number of datapoints used in the estimate, is finite. The aim is to find an upper bound  $\delta(\omega)$  such that

$$|G_0(e^{j\omega}) - G_{nom}(e^{j\omega})| \leq \delta(\omega)$$

for all frequencies in the interval  $[0, 2\pi)$ . It is straightforward to give a discrete upper bound  $\delta(\omega_k)$ . First note that  $\beta(\omega_k) = |\hat{G}(e^{j\omega_k}) - G_{nom}(e^{j\omega_k})|$  can be calculated exactly from the knowledge of  $G_{nom}$ . From the inequality

$$\begin{aligned} & |G_0(e^{j\omega_k}) - G_{nom}(e^{j\omega_k})| \\ & \leq |G_0(e^{j\omega_k}) - \hat{G}(e^{j\omega_k})| + |\hat{G}(e^{j\omega_k}) - G_{nom}(e^{j\omega_k})| \end{aligned}$$

it now follows that a possible choice for  $\delta(\omega_k)$  is  $\delta(\omega_k) = \alpha(\omega_k) + \beta(\omega_k)$ . Hence the problem is to find the behaviour of  $\delta(\omega)$  between the estimated frequency points for the prespecified nominal model. As argued in section 3.1, the data does essentially not contain more information about the transfer function of the system than is captured by the discrete estimate  $\hat{G}(e^{j\omega_k})$ . Therefore, assumptions about the system must be used to be able to bound the error at frequencies  $\omega \neq \omega_k$ . We will use smoothness assumptions on the system, and we will interpolate the discrete error bound  $\delta(\omega_k)$  using these smoothness properties.

#### 4.2 Bounds on derivatives.

Smoothness properties of the system in the form of upper bounds on the derivatives of  $G_0(e^{j\omega})$  with respect to the frequency, can be obtained from the assumed upper bound on the impulse response.

**Proposition 4.1** For a SISO system with  $|g_0(m)| \leq M\rho^{-m}$  there holds

$$\begin{aligned} \left| \frac{d G_0(e^{j\omega})}{d\omega} \right| & \leq \frac{M\rho}{(\rho-1)^2} \\ \left| \frac{d^2 G_0(e^{j\omega})}{d\omega^2} \right| & \leq \frac{M\rho(\rho+1)}{(\rho-1)^3} \end{aligned}$$

**Proof:** See deVries (1991).  $\square$

To be able to bound the derivatives of the magnitude of the error system  $|G_0(e^{j\omega}) - G_{nom}(e^{j\omega})|$  we need the following proposition.

**Proposition 4.2** For a SISO system there holds

$$\begin{aligned} & \left| \frac{d^k}{d\omega^k} |G_0(e^{j\omega}) - G_{nom}(e^{j\omega})| \right| \\ & \leq \left| \frac{d^k}{d\omega^k} (G_0(e^{j\omega}) - G_{nom}(e^{j\omega})) \right| \quad (9) \end{aligned}$$

$$\leq \left| \frac{d^k G_0(e^{j\omega})}{d\omega^k} \right| + \left| \frac{d^k G_{nom}(e^{j\omega})}{d\omega^k} \right| \quad (10)$$

for  $k = 1$  and  $k = 2$ .

**Proof:** See deVries (1991).  $\square$

An upper bound for (10) can be calculated using proposition 4.1 and the knowledge of  $G_{nom}(e^{j\omega})$ . If an upper bound on  $|g_0(m) - g_{nom}(m)|$  is known, we are able to calculate an upper bound for the error directly from proposition 4.1.

#### 4.3 Interpolation.

In this section we will address the problem of calculating an upper bound on the error  $|G_0(e^{j\omega}) - G_{nom}(e^{j\omega})|$  between the frequency points  $\omega_k$  where an upper bound  $\delta(\omega_k)$  is known. Hence, we have to find the highest possible value  $\delta(\omega)$  of this error for each frequency  $\omega$  between two given points, say  $\delta(\omega_k)$  and  $\delta(\omega_{k+1})$ . We are able to bound this error by taking into account the bounds on the first and second derivatives of  $|G_0(e^{j\omega}) - G_{nom}(e^{j\omega})|$  that were derived in section 4.1, say  $\gamma_1$  and  $\gamma_2$  respectively. The maximum value of the error  $\delta(\omega)$  now arises by interpolating the discrete error bound  $\delta(\omega_k)$  using the function  $f(x)$  depicted in figure 1. To explain the construction of this function  $f(x)$ , assume that there is a maximum between the two frequency points. Starting at the maximum ( $x = 0$ ,  $f(x) = 0$  and  $df(x)/dx = 0$ ) we want  $f(x)$ , in a smooth way, to decrease as fast as possible: the faster  $f(x)$  decreases, the higher the maximum lies above the two given points  $\delta(\omega_k)$ . Hence we use a function having a constant second derivative equal to the bound  $\gamma_2$  on this derivative. In this way parts II and III of the error bound are constructed. The absolute value of the first derivative of this function will clearly increase with the distance  $|x|$  to the maximum. At  $|x| = \gamma_1/\gamma_2$  the first derivative becomes equal to the bound  $\gamma_1$  on this derivative. Hence, from thereon we use a function having a constant first derivative equal to the bound  $\gamma_1$ . In this way part I or IV of the error bound is constructed. The function constructed in this way is unique and given by

$$\begin{aligned} f(x) &= -\frac{\gamma_2}{2} x^2 & \text{for } |x| \leq \frac{\gamma_1}{\gamma_2} & \quad (11) \\ &= -\gamma_1 |x| + \frac{\gamma_1^2}{2\gamma_2} & \text{for } |x| > \frac{\gamma_1}{\gamma_2} & \end{aligned}$$

The function  $f(x)$  given in (11) directly gives the value of  $\delta(\omega)$

$$\delta(\omega) = \delta(\omega_k) - f(\Delta x_1) + f(x) \quad \text{for } \omega \in [\omega_k, \omega_{k+1}] \quad (12)$$

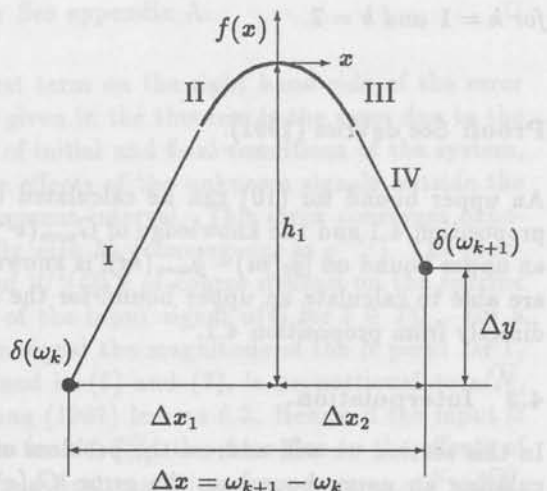


Fig. 1: The interpolating function  $f(x)$  for the discrete error bound.

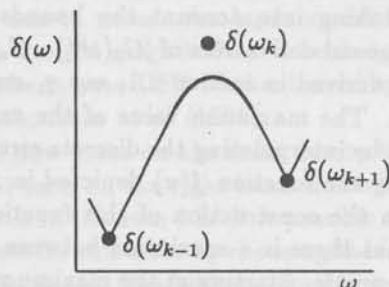


Fig. 2: A situation in which the point  $\delta(\omega_k)$  must not be used.

However, in (12) the values of  $\Delta x_1$  and  $x$  are unknown, because the location of the maximum is as yet unknown. Analytic expressions for the location of the maximum can be given, by specifying  $\Delta x_1$  or  $\Delta x_2$  as a function of  $\delta(\omega_k)$ ,  $\delta(\omega_{k+1})$ ,  $\gamma_1$  and  $\gamma_2$ . These expressions are given in appendix B.

When  $|\Delta y| > \gamma_1 \Delta x$  the estimated point of the discrete estimate with the highest error bound must not be used. Interpolation from neighbouring points, although over a greater distance, gives a lower error bound. This situation can also arise when  $|\Delta y| \leq \gamma_1 \Delta x$ , see figure 2.

#### 4.4 Remarks.

Taking a closer look at the results of this and the previous section, we can summarize in the following way. In section 3 a bound  $\alpha(\omega_k)$  has been derived

$$|G_0(e^{j\omega_k}) - \hat{G}(e^{j\omega_k})| \leq \alpha(\omega_k) \quad (13)$$

for all  $\omega_k$  in a set  $\Omega \subset \mathbb{R} \cap [0, 2\pi)$  containing a finite number ( $\leq N$ ) of elements. Since the nominal model is known, the error

$$\beta(\omega_k) := |\hat{G}(e^{j\omega_k}) - G_{nom}(e^{j\omega_k})| \quad (14)$$

can be calculated exactly for all  $\omega_k \in \Omega$ . In this section 4, a continuous bound  $\delta(\omega)$  is derived, such that

$$|G_0(e^{j\omega}) - G_{nom}(e^{j\omega})| \leq \delta(\omega) \quad (15)$$

with

$$\delta(\omega_k) = \alpha(\omega_k) + \beta(\omega_k) \quad \text{for } \omega_k \in \Omega \quad (16)$$

In the nonparametric discrete estimate, cf. (13), no error due to undermodelling is present, i.e. no error due to approximation is made, because complete freedom exist for each frequency point to fit  $G_0(e^{j\omega_k})$ . The approximation error therefore is completely due to the nominal model, cf. (14).

In the procedure presented, the determination of the nominal model and the determination of the error bound clearly are completely separated. We addressed the problem of determining the error bound. The problem of determining, from the discrete estimate, a nominal model such that the error bound is as low as possible is addressed in Helmicki *et al.* (1990a) and Gu and Khargonekar (1991). Methods for tuning the nominal model to nominal control design specifications are discussed in Bitmead and Zang (1991), Hakvoort (1990) and Schrama (1991).

The procedure presented can very well be used to obtain an upper bound on the unmodelled dynamics that is needed in Wahlberg and Ljung (1991) and Kosut *et al.* (1990).

## 5 Relation with control design specifications.

To show the applicability of the approach presented in this paper to robust control design, we will consider the following situation. In order to verify desired robustness properties of a designed controller for the system, an allowable error bound is specified for the difference between  $G_0$  and  $G_{nom}$ :

$$|G_0(e^{j\omega}) - G_{nom}(e^{j\omega})| \leq \delta_a(\omega)$$

The allowable error  $\delta_a(\omega)$  is a function of the nominal model, the designed controller and the robust control design specifications. Given measurement data from the system, it now has to be verified whether a specific nominal model lies within the

specified error bound. If not, there should be determined which action should be taken in order to solve the problem: either constructing a new nominal model, or performing additional experiments to reduce the uncertainty.

The actual error bound  $\delta(\omega)$  for the nominal model clearly is a function of the nominal model itself and of the discrete estimate  $\hat{G}$ . Therefore both should be tuned to the robust control design specifications. This can be done by comparing the allowable error  $\delta_a(\omega)$  with the actual error bound  $\delta(\omega)$ . For those values of  $\omega$  where  $\delta_a(\omega) \leq \delta(\omega)$  we can analyse  $\delta(\omega)$  and evaluate its different components.

At the finite number of frequency points  $\omega_k \in \Omega$ , we have  $\delta(\omega_k) = \alpha(\omega_k) + \beta(\omega_k)$ . Therefore we know that

1. when  $\alpha(\omega_k) \gg \beta(\omega_k)$ , the uncertainty is mainly due to the inherent uncertainty in the data  $\alpha(\omega_k)$ , i.e. effects of initial and final conditions, bad signal-to-noise ratio and/or restricted length of the data set. Actions to be taken to improve the bound include: increasing  $N_s$ , increasing the power of the input signal, and increasing  $N$ . In the case of periodic input signals, the signal-to-noise ratio in the frequency domain is proportional to  $\sqrt{N/N_0}$ . Consequently the error bound can also be improved by decreasing  $N_0$ .
2. when  $\alpha(\omega_k) \ll \beta(\omega_k)$ , the uncertainty is mainly due to a bad nominal model. A straightforward action is then to choose a new nominal model, that is better able to represent the system dynamics in the specific frequency range.

In between the finite number of frequency points  $\omega_k \in \Omega$ , say for  $\omega_k < \omega < \omega_{k+1}$ , the error bound  $\delta(\omega)$  is determined through interpolation between the adjacent points  $\delta(\omega_k), \delta(\omega_{k+1})$ . Therefore

3. when  $\delta(\omega) \gg \max(\delta(\omega_k), \delta(\omega_{k+1}))$ , the uncertainty is mainly due to the interpolation step. Note that uncertainty due to interpolation is strongly determined by the distance between two adjacent discrete frequency points. Consequently new experiments should be performed with a smaller distance between the discrete frequency points in the specific frequency region.

Note that it is possible to determine whether the main source of the actual error is the inherent uncertainty in the data, the nominal model, or the

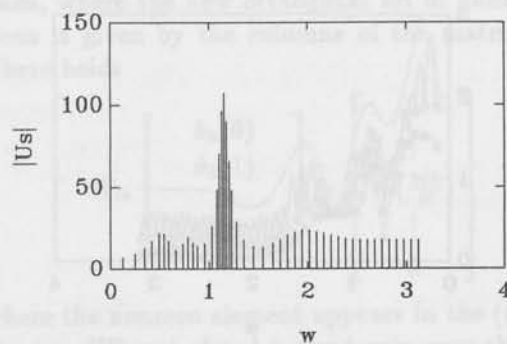


Fig. 3:  $|U^s(\omega_k)|$ , the magnitude of the DFT of the input signal in the interval  $T_{N_s}^N$ .

interpolation step caused by the absence of data due to the specific excitation of the system. Also it is possible to decrease the contribution of these different error sources almost independently. Now it is possible to iteratively decrease the error bound, until the level of the allowable error is reached, successively by input design and additional experiments, and by tuning the nominal model. Using this procedure we can determine whether or not specific robust control design specifications can be met.

Note that the error bound  $\alpha(\omega_k)$  is essentially frequency dependent and that the frequency points  $\omega_k \in \Omega$  need not be positioned equidistantly over the frequency axis. In comparison with the existing methods (see e.g. Helmicki *et al.* (1990a) and Gu and Khargonekar (1991)), this creates a lot of freedom to shape the error bound into an accepted (allowable) form, which from a control point of view definitely should be frequency-dependent.

## 6 Example.

To illustrate the properties of the method we made a simulation with a fifth order system whose impulse response satisfies a bound given by  $M = 2.5$  and  $\rho = 1.25$ , and a third order nominal model. There was 10 percent (in amplitude) noise on the output. The upper bound  $\bar{V}^s(\omega_k)$  was set to  $\bar{V}^s(\omega_k) = 2 \cdot \max_{\omega_k} |V^s(\omega_k)|$ . The input signal was chosen to obey  $\bar{u}^p = 2$  and  $\bar{u} = 1$ . We used 1074 points with  $N = 1024$ ,  $N_0 = 256$  and  $N_s = 50$ . The magnitude of the DFT of the input signal in the interval  $T_{N_s}^N$ ,  $|U^s(\omega_k)|$ , is given in figure 3. Note that the frequencies  $\omega_k$  are not equidistant. The input was designed iteratively to result in an error bound smaller than the allowable error by choosing the frequency grid and the magnitude of  $U^s(\omega_k)$ . In figure 4 the allowable error  $\delta_a(\omega)$ , the error bound  $\delta(\omega)$  and the error due to approximation  $\beta(\omega_k)$  are

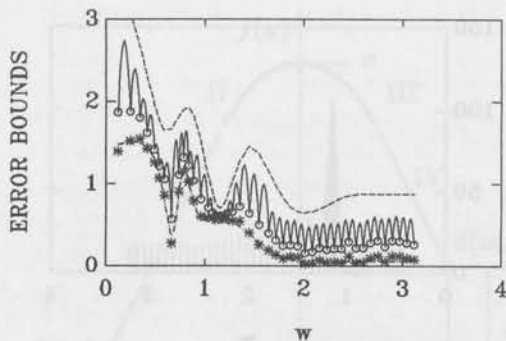


Fig. 4: The error bounds and the true error:  $\delta_a(\omega)$  (dash),  $\delta(\omega)$  (solid),  $\delta(\omega_k)$  (o),  $\beta(\omega_k)$  (\*),  $|G_0(\omega) - G_{nom}(\omega)|$  (dashdot).

given. The inherent uncertainty in the data  $\alpha(\omega_k)$  equals  $\delta(\omega_k) - \beta(\omega_k)$ . The error due to interpolation is indicated by the curves between the points  $\delta(\omega_k)$ . Note that  $\beta(\omega_k)$  provides a good indication of the true approximation error, and that the error bound  $\delta(\omega)$  can be made almost equal to the true approximation error by input design. Comparing  $\beta(\omega_k)$  and  $\delta(\omega)$ , it follows that in the frequency interval  $\omega \in [1.1, 1.3]$  the error due to approximation clearly dominates, whereas for  $\omega \in [2, \pi]$  the inherent uncertainty in the data and the error due to interpolation clearly dominate.

## 7 Conclusions.

In this paper a procedure is presented to quantify the model uncertainty of any prespecified nominal model, given a sequence of measurement data from a plant. In the procedure presented the empirical transfer function estimate (ETF) is used to construct a nonparametric estimate of the transfer function in a discrete number of frequency points, together with an upper bound on the error. Through interpolation, this error bound can be transformed to a bound which is available on a continuous frequency interval. A frequency dependent upper bound is obtained, which is much more tailored to the needs of a robust control design scheme, than an  $H_\infty$ -bound. In order to obtain a tight error bound, a special input signal is proposed (partly periodic) which has advantages over classical sine wave experiments.

The estimated upper bound for the model error of a prespecified nominal model can be split into three parts: one part due to the inherent uncertainty in the data, a second part due to interpolation, and a third part due to imperfections of the nominal model. These three components can be

tuned almost independently, by appropriate experiment design and by choosing an appropriate nominal model. When the error bound is too conservative in relation with control design specifications, information is provided as to which action should be taken (new experiments or alternative nominal model) in order to satisfy the design requirements. Because the nominal model is not a fixed function of the data, it is not necessary to change the nominal model when a new set of measurements is used. Therefore it is possible to restrict attention to a specific frequency region when designing the new input signal, the error bound for other frequencies remains valid if the nominal model is not changed.

## 8 References.

- Bitmead, R.R. and Z. Zang (1991). An iterative identification and control strategy. *Proc. 1st European Control Conf.*, Grenoble, France, pp. 1396-1400.
- deVries, D.K. (1991). Quantification of model uncertainty from data. *Submitted to Int. Journal of Control*.
- Goodwin, G.C. and B. Ninness (1991). Model error quantification for robust control based on quasi-bayesian estimation in closed loop. *Proc. American Control Conf.*, 77-82.
- Goodwin, G.C. and M.E. Salgado (1989). Quantification of uncertainty in estimation using an embedding principle. *Proc. American Control Conf.*, 1416-1421.
- Gu, G. and P.P. Khargonekar (1991). Linear and nonlinear algorithms for identification in  $H^\infty$  with error bounds. *Proc. American Control Conf.*, 64-69.
- Hakvoort, R.G. (1990). Optimal experiment design for prediction error identification in view of feedback design. *Selected Topics in Identification, Modelling and Control, 2*, 71-78. Delft University Press, The Netherlands.
- Helmicki, A.J., C.A. Jacobson and C.N. Nett (1990a). Identification in  $H_\infty$ : a robustly convergent, nonlinear algorithm. *Proc. American Control Conf.*, 386-391.
- Helmicki, A.J., C.A. Jacobson and C.N. Nett (1990b). Identification in  $H_\infty$ : linear algorithms. *Proc. American Control Conf.*, 2418-2423.
- Kosut, R.L., M. Lau, S. Boyd (1990). Identification of systems with parametric and nonparametric uncertainty. *Proc. American Control Conf.*, 2412-2417.
- LaMaire, R.O., L. Valavani, M. Athans and G. Stein (1991). A frequency-domain estimator for use in adaptive control systems. *Automatica*, 27, 23-38.
- Ljung, L. (1987). *System Identification: Theory for the User*. Prentice-Hall, Englewood Cliffs, NJ.
- Schoukens, J., P. Guillaume, R. Pintelon (1991). Design of multisine excitations. *IEE Control 91 confer-*

ence, Edinburgh.

Schrama, R.J.P. (1991). Control-oriented approximate closed-loop identification via fractional representations. *Proc. American Control Conf.*, 719-720.

Wahlberg, B. and L. Ljung (1991). On estimation of transfer function error bounds. *Proc. European Control Conf.*, 1378-1383.

## A Proof of theorem 3.2.

### A.1 Properties of the N point DFT.

To give the proof we have to start by taking a closer look at the properties of the N point DFT, and by dealing with some additional definitions and notation. The periodic continuation of a signal  $x(t)$  is denoted by  $x^R(t)$

$$x^R(t + kN) = x(t) \quad \text{for } k \in \mathbb{Z}, t \in T^N$$

The N point DFT and inverse DFT are defined in (5) and (6). A set of N complex orthogonal time domain elementary functions (complex sinewaves) now can be given as

$$\hat{x}_k(t) = \frac{1}{N} X\left(\frac{2\pi k}{N}\right) e^{j\frac{2\pi k}{N}t} \quad k \in T^N \quad (17)$$

There holds

$$\sum_{k=0}^{N-1} \hat{x}_i(t) \hat{x}_j(t) = 0 \quad \text{for } i \neq j$$

$$x(t) = \sum_{k=0}^{N-1} \hat{x}_k(t) \quad \text{for } t \in T^N$$

Note that the elementary functions are also defined outside  $T^N$ , and that outside  $T^N$  they are given by periodic continuation. Hence, for  $t \notin T^N$  the inverse N point DFT gives a periodic continuation

$$x^R(t) = \sum_{k=0}^{N-1} \hat{x}_k(t) \quad \text{for } t \in \mathbb{Z} \quad (18)$$

Consider the transformation matrix  $W_N \in \mathbb{C}^{N \times N}$

$$W_N = \begin{bmatrix} 1 & 1 & \dots & 1 \\ 1 & e^{-j\frac{2\pi}{N}} & \dots & e^{-j\frac{2\pi(N-1)}{N}} \\ \vdots & \vdots & \ddots & \vdots \\ 1 & e^{-j(N-1)\frac{2\pi}{N}} & \dots & e^{-j(N-1)\frac{2\pi(N-1)}{N}} \end{bmatrix} \quad (19)$$

Note that  $W_N/\sqrt{N}$  is an orthonormal matrix:  $W_N W_N^*/N = W_N^* W_N/N = I$ .  $W_N^*$  denotes the complex conjugate transpose of the matrix  $W_N$ . The N point DFT can now be seen as a change of

basis, where the new orthogonal set of basis functions is given by the columns of the matrix  $W_N$ . There holds

$$W_N \begin{bmatrix} \hat{x}_k(0) \\ \hat{x}_k(1) \\ \vdots \\ \hat{x}_k(N-1) \end{bmatrix} = \begin{bmatrix} 0 \\ \vdots \\ X\left(\frac{2\pi k}{N}\right) \\ \vdots \\ 0 \end{bmatrix} \quad (20)$$

where the nonzero element appears in the  $(k+1)$ -th row. When a signal is used only over the time interval  $T_{N_s}^N$  the DFT is defined according to (7), (8), and the elementary functions read

$$x(t) = \sum_{k=0}^{N-1} \hat{x}_k^s(t) \quad \text{for } t \in T_{N_s}^N \quad (21)$$

$$\hat{x}_k^s(t) = \frac{1}{N} X^s\left(\frac{2\pi k}{N}\right) e^{j\frac{2\pi k}{N}(t-N_s)} \quad \text{for } t \in T_{N_s}^N$$

Finally, the past values of the input signal ( $t < 0$ ) are sometimes denoted as  $u^P(t)$  to stress that they are unknown.

### A.2 Proof.

The key observation is that we are able to decompose the input signal  $u(t)$  over a measurement interval  $T^{N+N_s}$  in the basis  $W_N$ .

$$u(t) = \sum_{k=0}^{N-1} \hat{u}_k^s(t) \quad \text{for } t \in T^{N+N_s}$$

This can be done only for partly periodic input signals, see (18). For  $t \in T^{N+N_s}$  the output now can be written as

$$y(t) = \sum_{i=0}^t g_0(i) \sum_{k=0}^{N-1} \hat{u}_k^s(t-i) + \sum_{i=t+1}^{\infty} g_0(i) u^P(t-i) + v(t) \quad (22)$$

Note that for an elementary function there holds

$$g_0(t) * \hat{u}_k^s(t) = \frac{1}{N} \sum_{i=0}^{\infty} g_0(i) U^s\left(\frac{2\pi k}{N}\right) e^{j\frac{2\pi k}{N}(t-N_s-i)}$$

$$= \frac{1}{N} U^s\left(\frac{2\pi k}{N}\right) e^{j\frac{2\pi k}{N}(t-N_s)} \sum_{i=0}^{\infty} g_0(i) e^{-j\frac{2\pi k}{N}i}$$

$$= G_0\left(\frac{2\pi k}{N}\right) \hat{u}_k^s(t) \quad (23)$$

where  $*$  denotes convolution. Hence

$$\sum_{i=0}^t g_0(i) \sum_{k=0}^{N-1} \hat{u}_k^s(t-i) = \sum_{k=0}^{N-1} \sum_{i=0}^t g_0(i) \hat{u}_k^s(t-i)$$

$$= \sum_{k=0}^{N-1} \left( \sum_{i=0}^{\infty} g_0(i) \hat{u}_k^s(t-i) - \sum_{i=t+1}^{\infty} g_0(i) \hat{u}_k^s(t-i) \right)$$

$$= \sum_{k=0}^{N-1} G_0\left(\frac{2\pi k}{N}\right) \hat{u}_k^s(t) - \sum_{i=t+1}^{\infty} g_0(i) u^R(t-i) \quad (24)$$

Define

$$e(t) = \sum_{i=t+1}^{\infty} g_0(i)[u^P(t-i) - u^R(t-i)] \quad (25)$$

Writing down equation (22) for all  $t \in T_{N_s}^N$ , and using equations (21), (24) and (25) results in

$$\sum_{k=0}^{N-1} \begin{bmatrix} \hat{y}_k^s(N_s) \\ \hat{y}_k^s(N_s+1) \\ \vdots \\ \hat{y}_k^s(N_s+N-1) \end{bmatrix} = \sum_{k=0}^{N-1} G_0\left(\frac{2\pi k}{N}\right) \begin{bmatrix} \hat{u}_k^s(N_s) \\ \hat{u}_k^s(N_s+1) \\ \vdots \\ \hat{u}_k^s(N_s+N-1) \end{bmatrix} + \begin{bmatrix} e(N_s) \\ e(N_s+1) \\ \vdots \\ e(N_s+N-1) \end{bmatrix} + \begin{bmatrix} v(N_s) \\ v(N_s+1) \\ \vdots \\ v(N_s+N-1) \end{bmatrix} \quad (26)$$

Premultiplying with the  $(\ell+1)$ -th row of  $W_N$  and using equation (20) gives

$$Y^s\left(\frac{2\pi\ell}{N}\right) = G_0\left(\frac{2\pi\ell}{N}\right)U^s\left(\frac{2\pi\ell}{N}\right) + E^s\left(\frac{2\pi\ell}{N}\right) + V^s\left(\frac{2\pi\ell}{N}\right)$$

By using the assumptions made on the impulse response and the input signal, an upper bound for  $E^s\left(\frac{2\pi\ell}{N}\right)$  can be derived

$$\begin{aligned} |E^s\left(\frac{2\pi\ell}{N}\right)| &\leq \left| \sum_{t=N_s}^{N_s+N-1} e^{-j\frac{2\pi\ell}{N}(t-N_s)} \times \right. \\ &\quad \left. \times \sum_{i=t+1}^{\infty} g_0(i)[u^P(t-i) - u^R(t-i)] \right| \\ &\leq (\bar{u}^P + \bar{u}) \sum_{t=N_s}^{N_s+N-1} \sum_{i=t+1}^{\infty} |g_0(i)| \\ &\leq (\bar{u}^P + \bar{u}) \frac{M\rho}{(\rho-1)^2} \rho^{-N_s}(1-\rho^{-N}) \quad (27) \end{aligned}$$

The result now follows by using the assumption made on the noise. ■

## B Interpolation algorithm.

To be able to give analytic expressions for the location of the maximum one has to distinguish several cases, depending on which part of the interpolating function  $f(x)$  actually is used. It is e.g. possible that  $\gamma_1, \gamma_2, \delta(\omega_k)$  and  $\delta(\omega_{k+1})$  are such that the interpolating function  $f(x)$  reduces to part I. In all, there are ten possibilities: only part I, only part II, part I and II, etc.

**Algorithm B.1** All possibilities of the function given in equation (11) to interpolate two points are

given below, as a function of  $\Delta x, \Delta y, \gamma_1$  and  $\gamma_2$ . A maximum occurs if

$$|\Delta y| < \gamma_1 \Delta x - \frac{\gamma_1^2}{2\gamma_2} \quad \text{and} \quad \Delta x \geq \frac{\gamma_1}{\gamma_2}$$

or if

$$|\Delta y| < \frac{\gamma_2}{2} \Delta x^2 \quad \text{and} \quad \Delta x \leq \frac{\gamma_1}{\gamma_2}$$

If a maximum occurs we can distinguish the following four cases.

1. If  $\Delta x_1 \geq \gamma_1/\gamma_2$  and  $\Delta x_2 \geq \gamma_1/\gamma_2$  than  $\Delta x_1 = \frac{\Delta y + \gamma_1 \Delta x}{2\gamma_1}$ . All four parts of  $f(x)$ , as depicted in figure 1, are used.
2. If  $\Delta x_1 \geq \gamma_1/\gamma_2$  and  $\Delta x_2 < \gamma_1/\gamma_2$  than  $\Delta x_1 = \frac{\gamma_1}{\gamma_2} + \Delta x - \sqrt{\frac{2}{\gamma_2}(\gamma_1 \Delta x - \Delta y)}$ . Parts I, II and III of  $f(x)$  are used.
3. If  $\Delta x_1 < \gamma_1/\gamma_2$  and  $\Delta x_2 \geq \gamma_1/\gamma_2$  than  $\Delta x_1 = \sqrt{\frac{2}{\gamma_2}(\gamma_1 \Delta x + \Delta y)} - \frac{\gamma_1}{\gamma_2}$ . Parts II, III and IV of  $f(x)$  are used.
4. If  $\Delta x_1 < \gamma_1/\gamma_2$  and  $\Delta x_2 < \gamma_1/\gamma_2$  than  $\Delta x_1 = \frac{\Delta y}{\gamma_2 \Delta x} + \frac{\Delta x}{2}$ . Parts II and III of  $f(x)$  are used.

The maximum height  $h_1$  above  $f_1$  is given by  $h_1 = -f(x_1)$ , where  $f(x)$  is given in equation (11).

If no maximum occurs we can distinguish the following seven cases.

1. If  $\gamma_1 \Delta x - \frac{\gamma_1^2}{2} \Delta x^2 \leq \Delta y < \gamma_1 \Delta x$  than  $\Delta x_1 = \frac{\gamma_1}{\gamma_2} + \Delta x - \sqrt{\frac{2}{\gamma_2}(\gamma_1 \Delta x - \Delta y)}$ . Note that  $\Delta x_1 \geq \Delta x$ . Parts I and II of  $f(x)$  are used.
2. If  $\frac{\gamma_2}{2} \Delta x^2 \leq \Delta y < \gamma_1 \Delta x - \frac{\gamma_1^2}{2} \Delta x^2$  than  $\Delta x_1 = \frac{\Delta x}{2} + \frac{\Delta y}{\gamma_2 \Delta x}$ . Note that  $\Delta x_1 \geq \Delta x$ . Only part II of  $f(x)$  is used.
3. If  $\gamma_1 \Delta x - \frac{\gamma_1^2}{2} \Delta x^2 \leq -\Delta y < \gamma_1 \Delta x$  than  $\Delta x_2 = \frac{\gamma_1}{\gamma_2} + \Delta x - \sqrt{\frac{2}{\gamma_2}(\gamma_1 \Delta x + \Delta y)}$ . Note that  $\Delta x_2 \geq \Delta x$ . Parts III and IV of  $f(x)$  are used.
4. If  $\frac{\gamma_2}{2} \Delta x^2 \leq -\Delta y < \gamma_1 \Delta x - \frac{\gamma_1^2}{2} \Delta x^2$  than  $\Delta x_2 = \frac{\Delta x}{2} - \frac{\Delta y}{\gamma_2 \Delta x}$ . Note that  $\Delta x_2 \geq \Delta x$ . Only part III of  $f(x)$  is used.
5. If  $\Delta y = \gamma_1 \Delta x$  than  $\Delta x_1 = \frac{\gamma_1}{\gamma_2} + \Delta x$ . Only part I of  $f(x)$  is used.
6. If  $\Delta y = -\gamma_1 \Delta x$  than  $\Delta x_2 = \frac{\gamma_1}{\gamma_2} + \Delta x$ . Only part IV of  $f(x)$  is used.

**Proof:** Direct computation. □

## Accurate identification for control: the necessity of an iterative scheme

Ruud J.P. Schrama<sup>†</sup>

<sup>†</sup>*Mechanical Engineering Systems and Control Group  
Delft University of Technology, Mekelweg 2, 2628 CD Delft, The Netherlands.*

**Abstract.** If approximate identification and model-based control design are used to accomplish a high performance control system, then the two procedures have to be treated as a joint problem. Solving this joint problem by means of separate identification and control design procedures practically entails an iterative scheme. A frequency response identification technique and a robust control design method are used to set up such an iterative scheme. Its utility is illustrated by an example.

### 1 Introduction

Many control design techniques rest on the availability of a model. It is often taken that an appropriate model can be derived prior to the control design. Traditionally a nominal model  $\hat{P}$  is estimated from plant data, and subsequently a compensator  $C_{\hat{P}}$  is designed for  $\hat{P}$ . Since  $\hat{P}$  is just an approximate description of the plant  $P$ , the compensator  $C_{\hat{P}}$  must be robust. This has motivated the development of identification techniques that estimate an upper bound on the model error (Helmicki *et al.*, 1991, Goodwin and Ninness, 1991). With this upper bound a controller  $C_{\hat{P}}$  can ideally be designed to achieve some robust performance. However, this robust performance can be a *high* performance only if the nominal model  $\hat{P}$  has been chosen with care.

In this note we focus on the derivation of a nominal model  $\hat{P}$  for high-performance control design. Accordingly a nominal model  $\hat{P}$  is said to be appropriate, if it gives rise to a controller  $C_{\hat{P}}$ , that achieves similar high performances for  $P$  and  $\hat{P}$ . Thus the performance of the model-compensator pair  $\hat{P}, C_{\hat{P}}$  must be robust in view of the plant  $P$ . This is accomplished, if the feedback system composed of the nominal model  $\hat{P}$  and the model-based compensator  $C_{\hat{P}}$  approximately describes the feedback system containing the plant  $P$  and the same compensator  $C_{\hat{P}}$ . In this perspective the quality of

a nominal model  $\hat{P}$  depends on its compensator  $C_{\hat{P}}$ .

Now suppose we derive an approximate model first, and after that we design a compensator. Then, in the approximation stage, we have to select a nominal model  $\hat{P}$  without knowing fully the quality of each candidate model. The exact quality of the selected nominal model  $\hat{P}$  will remain unknown until the second stage of control design has been completed. In order that the model-compensator pair  $\hat{P}, C_{\hat{P}}$  approximately describes the plant-compensator pair  $P, C_{\hat{P}}$ , we have to treat the approximation and the control design as a *joint problem* instead of two individual problems. An iterative scheme is required to solve this joint problem by means of the separate stages of approximate identification and model-based control design.

The need of an iteration has been motivated already by e.g. Skelton (1985) and Schrama (1991a), and it is also advocated in philosophical terms by Anderson and Kosut (1991). However, to our knowledge, approximation of feedback properties rather than approximation of the plant itself has not been raised as a motivation before. Several iterative schemes of identification and control design have been proposed in literature. Rivera *et al.* (1990) used such an iteration to build prefilters for a control-relevant open-loop prediction-error identification. Instead of using one open-loop dataset we

take new data at each identification stage, while the plant is operated under feedback by the previously designed compensator. This is closely related to adaptive control, but as exposed by Bitmead *et al.* (1990) the iterative scheme enables an analysis of the interaction between the identification and control design stages. In the latter work prediction-error identification and LQG/LTR control design are combined in an iteration, that focusses on robust stability. The iterations of Hakvoort (1990) and Bitmead and Zang (1991) use prediction-error identification and they address LQ-performance.

We tackle the joint problem by an iteration of repeated frequency response identification and robust control design. In this note we delineate our iterative scheme, and we focus on the identification part in particular. A full discussion is provided by Schrama (1992). In Section 2 we discuss the robust control design method, which leads to the problem of feedback-relevant approximate identification from closed-loop data. Then in Section 3 we frame the identification problem in terms of coprime factorizations. Section 4 contains an example of the proposed iteration and the final section provides some concluding remarks.

## 2 Control design and approximation

From Bongers and Bosgra (1990) we adopt the following control design paradigm. The feedback configuration of interest is depicted in Fig. 1. The transfer matrix, which maps  $\text{col}(r_2, r_1)$  into

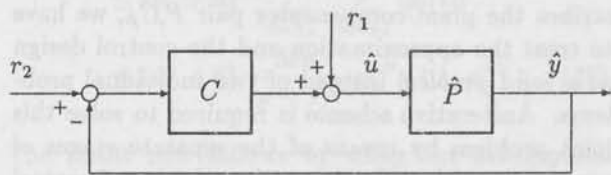


Fig. 1: Feedback configuration for control design

$\text{col}(\hat{y}, \hat{u})$ , is denoted  $T(\hat{P}, C)$ ; i.e.

$$T(\hat{P}, C) = \begin{bmatrix} \hat{P}(I + C\hat{P})^{-1}C & \hat{P}(I + C\hat{P})^{-1} \\ (I + C\hat{P})^{-1}C & (I + C\hat{P})^{-1} \end{bmatrix}. \quad (1)$$

The model-based controller  $C_{\hat{P}}$  is derived from  $\hat{P}$  as

$$C_{\hat{P}} = \arg \min_C \|T(\hat{P}, C)\|_{\infty}. \quad (2)$$

The resulting controller is robust in the sense that it anticipates stable factor perturbations (for details see Bongers and Bosgra, 1990 and Vidyasagar,

1985). Moreover  $C_{\hat{P}}$  pursues traditional design specifications such as a small sensitivity at the lower frequencies and a small complementary sensitivity at the higher frequencies (McFarlane and Glover, 1988).

If  $\|T(\hat{P}, C_{\hat{P}})\|_{\infty}$  is small, then the nominal performance is high. The performance for the actual plant  $P$  can be examined through

$$\|T(P, C_{\hat{P}})\|_{\infty} \leq \|T(\hat{P}, C_{\hat{P}})\|_{\infty} + \|T(P, C_{\hat{P}}) - T(\hat{P}, C_{\hat{P}})\|_{\infty}. \quad (3)$$

The term on the left reflects the performance of the controlled plant.  $\|T(\hat{P}, C_{\hat{P}})\|_{\infty}$  is the minimum achieved in (2); and  $\|T(P, C_{\hat{P}}) - T(\hat{P}, C_{\hat{P}})\|_{\infty}$  is the 'worst-case' performance degradation due to the fact that  $C_{\hat{P}}$  has been designed for the nominal model  $\hat{P}$  rather than for the plant  $P$ .

The feedback systems corresponding to  $T(P, C_{\hat{P}})$  and  $T(\hat{P}, C_{\hat{P}})$  have similar performances if  $\|T(P, C_{\hat{P}}) - T(\hat{P}, C_{\hat{P}})\|_{\infty}$  is small. At the same time  $\|T(\hat{P}, C_{\hat{P}})\|_{\infty}$  must be made as small as possible in order to achieve a high performance. As the latter is pursued in the control design stage, cf. (2), we would like to minimize  $\|T(P, C_{\hat{P}}) - T(\hat{P}, C_{\hat{P}})\|_{\infty}$  in the preceding approximation stage. And since  $C_{\hat{P}}$  is not known a priori, the approximation and control design have to be treated as a joint problem.

We propose the following iterative scheme to tackle the joint problem. In the  $i$ -th step we obtain data from the plant, while it operates under feedback by  $C_{i-1}$ . The nominal model  $\hat{P}_i$  is derived according to

$$\hat{P}_i = \arg \min_{\hat{P} \in \mathcal{P}} \|T(P, C_{i-1}) - T(\hat{P}, C_{i-1})\|_{\infty} \quad (4)$$

where  $\mathcal{P}$  is the set of candidate models. This minimizes the performance degradation for  $C_{i-1}$ . Subsequently  $\hat{P}_i$  is used to construct  $C_i$  as in (2), which produces a small nominal performance term  $\|T(\hat{P}_i, C_i)\|_{\infty}$ . Then this controller is applied to the plant  $P$  and new data can be collected.

In a straightforward application of the identification in (4) and the control design in (2) we would encounter the following problem. Since by (2)  $C_i$  is based solely on the nominal model  $\hat{P}_i$ , the 'new' compensator  $C_i$  may be completely different from the 'old' compensator  $C_{i-1}$ . And although  $T(\hat{P}_i, C_{i-1})$  approximately describes  $T(P, C_{i-1})$ , cf. (4), this does not necessarily hold if  $C_{i-1}$  is replaced by  $C_i$ . Consequently the performance degradation  $\|T(P, C_i) - T(\hat{P}_i, C_i)\|_{\infty}$  can be very large, despite the fact that  $C_i$  is maximally robust in view of the

achieved nominal performance. In order to provide for a small performance degradation, we have to introduce weighting functions in the control design of (2).

In this note we just use an adjustable scalar weight  $\alpha_i$ . The controller  $C_i$  is designed as

$$C_i = \arg \min_C \|T(\alpha_i \hat{P}_i, C/\alpha_i)\|_\infty. \quad (5)$$

This causes  $C_i$  to maximize robustness for a nominal performance level associated with  $\alpha_i$ . The resulting designed feedback system will have its bandwidth close to the cross-over frequency of  $\alpha_i \hat{P}_i$  (McFarlane and Glover, 1988). Thus a large  $\alpha_i$  corresponds to a high nominal performance, and it can be adjusted to cause only a slight improvement upon  $C_{i-1}$ . Thereby we keep the performance degradation small at each step of the iteration. By gradually increasing the weight during the iteration we end up with a large weight and a high performance controller for the plant.

The identification problem that has to be solved at each iteration step is

$$\hat{P}_i = \arg \min_{\hat{P} \in \mathcal{P}} \|T(\alpha_i P, C_{i-1}/\alpha_i) - T(\alpha_i \hat{P}, C_{i-1}/\alpha_i)\|_\infty \quad (6)$$

As there exists no identification technique that can be used to solve (6), we replace the above  $H_\infty$  (or  $L_\infty$ ) approximation by an  $L_2$  approximation. The rationale for this replacement is that the  $L_2$  approximation will yield a reasonably good nominal model in  $L_\infty$  sense, provided that the error-term is sufficiently smooth. This observation is backed up by the result of Caines and Bayukal-Gürsoy (1989) on the  $L_\infty$  consistency of  $L_2$  estimators. The  $L_2$ -identification problem is discussed in the next section.

### 3 Framework for identification

We consider the case in which the plant  $P$  is controlled by  $C_{i-1}$  as in Fig. 2. In order to simplify

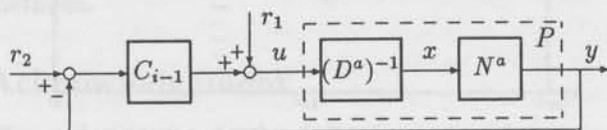


Fig. 2: Feedback configuration for identification

notation we take  $\alpha_i = 1$ . The problem of interest is to identify a nominal model  $\hat{P}_i$  from measurements of the plant's input  $u$  and output  $y$  such that

$$\hat{P}_i = \arg \min_{\hat{P} \in \mathcal{P}} \|T(P, C_{i-1}) - T(\hat{P}, C_{i-1})\|_2. \quad (7)$$

With  $P \notin \mathcal{P}$  the minimization of (7) from  $u$  and  $y$  combines all problems that are encountered in approximate identification and closed-loop identification. Therefore direct application of standard identification methods to  $u$  and  $y$  will not yield the desired  $\hat{P}_i$  (see Schrama (1991b) for a discussion). In order to solve (7) we represent the plant  $P$  by a right coprime factorization (definitions are found in Vidyasagar (1985)), which is dual to representation of  $P$  used by Hansen (1989).

We assume that the plant  $P$  is stabilized by the controller  $C_{i-1}$ . Since  $C_{i-1}$  is known from the previous design step, it can be used to parameterize the set of all stabilized systems by their right coprime factorizations. — This result is dual to the parameterization of all stabilizing compensators (Vidyasagar, 1985). — One of these factorizations corresponds to the unknown plant  $P$ . Hence  $P$  can be written as

$$P = (N_a + D_c R)(D_a - N_c R)^{-1}, \quad (8)$$

where  $R$  is stable, the pairs  $(N_c, D_c)$ ,  $(N_a, D_a)$  are coprime factorizations satisfying  $C_{i-1} = N_c D_c^{-1}$  and  $P_a = N_a D_a^{-1}$ , and  $P_a$  is just an auxiliary model, that is stabilized by  $C_{i-1}$ . Next we define

$$N^a \doteq N_a + D_c R; \quad D^a \doteq D_a - N_c R, \quad (9)$$

so that  $N^a (D^a)^{-1}$  is a right coprime factorization of  $P$  by virtue of (8). With this representation of  $P$  we can obtain the following two results.

**Lemma 3.1** *Let the feedback system of Fig. 2 be stable and let controller  $C_{i-1}$  be known. Further let  $(N_a, D_a)$  be a right coprime factorization of an auxiliary model  $P_a$ , that is stabilized by  $C_{i-1}$ . Then the variable  $x$  of Fig. 2 can be reconstructed from  $u$  and  $y$  via*

$$x = (D_a + C_{i-1} N_a)^{-1} (u + C_{i-1} y). \quad (10)$$

**Proof:** From Fig. 2 we have  $y = N^a x$  and  $u = D^a x$ , and by straightforward calculation we obtain  $x = (D^a + C_{i-1} N^a)^{-1} (u + C_{i-1} y)$ . With the equality

$$D^a + C_{i-1} N^a = D_a + C_{i-1} N_a, \quad (11)$$

in which the right hand side follows from substituting (9) in the left hand side, we arrive at (10).  $\square$

**Theorem 3.2** *Let the assumptions of Lemma 3.1 hold. Then the frequency response of  $T(P, C_{i-1})$  can be estimated from  $u$  and  $y$ .*

**Proof:** With the use of  $P = N^a(D^a)^{-1}$  and (11) the transfer function  $T(P, C_{i-1})$  can be rewritten as

$$\begin{aligned} T(P, C_{i-1}) &= \begin{bmatrix} N^a(D^a)^{-1}[(D^a + C_{i-1}N^a)(D^a)^{-1}]^{-1} \\ [(D^a + C_{i-1}N^a)(D^a)^{-1}]^{-1} \end{bmatrix} [C_{i-1} \ I] \\ &= \begin{bmatrix} N^a \\ D^a \end{bmatrix} (D_a + C_{i-1}N_a)^{-1} [C_{i-1} \ I]. \end{aligned} \quad (12)$$

The terms  $(D_a + C_{i-1}N_a)$  and  $[C_{i-1} \ I]$  are known, and thus their frequency responses can be calculated. Further the frequency responses of  $N^a$  and  $D^a$  can be estimated from  $y = N^a x$  and  $u = D^a x$  with  $x$  reconstructed as in Lemma 3.1. Together these frequency responses make up an estimate of the frequency response of  $T(P, C_{i-1})$ .  $\square$

Lemma 3.1 and Theorem 3.2 do also hold in case the plant output  $y$  is contaminated by an unmeasurable noise (Schrama, 1991b). That is,  $x$  can still be reconstructed from  $u$  and  $y$ , and the identification of  $N^a$  and  $D^a$  from  $u, y$  and  $x$  turns out to be an open-loop identification problem.

With Theorem 3.2 we have access to the frequency response of  $T(P, C_{i-1})$  and thus  $\hat{P}_i$  can be identified from (7). This frequency-domain identification problem is not trivial, because  $\hat{P}$  appears in  $T(\hat{P}, C_{i-1})$  in a multiple and non-linear fashion. The optimization of (7) can be solved by estimating  $\hat{P}_i$  in terms of coprime factors (Schrama, 1992).

## 4 Example

The plant  $P$  under investigation is a real rational continuous-time system of order 9:  $P(s) = n(s)/d(s)$  with

$$\begin{aligned} n(s) &= 6.599 \cdot 10^{-5} s^9 - 2.552 \cdot 10^{-3} s^8 - 0.1264 s^7 \\ &\quad - 0.2836 s^6 - 4.195 s^5 + 6.983 s^4 - 13.74 s^3 \\ &\quad + 215.2 s^2 + 144.0 s + 1057 \\ d(s) &= s^9 + 2.401 s^8 + 32.68 s^7 + 54.78 s^6 + 347.2 s^5 \\ &\quad + 351.2 s^4 + 1256 s^3 + 488.8 s^2 + 635.3 s \\ &\quad + 105.9. \end{aligned}$$

The iterative scheme started from open-loop, i.e.  $C_0 = 0$ . The identified nominal models  $\hat{P}_i$  are of order 5, and the controllers  $C_i$  are of order 4. The design objective is to reduce the sensitivity at the lower frequencies. Pretending that the plant  $P$  is unknown, we cannot tell a priori what performance is attainable with a reduced-order controller.

The number of performed iteration steps is 19. The log-magnitude Bode diagrams of the nominal models  $\hat{P}_1, \hat{P}_{12}$  and  $\hat{P}_{19}$  have been drawn in Fig. 3

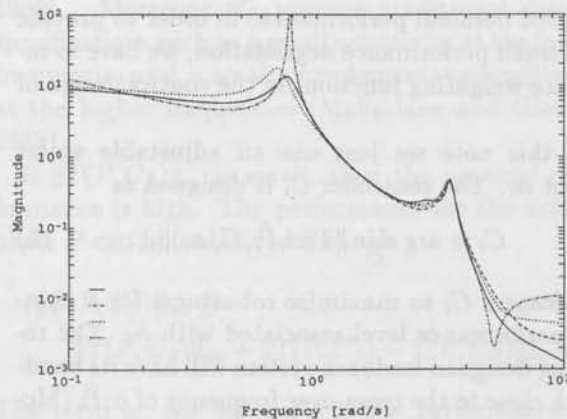


Fig. 3: Bode plots of  $P$  (—),  $\hat{P}_1$  (---),  $\hat{P}_{12}$  (····) and  $\hat{P}_{19}$  (-·-·).

together with that of the plant  $P$ . The curves corresponding to  $P$  and the open-loop nominal model  $\hat{P}_1$  are indiscernible at the frequencies where the magnitude of  $P$  is high. The other two nominal models show a good match only in the frequency range from 1 to 2 rad/s. Based on Fig. 2  $\hat{P}_{12}$  and  $\hat{P}_{19}$  should be marked as bad nominal models. Similar observations apply to the phase plots.

The scalar design weight  $\alpha_i$  has been increased during the iteration:  $\alpha_1 = 1$ ,  $\alpha_{12} = 5.4$  and  $\alpha_{19} = 9.2$ . For completeness we mention that the design from  $\hat{P}_1$  would have resulted in a destabilizing controller if  $\alpha_{19}$  had been used instead of  $\alpha_1$ .

The sensitivity  $(I + C_i P)^{-1}$  has been depicted in Fig. 4 for the controllers  $C_1, C_{12}$  and  $C_{19}$ . These

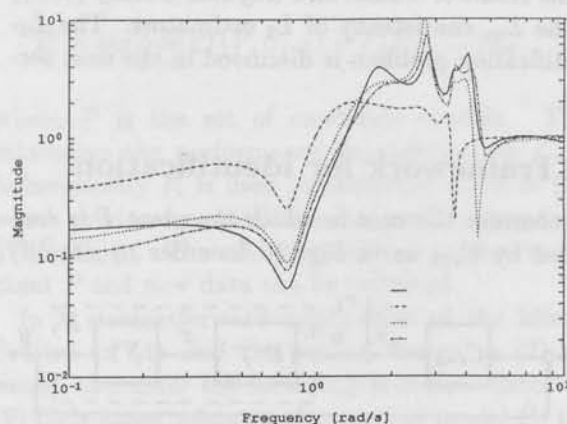


Fig. 4: Bode plots of the sensitivities  $(I + C_P P)^{-1}$  (—),  $(I + C_1 P)^{-1}$  (---),  $(I + C_{12} P)^{-1}$  (····) and  $(I + C_{19} P)^{-1}$  (-·-·).

curves show that a reduction of the sensitivity at lower frequencies has been realized at the expense

of some increase at higher frequencies. For comparison we have also designed controllers from the plant  $P$  itself. The controller  $C_P$ , which has order 4 also, has been designed with the scalar weight  $\alpha_{19}$ . The resulting sensitivity  $(I+C_P P)^{-1}$  shows a great resemblance to  $(I+C_{19} P)^{-1}$ . From this we conclude that the nominal model  $\hat{P}_{19}$  is very well-suited to high-performance control design in the sense, that the resulting model-based controller  $C_{19}$  is as good as the 'plant-based' controller  $C_P$ . Lastly we remark that  $\hat{P}_{19}$  exhibits the worst open-loop match, and at the same time it is the best nominal model for high-performance control design.

## 5 Concluding remarks

We observed that approximate identification and model-based control design have to be treated as a joint problem, if they are combined to achieve a high performance control system. Solving this joint problem with individual identification and control design methods requires an iterative approach.

The proposed iterative scheme is based on a robust control design method. Each identification step uses the previously designed controller to obtain new data from the plant. The associated identification problem has been solved by means of a coprime factorization of the unknown plant. An example has given evidence of the utility of the iterative scheme. It also illustrated the need of an iteration, since a good controller is required for the identification of an appropriate nominal model for high-performance control design. As an additional pay-off, the iteration reveals the performance, that is attainable for the unknown plant.

A drawback of our iteration is that the identification stage focusses on the 'old' compensator. In order to speed up the iteration the identification should anticipate the 'new' compensator. This is a topic for future investigations, together with the application of the same identification framework in case of time-domain data and other control design methods.

## Acknowledgement

The author wishes to thank Paul van den Hof and Okko Bosgra for their helpful discussions and suggestions.

## References

Anderson, B.D.O. and R.L. Kosut (1991). Adaptive robust control: on-line learning. in

*Proc. 30th IEEE Conf. Decision and Control*, Brighton, England.

Bitmead, R.R., M. Gevers and V. Wertz (1990). *Adaptive Optimal Control, The Thinking Man's GPC*. Prentice-Hall, Inc., Englewood Cliffs, NJ.

Bitmead, R.R. and Z. Zang (1991). An iterative identification and control strategy. in *Proc. European Control Conf.*, Grenoble, France, 1396-1400.

Bongers, P.M.M. and O.H. Bosgra (1990). Low order robust  $H_\infty$  controller synthesis. in *Proc. 29th IEEE Conf. Decision and Control*, Honolulu, HA, USA, 194-199.

Caines, P.E. and M. Baykal-Gürsoy (1989). On the  $L_2$  consistency of  $L_\infty$  estimators. *Syst. Control Lett.*, **12**, 71-76.

Goodwin, G.C. and B. Ninness (1991). Model error quantification for robust control based on quasi-Bayesian estimation in closed-loop. in *Proc. American Control Conf.*, Boston, MA, USA, 77-82.

Hakvoort, R.G. (1990). Optimal experiment design for prediction error identification in view of feedback design. *Selected Topics in Identification, Modelling and Control*, Delft University Press, **2**, 71-78.

Hansen, F.R. (1989). *A Fractional Representation Approach to Closed-Loop System Identification and Experiment Design*. Ph.D. Thesis, Stanford University, Stanford, CA, USA, march, 1989.

Helmicki, A.J., C.A. Jacobson and C.N. Nett (1991). Fundamentals of control-oriented system identification and their application for identification in  $H_\infty$ . in *Proc. American Control Conf.*, Boston, MA, USA, 89-99.

McFarlane, D. and K. Glover (1988). An  $H_\infty$  design procedure using robust stabilization of normalized coprime factors. in *Proc. 27th IEEE Conf. Decision and Control*, Austin, TX, USA, 1343-1348.

Rivera, D.E., J.F. Pollard and C.E. García (1990). Control-relevant parameter estimation via prediction-error methods: implications for digital PID and QDMC control. in *Annual AIChE Meeting*, Chicago, USA, paper 4a.

Schrama, R.J.P. (1991a). Control-oriented approximate closed-loop identification via fractional representations. in *Proc. American Control Conf.*, Boston, MA, USA, 719-720.

Schrama, R.J.P. (1991b). An open-loop solution to the approximate closed-loop identification problem. in *Preprints 9th IFAC/IFORS Symp. on Identification and System Parameter Estimation*, Budapest, Hungary, 1602-1607.



## An indirect method for transfer function estimation from closed loop data

Paul M.J. Van den Hof , Ruud J.P. Schrama

*Mechanical Engineering Systems and Control Group  
Delft University of Technology, Mekelweg 2, 2628 CD Delft, The Netherlands.*

**Abstract.** An indirect identification method is introduced that is able to consistently estimate the transfer function of a linear plant on the basis of data obtained from closed loop experiments, even in the situation that the model of the noise disturbance on the data is not accurate. Moreover the method allows approximate identification of the open loop plant with an explicit and tunable expression for the bias distribution of the resulting model.

**Keywords.** system identification, closed loop systems, identifiability.

### 1 Introduction

The problem of parametric identification of a linear system on the basis of data obtained from closed loop experiments, has obtained considerable attention in the literature. Several methods have been proposed and analysed, either in the framework of (least-squares) prediction error methods, see e.g. Söderström *et al.* (1976), Gustavsson *et al.* (1977), or in terms of instrumental variable methods, Söderström and Stoica (1981). In the prediction error context, well known approaches are the direct method, the indirect method and the joint input-output method. It has been established that - under weak conditions - the system's transfer function can be consistently identified, provided that the system is in the set of models that is considered. This rather restrictive condition refers to both the input-output transfer function of the system, as to the noise-shaping filter of the noise contribution on the data. For instrumental variable methods, similar results have been derived, restricting only the input-output transfer function of the system to be present in the model set.

In many practical situations, our primary interest is not the consistent identification of the system, but the gathering of a good approximation of its input-output transfer function. In this paper this

problem will be discussed for a closed loop system configuration, in which an external (sufficiently exciting) reference signal or setpoint signal is present and measurable. In the light of the remarks made above, we would like to come up with an identification method that is able to

- (i) consistently identify the i/o transfer function regardless of the fact whether the noise contribution on the data can be modelled exactly, and
- (ii) formulate an explicit expression for the asymptotic bias distribution of the identified model when the i/o transfer function of the system is not modelled exactly.

Note that property (i) alone can also be reached through instrumental variable methods, Söderström and Stoica (1981). A nonparametric solution to the problem, requiring knowledge of the controller, is discussed in Schrama (1991).

We will propose and analyse a two-stage identification method that reaches the two requirements mentioned above, while still being composed of - classical - prediction error methods. Knowledge of the controller will not be required. Firstly the sensitivity function of the closed loop system is identified through a high order linear model. This sensitivity

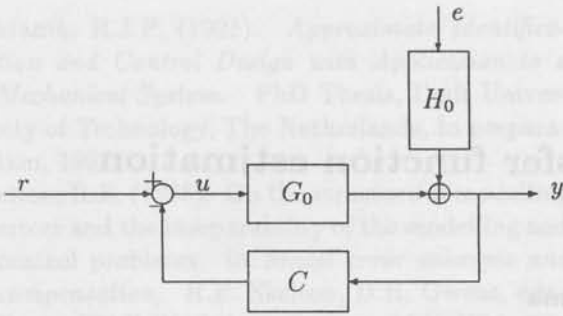


Fig. 1: The closed loop system configuration

function is used to simulate a noise free input signal for an open loop identification of the plant to be identified. Using output error methods, in accordance with Ljung (1987), an explicit approximation criterion can be formulated, characterizing the bias of identified models in the case of undermodelling.

## 2 Problem setting

We will consider a data generating system that is defined as:

$$S: \quad y(t) = G_0(q)u(t) + H_0(q)e(t) \quad (1)$$

with  $y(t)$  the output signal,  $u(t)$  the input signal, and  $e(t)$  a unit variance white noise signal.  $G_0(q)$  and  $H_0(q)$  are rational functions in  $q$ , the forward shift operator, with  $H_0(q)$  stable and stably invertible. The input signal is determined according to:

$$u(t) = r(t) - C(q)y(t) \quad (2)$$

with  $C$  a linear controller and  $r(t)$  a reference or setpoint signal. The closed loop system configuration that we consider is depicted in figure 1. The parametrized set of models, considered to model the system  $S$  is denoted by

$$\mathcal{M}: \quad y(t) = G(q, \theta)u(t) + H(q, \theta)e(t), \quad \theta \in \Theta \subset \mathbb{R}^d \quad (3)$$

with  $G(q, \theta)$  and  $H(q, \theta)$  proper rational transfer functions, depending on a real-valued parameter vector  $\theta$  that is lying in a set  $\Theta$  of admissible values, and  $\varepsilon$  the one step ahead prediction error, see Ljung (1987). The notation  $S \in \mathcal{M}$  is used to indicate that there exists a  $\theta_0 \in \Theta$  such that  $G(z, \theta_0) = G_0(z)$  and  $H(z, \theta_0) = H_0(z)$  for almost all  $z \in \mathbb{C}$ . The notation  $G_0 \in \mathcal{G}$  accordingly refers to the situation that only  $G(z, \theta_0) = G_0(z)$  for almost all  $z \in \mathbb{C}$ .

In the open loop case  $C(q) \equiv 0$ , it is well known, Ljung (1987), that when  $G_0 \in \mathcal{G}$ ,  $S \notin \mathcal{M}$ , it is

possible - under weak conditions - to consistently estimate  $G_0$  using prediction error methods, provided that  $G(q, \theta)$  and  $H(q, \theta)$  are independently parametrized within  $\mathcal{M}$ . To this end very often prediction error estimates are suggested with a fixed noise model:  $H(q, \theta) = L(q)$ , as e.g. the output error model structure, having  $L(q) = 1$ . In this situation the asymptotic parameter estimate is characterized by the explicit approximation criterion:  $\lim_{N \rightarrow \infty} \hat{\theta}_N =$

$$\arg \min_{\theta} \int_{-\pi}^{\pi} |G_0(e^{i\omega}) - G(e^{i\omega}, \theta)|^2 \frac{\Phi_u(\omega)}{|L(e^{i\omega})|^2} d\omega, \quad (4)$$

with probability 1, where  $\Phi_u(\omega)$  the spectral density of  $u$ .

In the closed loop situation, this consistency-property of  $G_0$  is lost, as well as the validity of the approximation criterion (4), due to the fact that the input signal  $u$  is not uncorrelated with the noise disturbance  $e$ . We will show that, by reorganizing the closed loop configuration (1), (2), we are able to create a situation where we can repeatedly apply the open loop results in order to reach our goals.

## 3 A two-stage identification strategy

Let us consider the sensitivity function of the closed loop system (1), (2),

$$T_0(q) = \frac{1}{1 + G_0(q)C(q)} \quad (5)$$

Using  $T_0$  we can rewrite equations (1), (2):

$$u(t) = T_0(q)r(t) - C(q)T_0(q)H_0(q)e(t) \quad (6)$$

$$y(t) = G_0(q)u(t) + H_0(q)e(t) \quad (7)$$

Since  $r$  and  $e$  are uncorrelated signals, and  $u$  and  $r$  are available from measurements, it follows from (6) that we can identify the sensitivity function  $T_0$  in an open loop way. Using the open loop results as mentioned in the previous section, we can even identify  $T_0(q)$  consistently, irrespective of the noise contribution  $C(q)T_0(q)H_0(q)e(t)$  in (6), using any model structure

$$u(t) = T(q, \beta)r(t) + R(q, \gamma)\varepsilon_u(t), \quad (8)$$

$\beta \in B \subset \mathbb{R}^{d_\beta}$ ;  $\gamma \in \Gamma \subset \mathbb{R}^{d_\gamma}$ , where  $\varepsilon_u(t)$  the one step ahead prediction error of  $u(t)$ , and  $T$  and  $R$  parametrized independently.

Consistency of  $T$  can of course only be reached

when  $T_0 \in \mathcal{T} := \{T(q, \beta) \mid \beta \in B\}$ . The estimate  $T(q, \hat{\beta}_N)$  of  $T_0(q)$  is determined according to a least squares criterion:

$$\hat{\beta}_N = \arg_{\beta} \min_{\beta, \gamma} \frac{1}{N} \sum_{t=1}^N \varepsilon_u(t)^2 \quad (9)$$

By again manipulating equations (6), (7), we can write:

$$u^r(t) := T_0(q)r(t) \quad (10)$$

$$y(t) = G_0(q)u^r(t) + T_0(q)H_0(q)e(t) \quad (11)$$

Since  $u^r$  and  $e$  are uncorrelated, it follows from (11) that when  $u^r$  would be available from measurements,  $G_0$  could be estimated in an open loop way, using the common open-loop techniques. In stead of knowing  $u^r$ , we have an estimate of this signal available through

$$\hat{u}_N^r(t) = T(q, \hat{\beta}_N)r(t) \quad (12)$$

Consider the model structure

$$y(t) = G(q, \theta)\hat{u}_N^r(t) + H(q, \eta)\varepsilon_y(t) \quad (13)$$

with  $G(q, \theta)$ ,  $H(q, \eta)$  parametrized independently,  $\theta \in \Theta \subset \mathbb{R}^{d_\theta}$ ,  $\eta \in \Omega \subset \mathbb{R}^{d_\eta}$ . It will be shown that the estimate  $G(q, \hat{\theta}_N)$  of  $G_0(q)$ , determined by

$$\hat{\theta}_N = \arg_{\theta} \min_{\theta, \eta} \frac{1}{N} \sum_{t=1}^N \varepsilon_y(t)^2 \quad (14)$$

under weak conditions converges to  $G_0(q)$  with probability 1. This result is formalized in the following theorem.

**Theorem 3.1** *Given the closed loop system determined by (1), (2), with  $T_0(q)$  asymptotically stable,  $e$  and  $r$  uncorrelated quasi-stationary signals, and  $r$  persistently exciting of sufficient order.*

*Consider the two-stage identification procedure presented in this section with model structures and identification criteria (8), (9) for step 1, and (13), (14) for step 2.*

*If  $T_0 \in \mathcal{T}$  and  $G_0 \in \mathcal{G}$  then, under weak conditions,  $G(q, \hat{\theta}_N) \rightarrow G_0(q)$  with probability 1 as  $N \rightarrow \infty$ .*

**Proof:** The identification procedure in the first step, determined by (8), (9), is known to yield a consistent estimate of the transfer function  $T_0$ , provided that  $r$  is persistently exciting of sufficient order. This implies that

$$T(q, \hat{\theta}_N) \rightarrow T_0(q) \text{ with probability 1, as } N \rightarrow \infty \quad (15)$$

For the second step (13), (14), we can write:

$$\hat{\theta}_N = \arg_{\theta} \min_{\theta, \eta} \frac{1}{N} \sum_{t=1}^N V_N(\theta, \eta, t)$$

with  $V_N(\theta, \eta, t) =$

$$= \{H(q, \eta)^{-1}[y(t) - G(q, \theta)T(q, \hat{\beta}_N)r(t)]\}^2 \quad (16)$$

$$= \{H(q, \eta)^{-1}[G_0(q)T_0(q) - G(q, \theta)T(q, \hat{\beta}_N)]r(t) + H(q, \eta)^{-1}[H_0(q) - 1 + T_0(q)]e(t)\}^2 \quad (17)$$

We know from Ljung (1987) that under weak conditions, for  $N \rightarrow \infty$ ,

$$\hat{\theta}_N \rightarrow \arg_{\theta} \min_{\theta, \eta} EV_N(\theta, \eta, t) \text{ with probability 1.}$$

Since  $T(q, \hat{\beta}_N) \rightarrow T_0(q)$  with probability 1 as  $N \rightarrow \infty$ , and  $r$  and  $e$  uncorrelated, it follows that  $\hat{\theta}_N \rightarrow$

$$\arg_{\theta} \min_{\theta, \eta} E\{\{H(q, \eta)^{-1}[G_0(q) - G(q, \theta)]T_0(q)r(t)\}^2 + \{H(q, \eta)^{-1}[H_0(q) - 1 + T_0(q)]e(t)\}^2\} \quad (18)$$

If  $r$  is persistently exciting of sufficient order,  $G_0 \in \mathcal{G}$ , and  $G$  and  $H$  parametrized independently, (18) implies that  $G(q, \hat{\theta}_N) \rightarrow G_0(q)$  with probability 1 as  $N \rightarrow \infty$ .  $\square$

In the case that we accept undermodelling in the second step of the procedure, ( $G_0 \notin \mathcal{G}$ ), the bias distribution of the asymptotic model can be characterized.

**Proposition 3.2** *Consider the situation of theorem 3.1.*

*If  $T_0 \in \mathcal{T}$ , and if in step 2 of the identification procedure, determined by (13), (14), a fixed noise model is used, i.e.  $H(q, \eta) = L(q)$ , then, under weak conditions,  $\hat{\theta}_N \rightarrow \theta^*$  with probability 1 as  $N \rightarrow \infty$ , with  $\theta^* =$*

$$\arg \min_{\theta} \int_{-\pi}^{\pi} |G_0(e^{i\omega}) - G(e^{i\omega}, \theta)|^2 \frac{|T_0(e^{i\omega})|^2 \Phi_r(\omega)}{|L(e^{i\omega})|^2} d\omega \quad (19)$$

**Proof:** The proposition follows from transforming equation (18) to the frequency domain, employing Parseval's relation.  $\square$

In this situation of approximate modelling of  $G_0$ , the asymptotic estimate can be characterized by the explicit approximation criterion (19). It is remarkable, and at the same time quite appealing, that in this closed loop situation, the approximation of  $G_0$

is obtained with an approximation criterion that has the sensitivity function  $T_0$  of the closed loop system as a weighting function in the frequency domain expression (19). An even more general result is formulated in the following proposition, dealing also with the situation  $T_0 \notin \mathcal{T}$ .

**Proposition 3.3** Consider the situation of theorem 3.1.

If both in step 1 and step 2 of the identification procedure fixed noise models are used, i.e.  $R(q, \gamma) = K(q)$  and  $H(q, \eta) = L(q)$ , then, under weak conditions,  $\hat{\theta}_N \rightarrow \theta^*$  with probability 1 as  $N \rightarrow \infty$ , with  $\theta^* = \arg \min_{\theta}$

$$\int_{-\pi}^{\pi} |G_0(e^{i\omega})T_0(e^{i\omega}) - G(e^{i\omega}, \theta)T(e^{i\omega}, \beta^*)|^2 \cdot \frac{\Phi_r(\omega)}{|L(e^{i\omega})|^2} d\omega \quad (20)$$

and

$$\beta^* = \arg \min_{\beta} \int_{-\pi}^{\pi} |T_0(e^{i\omega}) - T(e^{i\omega}, \beta)|^2 \frac{\Phi_r(\omega)}{|K(e^{i\omega})|^2} d\omega \quad (21)$$

**Proof:** The proof follows from similar reasoning as in the proof of theorem 3.1, and proposition 3.2, however now with the sensitivity function  $T_0$  substituted by its limiting estimate  $T(q, \beta^*)$ .  $\square$

Proposition 3.3 shows that even when in both steps of the procedure nonconsistent estimates are obtained, the bias distribution of  $G(q, \theta^*)$  is characterized by a frequency domain expression which is dependent on the identification result from the first step (cf. (21)).

**Remark 3.4** Note that in (20) the integrand expression can be rewritten, using the relation:

$$\begin{aligned} G_0(e^{i\omega})T_0(e^{i\omega}) - G(e^{i\omega}, \theta)T(e^{i\omega}, \beta^*) &= \\ &= [G_0(e^{i\omega}) - G(e^{i\omega}, \theta)]T_0(e^{i\omega}) + \\ &+ G(e^{i\omega}, \theta)[T_0(e^{i\omega}) - T(e^{i\omega}, \beta^*)] \quad (22) \end{aligned}$$

which shows how an error made in the first step affects the estimation of  $G_0$ . If  $T(q, \beta^*) = T_0(q)$  then (20) reduces to (19). If the error made in the first step is sufficiently small it will have a limited effect on the final estimate  $G(q, \theta^*)$ .

Note that the results presented in this section show that a consistent estimation of the sensitivity function  $T_0$  is not even necessary to get a good approximate identification of the transfer function  $G_0$ . Equations (20) and (22) suggest that as long as the error in the estimated sensitivity function is sufficiently small, the i-o transfer function can be identified accurately. In this respect one could also think of applying an FIR (finite impulse response) model structure (Ljung, 1987) in the first step, having a sufficient polynomial degree in order to describe the essential dynamics of the sensitivity function. This model structure will be applied in the simulation example described in the next section. As an alternative to the FIR structure, orthogonal functions other than the pulse functions, may be applied as a basis for modelling the sensitivity function in the first step of the procedure. This could substantially reduce the number of parameters to be estimated, see e.g. Heuberger (1990) and Wahlberg (1991). The fixed noise model  $L(q)$  can be used as a design variable in order to "shape" the bias distribution (20) to a desired form.

## 4 Simulation example

In order to illustrate the results presented in this paper, we consider a linear system operating in closed loop according to figure 1, with

$$G_0 = \frac{1}{1 - 1.6q^{-1} + 0.89q^{-2}} \quad (23)$$

$$C = q^{-1} - 0.8q^{-2} \quad (24)$$

$$H_0 = \frac{1 - 1.56q^{-1} + 1.045q^{-2} - 0.3338q^{-3}}{1 - 2.35q^{-1} + 2.09q^{-2} - 0.6675q^{-3}} \quad (25)$$

The noise signal  $e$  and the reference signal  $r$  are independent unit variance zero mean random signals. The controller is designed in such a way that the closed loop transfer function  $G_0T_0$  has a denominator polynomial  $z^2(z - 0.3)^2$ .

The two-step identification strategy is applied to a data set generated by this closed loop system, using data sequences of length  $N = 2048$ .

In the first step, the sensitivity function is estimated by applying an FIR output error model structure, estimating 15 Markov parameters:

$$T(q, \beta) = \sum_{k=0}^{14} \beta(k)q^{-k}; \quad R(q, \gamma) = 1 \quad (26)$$

Note that the real sensitivity function  $T_0$  is a rational transfer function of order 4. The magnitude

Bode plot of the estimated sensitivity function is depicted in figure 2, together with the exact one. The estimate  $T(q, \hat{\beta}_N)$  is used to reconstruct a noise free input signal  $\hat{u}_N^r$  according to (12). Figure 3 shows this reconstructed input signal, compared with the real input  $u(t)$  and the optimally reconstructed input signal  $u^r(t) = T_0(q)r(t)$ . Note that, despite of the severe noise contribution on the signal  $u$  caused by the feedback loop, the reconstruction of  $u^r$  by  $\hat{u}_N^r$  is extremely accurate. In the second step an output error model structure is applied such that  $G_0 \in \mathcal{G}$ , by taking

$$G(q, \theta) = \frac{b_0 + b_1q^{-1} + b_2q^{-2}}{1 + a_1q^{-1} + a_2q^{-2}} \quad \text{and} \quad H(q, \eta) = 1 \quad (27)$$

Figure 4 shows the result of estimating  $G_0$ . The magnitude Bode plot is compared with the second order model obtained from a direct (one-step) output error method, using only the measurements of  $u$  and  $y$ . The results clearly show the degraded performance of the direct identification strategy, while the indirect method gives accurate results. This is also clearly illustrated in the Nyquist plot of the same transfer functions, as depicted in figure 5.

## 5 Conclusions

An indirect method has been analysed for identification of transfer functions based on data obtained from closed loop experiments. It is assumed that a persistently exciting external reference signal is available. Using classical prediction error methods, the two-stage procedure has been shown to yield consistent estimates of the open loop plant, irrespective of the noise dynamics. Similar to the open loop case, an explicit and tunable frequency domain expression is given for the bias distribution of the asymptotic model.

## References

- Heuberger, P.S.C. (1990). Approximate system identification using system based orthonormal functions. *Proc. 29th IEEE Conf. Decision and Control*, Honolulu, HI, pp. 1086-1092.
- Söderström, T., L. Ljung and I. Gustavsson (1976). Identifiability conditions for linear multivariable systems operating under feedback. *IEEE Trans. Automat. Contr.*, AC-21, 837-840.
- Söderström, T., and P. Stoica (1981). Comparison of some instrumental variable methods - consistency and accuracy aspects. *Automatica*, 17, pp. 101-115.

- Gustavsson, I., L. Ljung and T. Söderström (1977). Identification of processes in closed loop - identifiability and accuracy aspects. *Automatica*, 13, 59-75.
- Ljung, L. (1987). *System Identification - Theory for the User*. Prentice-Hall, Englewood Cliffs NJ.
- Schrama, R. (1991). An open-loop solution to the approximate closed-loop identification problem. *Proc. 9th IFAC/IFORS Symposium Identification and System Param. Estim.*, July 8-12, 1991, Budapest, Hungary.
- Wahlberg, B. (1991). System identification using Laguerre models. *IEEE Trans. Automat. Contr.*, AC-36, pp. 551-562.

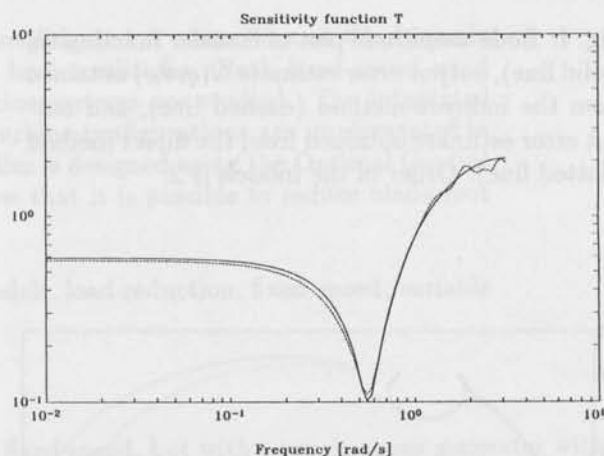


Fig. 2: Bode amplitude plot of exact sensitivity function  $T_0$  (solid line) and estimated sensitivity function  $T(q, \hat{\beta}_N)$  (dashed line).

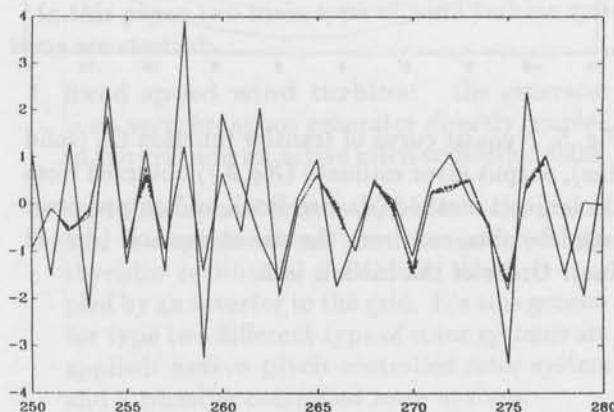


Fig. 3: Simulated input signal  $u$  (solid line), non-measurable input signal  $u^r$  caused by  $r$  (dashed line) and reconstructed input signal  $\hat{u}_N^r$  (dotted line)

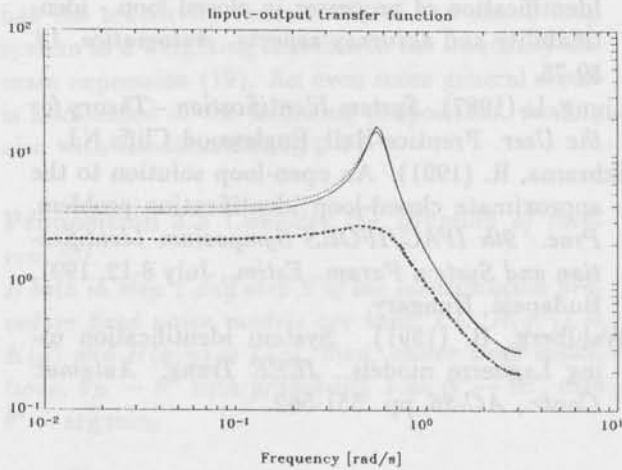


Fig. 4: Bode amplitude plot of transfer function  $G_0$  (solid line), output error estimate  $G(q, \hat{\theta}_N)$  obtained from the indirect method (dashed line), and output error estimate obtained from the direct method (dotted line). Order of the models is 2.

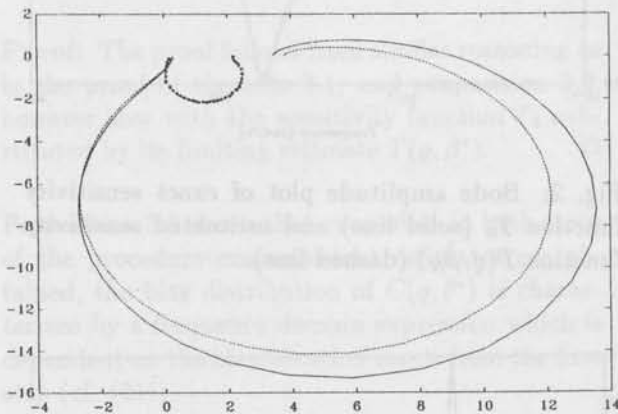


Fig. 5: Nyquist curve of transfer function  $G_0$  (solid line), output error estimate  $G(q, \hat{\theta}_N)$  obtained from the indirect method (dashed line), and output error estimate obtained from the direct method (dotted line). Order of the models is 2.

## Control of Wind Turbine Systems for Load Reduction † §

Peter M.M. Bongers <sup>‡</sup>, Theo van Holten <sup>‡</sup>, Sjoerd Dijkstra <sup>‡</sup>

<sup>‡</sup>*Mechanical Engineering Systems and Control Group  
Delft University of Technology, Mekelweg 2, 2628 CD Delft, The Netherlands,  
e-mail: bongers@tudw03.tudelft.nl*

<sup>‡</sup>*Stork Product Engineering, Postbus 379, 1000 AJ Amsterdam, The Netherlands*

**Abstract.** In this paper the implications are investigated of controllers on the dynamic loads occurring in the wind turbine under full load conditions. Both fixed speed wind turbine systems and variable speed wind turbine systems are studied. The integrated dynamic models describing the various wind turbine configurations are implemented in DUWECS. For each wind turbine the controller is designed using the Optimal Control design techniques. The simulations clearly show that it is possible to reduce blade root moments for a variable speed wind turbine.

**Keywords.** wind turbine control, dynamic models, load reduction, fixed speed, variable speed

### 1 Introduction

In general a controlled wind turbine is operating satisfactory if two objectives are met:

- a) the loads under operating conditions are minimal.
- b) the electrical energy production is optimal;
  - in partial load as much energy as possible
  - in full load a constant amount of energy

These objectives are conflicting, for example the loads are minimal if the wind turbine is not operating at all, hence a trade-off has to be made between the amount of acceptable dynamic loads and the desired energy production. Every designed controller, or even the absence of a controller, will imply a compromise between these objectives.

In what way an optimum can be achieved depends strongly on the applied type of wind turbine system. For example with a asynchronous generator in which case the turbine is operating at a

fixed speed, but with a synchronous generator with AC/DC/AC link speed variations are allowed.

For every wind turbine design the choice of a generator system (synchronous generator with AC/DC/AC link or asynchronous generator) and a rotor system (such as active pitch control, passive pitch control) are important decisions to make.

In this paper two main type of wind turbine systems are studied:

1. **fixed speed wind turbine:** the generator is an asynchronous generator directly coupled to the grid and an active pitch controlled rotor.
2. **variable speed wind turbine:** the generator is a synchronous generator coupled by a thyristor rectifier to a DC-link, which is coupled by an inverter to the grid. For this generator type two different type of rotor systems are applied: **active pitch** controlled rotor system and a **passive** controlled rotor system.

The fixed speed wind turbine is the cheapest configuration, the active pitch controlled variable speed wind turbine the most expensive configuration. The idea behind a passive pitch controlled wind turbine (van Holten (1988)) is the reduction of costs

<sup>†</sup>The original version of this paper was presented at the European Wind Energy Conference, October 14-18, 1991, Amsterdam, The Netherlands. Copyright of this paper remains with Elsevier Science Publishers

<sup>§</sup>This research was supported by the CEC under grant JOUR-0110

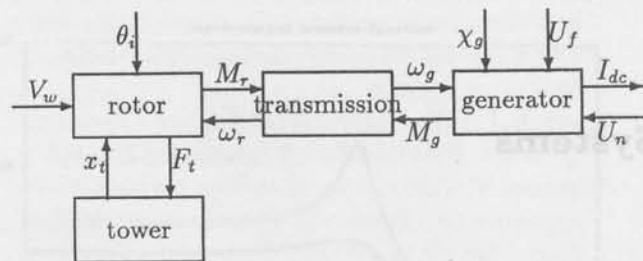


Fig. 1: schematic overview of a wind turbine

while retaining almost the same performance as an active pitch controlled turbine.

Section 2 discusses the integrated dynamic models of the wind turbine systems. These models are implemented in the DUWECS package (Bongers (1990)) which is used to obtain linear models and simulate the dynamic behaviour.

The control systems are designed using the Linear Quadratic Optimal Control Theory (Anderson and Moore (1989), Mäkilä and Toivonen (1987)). This implies that the controllers are designed on a linear state-space description of the non-linear wind turbine model. Because each wind turbine configuration has different control possibilities in Section 3 different control systems for each type of wind turbine system are designed.

In Section 4 the dynamic models of Section 2 controlled by the controllers of Section 3 are used in the DUWECS program to obtain dynamic responses of the different wind turbine configurations.

The conclusions of this paper are given in Section 5.

## 2 Wind turbine configurations

A variable speed wind turbine and a fixed speed wind turbine are studied in this paper. The fixed speed wind turbine has an asynchronous generator directly coupled to the public grid and allows an active pitch control. The variable speed turbine has a synchronous generator coupled with a direct current link to the public grid. Both wind turbine configurations fit into the integrated dynamic model description of flexible wind turbines (Bongers et. al. (1990)). Each wind turbine, schematically depicted in Fig. 1, can be seen as a set of interacting submodels. In the following a brief overview of the contents of the submodels is given. The variable speed wind turbine consists of the rotor: a two bladed rigid rotor with pitch, yaw and tilt freedom. The equations of motion are derived by using the method of Kane (Kane and Levinson (1985)). Each blade is divided into 10 sections with

section dependent 2D blade profile characteristics, corde, mass and twist. A simple model of dynamic inflow and wind shear is assumed. The dynamics of the blade pitch adjustment mechanism is described as a torsion mode with a pitch moment as input. The tower is described by the lowest bending mode. The transmission is described by the lowest torsion mode. The generator consists of a synchronous machine coupled by a thyristor rectifier to a DC-link (Hoeijmakers (1989)). This DC-link is coupled by an inverter to the public grid. The excitation voltage and the delay angle of the rectifier can be used for control purposes. Two type of pitch mechanisms are applied to the rotor system: When a **passive pitch mechanism** is used the pitch moment is generated by centrifugal forces and proportional to the rotor speed squared:  $M_{pitch} \propto \omega_r^2$ . Secondly when an **active pitch mechanism** is applied the pitch moment is generated via the controller.

The **fixed speed wind turbine** consists of the same rotor, transmission and tower as the variable speed wind turbine. Only the active pitch mechanism will be studied because the passive pitch mechanism responds to rotor speed variations which are minor for fixed speed wind turbines. The generator is an asynchronous generator (Schumacher (1985), Leonhard (1985)) coupled directly to the grid.

The mathematical models describing each of the wind turbines is implemented in DUWECS (Bongers (1990)).

## 3 Controller design

In this section the control design method will be discussed. The non-linear integrated dynamic model (Section 2) of each wind turbine can be written as:

$$\begin{aligned} \dot{x} &= \mathcal{F}(x, u, v, t) \\ y &= \mathcal{H}_y(x, u, v, t) \\ z &= \mathcal{H}_z(x, u, v, t) \end{aligned} \quad (1)$$

with  $\mathcal{F}, \mathcal{H}_y, \mathcal{H}_z$  non-linear functions,  $x$  state vector and  $v$  the wind speed. In (1)  $y$  are the measurable outputs such as produced energy  $I_g$  and rotor shaft angular velocity  $\omega_r$ . The controllable inputs  $u$  are: blade pitch angle  $\theta$ , excitation voltage  $u_F$  and delay angle of the rectifier  $\chi_g$ . In full load the excitation voltage is superfluous. The observed signals  $z$ : lead-lag blade root moment  $M_l$ , flap moment  $M_f$  and rotor shaft torque  $M_{shaft}$  are measured to judge the effectiveness of the controllers but not used for control purposes.

Each wind turbine configuration has its own set of input and output variables:

In this paper we will use a linear quadratic control design method, therefore the non-linear

| wind turbine   | inputs   | outputs   |
|----------------|--|---|
| fixed speed    | $\theta$   | $I_g$   |
| passive pitch  | $\chi_g$   | $\begin{pmatrix} I_g \\ \omega_r \end{pmatrix}$ |
| variable speed | $\begin{pmatrix} \theta \\ \chi_g \end{pmatrix}$ | $\begin{pmatrix} I_g \\ \omega_r \end{pmatrix}$ |

Table 1: input/output signals for different wind turbines

model (1) is linearized in an operating condition  $w$ , with  $w$  representing the steady-state condition ( $\mathcal{F}(x, u, v, t) = 0$ ) of (1):

$$\begin{aligned} \delta \dot{x} &= A_1 \delta x + B_1 \delta u + G_1 \delta v \\ \delta y &= C_1 \delta x \\ \delta z &= H_1 \delta x \end{aligned} \quad (2)$$

with  $A = \frac{\partial \mathcal{F}}{\partial x} \Big|_w$  etc. Because all modern controllers are implemented in digital hardware (for reasons of flexibility and allowing more complex controllers) the continuous equations (2) are discretized:

$$\begin{aligned} x_{k+1} &= A x_k + B u_k + G v_k \\ y_k &= C x_k \\ z_k &= H x_k \end{aligned} \quad (3)$$

In the linear system description the periodic information about the wind shear, tower shadow, gravity is lost therefore these effects are assumed in the wind signal  $v_k$ :

$$\begin{aligned} x_{k+1}^w &= A_w x_k^w + B_w e_k \\ v_k &= C_w x_k^w \end{aligned} \quad (4)$$

with  $e_k$  white noise. The controller can also be written in state-space form:

$$\begin{aligned} c_{k+1} &= A_c c_k + B_c y_k \\ u_k &= C_c c_k + D_c y_k \end{aligned} \quad (5)$$

The state-space descriptions of wind turbine (3), wind velocity (4) and controller (5) can be written in one state-space form:

$$\begin{aligned} x_{k+1}^e &= A^e x_k^e + B^e u_k + G^e e_k \\ y_k^e &= C^e x_k^e \\ z_k^e &= H^e x_k^e \end{aligned} \quad (6)$$

The LQ control design method (Kwakernaak and Sivan (1972)), Anderson and Moore (1989)) aims at minimizing:

$$J = \sum_{k=0}^{\infty} \{x_k^{eT} Q x_k^e + u_k^T R u_k\} \quad (7)$$

This means that the elements of the matrices ( $A_c, B_c, C_c, D_c$ ) are chosen such that (7) is minimal. The influence of the wind velocity can be written as an initial condition:  $x_0^e x_0^{eT} = G^e G^{eT}$ , the objective of minimizing the mechanical loads as  $Q = H^{eT} H^e$ , the magnitude of the allowable input signals can be chosen by  $R$ .

The mathematical restrictions on (4), (3), (6),(7) such that a stabilizing controller in the form of (5) exists is given in (Anderson and Moore (1989), Davison and Copeland (1985), Davison (1976), Mäkilä and toivonen (1987)).

The fixed speed wind turbine allows only single input single output (SISO) control (see Table 1) a second order controller is designed, which can be seen as a sophisticated tuned PID controller.

The passive pitch controlled variable speed wind turbine allows multi input single output (MISO) control. The controller can be seen as a more sophisticated tuned PID controller.

Most existing wind turbines are controlled by PID controllers, usually a retuning of these controllers will lead to the "so called" sophisticated PID controllers described here.

The active pitch controlled variable speed wind turbine allows multi input multi output (MIMO) controllers. Using a MIMO controller the interaction between blade pitch control and generator control can be exploited to obtain a better performance.

For computational convenience the order of the MIMO controller equals the order of the wind turbine model, which implies that there exists an explicit solution to (7): the LQG controller. The order of the SISO controllers are restricted, which implies that the solution to (7) has to be found iteratively. Both controller design algorithms are implemented at the Delft University of Technology using MATLAB.

## 4 Simulations

In this section we will show simulation results for five wind turbine configurations:

- 1) uncontrolled variable speed wind turbine
- 2) passive pitch controlled variable speed wind turbine and a controlled generator
- 3) LQG controlled variable speed wind turbine
- 4) uncontrolled fixed speed wind turbine
- 5) pitch controlled fixed speed wind turbine

The simulations are performed using DUWECS (Bongers (1990)), we have assumed an averaged wind speed at hub height according to Fig. 2. The rotor blades also experience a wind shear of + 7% of the wind speed at hub height at the highest point and -10% at the lowest point.

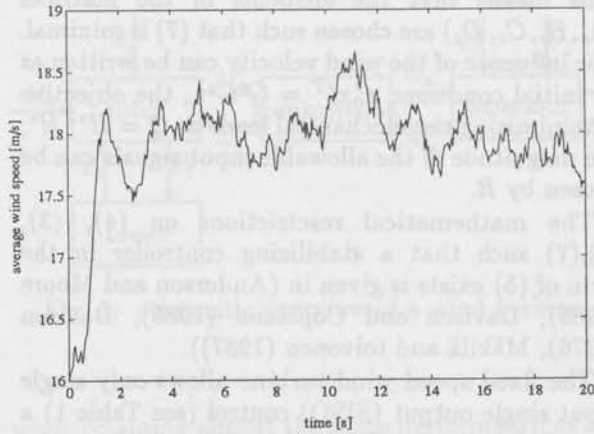


Fig. 2: wind speed at rotor shaft height

The time history of the produced electrical power is given in Fig. 3. It can be seen in Fig. 3 that the

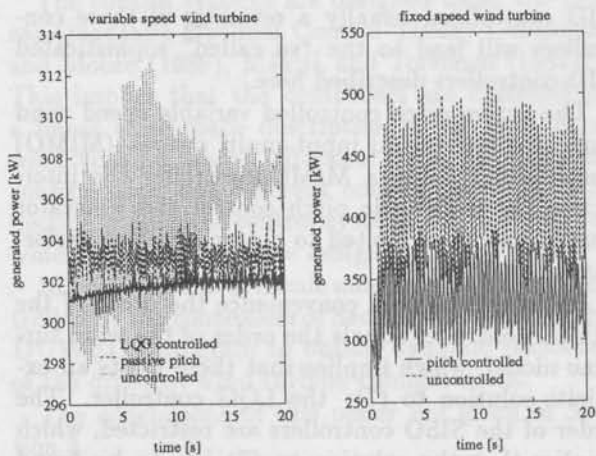


Fig. 3: produced electrical power

generated power can be kept almost constant for the variable speed wind turbine. For the fixed speed wind turbine it is possible to reduce the power variations by almost 70%.

The rotor shaft torque (Fig. 4) can be reduced significantly for both type of wind turbines compared to the uncontrolled turbine. The LQG controlled variable speed wind turbine shows the least torque variations. Although the torque variations of the fixed speed wind turbine are reduced significantly they are larger than the variable speed wind turbine.

Based on the simulated time histories the spectra of these signals are calculated. By applying a fast Fourier transformation on the finite data damping will be introduced in the spectra of the signals. In Fig. 5 the spectrum of the rotor shaft torque is given. The frequency response of the rotor shaft

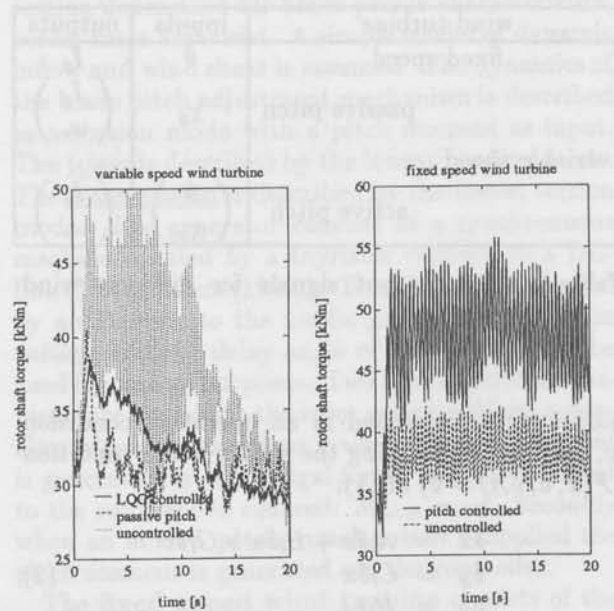


Fig. 4: rotor shaft torque

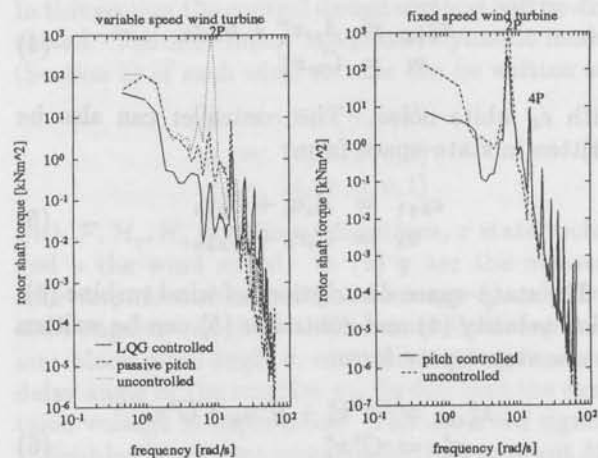


Fig. 5: rotor shaft torque

torque is given in Fig. 4. For the variable speed wind turbine the LQG controller suppresses almost all of the 2P and 4P oscillations<sup>1</sup>. For the fixed wind turbine however it appears that the 2P oscillation has been reduced significantly but an oscillation of approximately 4P has occurred.

In Fig. 6 the blade root bending moment in flap direction is given. It can be seen in Fig. 6 that

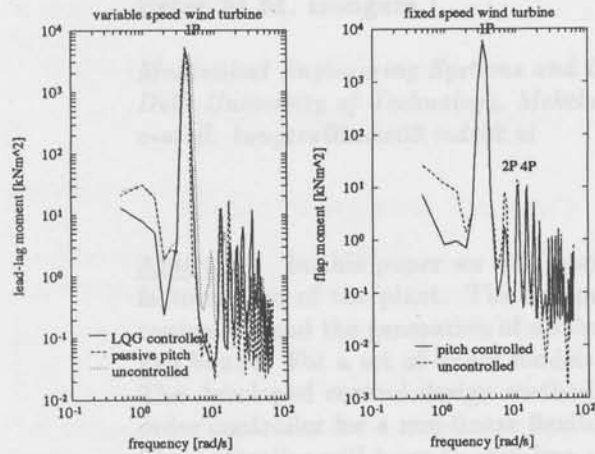


Fig. 6: blade root flap moment

the 1P oscillation of the blade root flap moment remains unchanged under the application of a controller. Note that this frequency is shifted for the uncontrolled variable speed wind turbine because of the large increase of rotor speed. The LQG controller reduces the remaining part of the spectrum more than the passive pitch controlled wind turbine. The controlled fixed speed wind turbine has lower loads than the uncontrolled wind turbine except at 4P where the loads are significantly higher.

## 5 Conclusions

Although the simulation results of the previous section are obtained with specific wind turbine configurations (rated power, rotor diameter, wind shear, etc.) the conclusions can be extended to the more general difference between fixed speed wind turbines and variable speed wind turbines, individual control (like passive pitch) or multivariable control (like LQG).

Using a fixed speed wind turbine it is possible to reduce the variations in produced power and rotor shaft loads. It is not possible to give statements about the reduction of blade loads yet because the link between a spectrum and the load sequence is not transparent.

<sup>1</sup>An oscillation at 2P means an oscillation with a frequency of two times the rotor speed. For example an unbalance in a two-bladed rotor causes a 2P excitation on the rotor shaft.

Using a more expensive variable speed wind turbine it is possible to keep the produced electrical energy constant and simultaneously reduce the mechanical loads.

The multivariable controller gives a better performance than two individual controllers (passive pitch control and generator control).

## References

- Anderson B.D.O., J.B. Moore (1989). *Optimal control, linear quadratic methods*. Prentice-Hall, Inc. Englewood Cliffs, N.J., USA, .
- Bongers P.M.M. (1990). *DUWECS Reference Guide, Delft University Wind Energy Conversion Simulation Program*. Delft University of Technology, The Netherlands, .
- Bongers P.M.M., W.A.A.M. Bierbooms, Sj. Dijkstra, Th. van Holten (1990). *An Integrated Dynamic Model of a Flexible Wind Turbine*. Delft University of Technology, The Netherlands, .
- Davison E.J. (1976). The robust control of a servo mechanism problem for linear time-invariant multivariable systems. *IEEE Trans. Automat. Contr.*, **AC-21**,25-34.
- Davison E.J., B.R. Copeland (1985). Gain margin and time lag tolerance constraints applied to the stabilization problem and robust servomechanism problem. *IEEE Trans. Automat. Contr.*, **AC-30**,229-239.
- Hoeijmakers M.J. (1989). *A possibility to incorporate saturation in the simple global model of a synchronous machine with rectifier*. Eindhoven university of Technology, The Netherlands, .
- Holten Th. van (1988). Voortgangsrapport van het FLEXHAT onderzoek (in Dutch). in *Proc. Nederlandse Wind Energie Conferentie 1988, Noordwijkerhout*, 370-375.
- Kane T.R., D.A. Levinson (1985). *Dynamics, theory and applications*. McGraw-Hill series in mechanical engineering, .
- Kwakernaak H., R. Sivan (1972). *Linear Optimal Control Systems*. Wiley Interscience, New York, USA, .
- Leonhard W. (1985). *Control of Electrical Drives*. Springer Verlag, Berlin, Germany, .
- Makila P.M., H.T. Toivonen (1987). Computational methods for parametric LQ problems - A survey. *IEEE Trans. Automat. Contr.*, **AC-32**,658-671.
- Matlab (1989). *Matlab User's guide*. The Mathworks Inc., South Natick, MA, USA, .
- Schumacher W. , *Mikrorechner geregelter asynchron-stellantrieb*. PhD Thesis, Technische Universität Carolo-Wilhelmina, Braunschweig, 1985.



## Robust control using coprime factorizations, application to a flexible wind turbine

Peter M.M. Bongers<sup>†</sup>

*Mechanical Engineering Systems and Control Group  
Delft University of Technology, Mekelweg 2, 2628 CD Delft, The Netherlands.  
e-mail: bongers@tudw03.tudelft.nl*

**Abstract.** In this paper we will propose a control design method based on a coprime factorization of the plant. The design method includes the synthesis of low order  $H_\infty$  controllers and the generation of a robustness margin which is less conservative than the gap bound. For a set of linear models the choice of a nominal model will be discussed. The developed control design method will then be used to design a robust linear low order controller for a non-linear flexible wind turbine model under full load conditions. The controller will have to stabilize a set of linear models representing the non-linear wind turbine under various operating conditions. It will be shown that using the new robustness test this controller stabilizes the whole set with the desired performance.

**Keywords.** low order  $H_\infty$  controllers, coprime factorizations, robustness margins, flexible wind turbines

### 1 Introduction

To increase the operational life and energy output of a wind turbine without raising the construction costs flexible wind turbines can be realized with soft characteristics in all subsystems in order to reduce the internal stresses, and essentially allowing the application of lighter and less costly components (Bongers et. al. (1990)). The efficiency of wind energy conversion into electrical energy is of importance in partial load, where the maximal amount of the available wind energy has to be converted. This has to be achieved without an excess of mechanical loads, to maintain a reasonable operational life of the wind turbine. The application of a variable speed generator (like a synchronous generator with DC-link) enables a high efficiency energy conversion. In full load however the rated amount energy production must be maintained at minimal fatigue loads occurring in the wind turbine. By variable speed wind turbines variations of

wind speed can partially be buffered variations in rotor speed. The design of well controlled flexible wind turbines seems to be attractive for commercial applications.

After the Preliminaries in Section 2 the controller design method is presented in Section 3. First in Section 3 stability of the feedback configuration stated in terms of coprime factorizations of the plant and controller. Using this stability expression a robustness margin is derived which is less conservative than the gap-metric robustness bound (Bongers (1991)). The gap-metric expression for robust stability clearly shows the necessity of good choice of a nominal model. Based on such a nominal model and the coprime controller design by McFarlane and Glover (1989) an extension to low order controller synthesis will be made according to (Bongers and Bosgra (1990)).

The actual control in Section 4 design is done along the following lines. A non-linear model is used to describe a flexible wind turbine over a range of operating conditions. The non-linear model will be approximated by a set of linear models. The

<sup>†</sup>This research was supported by the CEC under grant JOUR-0110

deviation of each model in the model set from the nominal model is represented by coprime factor perturbations. The nominal model will be chosen such that the coprime factor perturbations used to describe the set are minimal. Hence the model set will be characterized by the nominal model and a gap distance to the boundary of the set. In order to determine the nominal model and the gap distance we have chosen a desired performance of the closed loop. Given the nominal model and the desired performance a low order controller will be calculated. It will be shown that this controller will stabilize all models in the model set with the desired performance.

## 2 Preliminaries

In this paper we adopt the ring theoretic setting of (Desoer et. al. (1980), Vidyasagar et. al. (1982)) to study stable multivariable linear systems by considering them as transfer function matrices having all entries belonging to a ring  $\mathcal{H}$ . For the application of state-space algorithms we will identify the ring  $\mathcal{H}$  with  $\text{IRH}_\infty$ , the space of stable real rational finite dimensional linear time-invariant continuous-time systems. We consider the class of stable/unstable multivariable systems as transfer function matrices whose entries are elements of the quotient field  $\mathcal{F}$  of  $\mathcal{H}$  ( $\mathcal{F} := \{a/b \mid a \in \mathcal{H}, b \in \mathcal{H} \setminus \{0\}\}$ ). The set of multiplicative units of  $\mathcal{H}$  is defined as:  $\mathcal{J} := \{h \in \mathcal{H} \mid h^{-1} \in \mathcal{H}\}$ . In the sequel systems  $P \in \mathcal{F}^{p \times m}$  are denoted as  $P \in \mathcal{F}$ , a system with McMillan degree  $n$  as  $P \in \mathcal{F}_n$ . A system  $P \in \mathcal{F}$  can be written as  $P = P_1 + P_2$  with  $P_1 \in \mathcal{H}$ ,  $P_2 \in \mathcal{H}^\perp$ ,  $P_1$  can be denoted as  $[P]_{\mathcal{H}}$ .

**Proposition 2.1** Let  $P \in \mathcal{H}$ . The Hankel singular values of  $P$  are:

$$\sigma_i^H\{P\} = \lambda_i(W_c W_o)^{\frac{1}{2}} = \sigma_i$$

where  $W_c, W_o$  are the symmetric positive definite solutions to the controllable and observable gram-mians of  $P$ . The Hankel norm of  $P$  is defined as  $\|P\|_H = \sigma_1^H$ .

If  $P \in \mathcal{F}$  then the Hankel singular values of  $P$  are the Hankel singular values of the proper stable part of  $P$  i.e.  $[P]_{\mathcal{H}}$ .

The  $H_\infty$ -norm of  $P$  is defined as  $\|P\|_\infty = \sup_\omega \max \sigma_i[P(j\omega)]$ , with  $P \in \mathcal{H}$ .

### Factorizations

**Definition 2.2** (Vidyasagar et. al. (1982))

A system  $P \in \mathcal{F}$  has a right (left) fractional representation if there exist  $N, M(\tilde{N}, \tilde{M}) \in \mathcal{H}$  such that  $P = NM^{-1} (= \tilde{M}^{-1}\tilde{N})$ .

The pair  $M, N(\tilde{M}, \tilde{N})$  is right (left) coprime fractional representation (rcf or lcf) if it is a right (left) fractional representation and there exists  $U, V(\tilde{U}, \tilde{V}) \in \mathcal{H}$  such that:  $UN + VM = I$  ( $\tilde{N}\tilde{U} + \tilde{M}\tilde{V} = I$ ).

The pair  $M, N(\tilde{M}, \tilde{N})$  is called normalized right (left) coprime fractional representation (nr cf or nlcf) if it is a coprime fractional representation and:  $M^*M + N^*N = I$  ( $\tilde{M}\tilde{M}^* + \tilde{N}\tilde{N}^* = I$ ) with  $M^* = M^T(-s)$ .

According to Meyer (1988) the graph Hankel singular values  $\sigma_i^G(P)$  are defined as  $\sigma_i^H\left(\begin{matrix} M \\ N \end{matrix}\right)$

## 3 Control Design Method

In this section we will outline a low order robust controller design method based on a coprime factor plant description.

### Closed loop stability

The feedback configuration under consideration is given in Fig. 1 with the plant  $P$  and the controller  $C$ . The closed loop transfer function  $T(P, C)$  map-

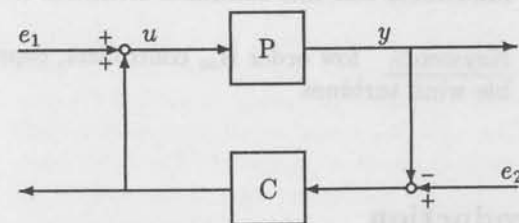


Fig. 1: Feedback configuration

ping the inputs  $(e_1, e_2)$  onto the outputs  $(u, y)$  is:

$$T(P, C) = \begin{bmatrix} I \\ P \end{bmatrix} (I + CP)^{-1} \begin{bmatrix} I & C \end{bmatrix} \quad (1)$$

with the restriction on  $C$  that  $\det(I + CP) \neq 0$ . The feedback configuration of Fig. 1 is called internally stable if and only if the four transfer functions in (1) are stable. Note that stability of three transfer functions in (1) does not imply stability of the fourth transfer function (Desoer and Chan (1975)). If  $T(P, C) \in \mathcal{H}$  we say that  $C$  stabilizes  $P$ . The stability of  $T(P, C)$  can be checked by inspecting each of the four transfer functions. However as stated in Theorem 3.1 it is possible to check the stability of  $T(P, C)$  by inspecting just one transfer function.

**Theorem 3.1** Let  $P \in \mathcal{F}$  have a rcf  $(N, M)$  and let  $C \in \mathcal{F}$  have a rcf  $(X, Y)$  and a lcf  $(\tilde{Y}, \tilde{X})$ , then the following statements are equivalent:

(a)  $C$  stabilizes  $P$

$$(b) \begin{bmatrix} M & -Y \\ N & X \end{bmatrix} \in \mathcal{J}$$

$$(c) (\tilde{X}M + \tilde{Y}N) \in \mathcal{J}$$

**Proof:** (a)  $\Leftrightarrow$  (b) is proved by in (Vidyasagar and Kimura (1986))

(a)  $\Leftrightarrow$  (c)

$$T(P, C) = \begin{bmatrix} I \\ P \end{bmatrix} (I + CP)^{-1} [I \ C]$$

can be written as:

$$T(P, C) = \begin{bmatrix} M \\ N \end{bmatrix} (\tilde{X}M + \tilde{Y}N)^{-1} [\tilde{X} \ \tilde{Y}]$$

Hence  $T(P, C) \in \mathcal{H}$  iff  $(\tilde{X}M + \tilde{Y}N) \in \mathcal{J}$ , since  $\begin{bmatrix} M \\ N \end{bmatrix}, [\tilde{X} \ \tilde{Y}]$  are coprime by definition.  $\square$

### Robustness

For robust control the controller  $C$  must not only stabilize  $P$  with a given performance but also stabilize plants  $P_\Delta$  in the neighbourhood of  $P$ . A bounded set of  $P_\Delta$  such that all plants in that set are stabilized is given in the following theorem.

**Theorem 3.2** Let the controller  $C \in \mathcal{F}$  internally stabilizing  $P$  be given as  $C = \tilde{X}_n^{-1}\tilde{Y}_n$  with  $(\tilde{Y}_n, \tilde{X}_n)$  nlc and let  $P \in \mathcal{F}$  be given as  $P = N_n M_n^{-1}$  with  $(N_n, M_n)$  a nrcf of  $P$ . Define:

$$\Lambda = [\tilde{X}_n \ \tilde{Y}_n] \begin{bmatrix} M_n \\ N_n \end{bmatrix}$$

and let a specific rcf of  $P$  be given by:  $\begin{bmatrix} M \\ N \end{bmatrix} =$

$$\begin{bmatrix} M_n \\ N_n \end{bmatrix} \Lambda^{-1}$$
 let another plant  $P_\Delta \in \mathcal{F}$  be given as:

$$P_\Delta = (N_\Delta Q)(M_\Delta Q)^{-1} = (N - \Delta N)(M - \Delta M)^{-1}$$

with  $Q \in \mathcal{H}$ . Define the set  $\mathcal{S}_b$  by:

$$\mathcal{S}_b = \{P_\Delta | T(P, C) \in \mathcal{H} \text{ and } \left\| \begin{bmatrix} \Delta M \\ \Delta N \end{bmatrix} \right\|_\infty < 1\}$$

Then the set  $\mathcal{S}_b$  is robustly stabilized by  $C$ .

**Proof:** The stability condition for the perturbed closed loop can be written as:

$$[\tilde{X}_n \ \tilde{Y}_n] \begin{bmatrix} M_\Delta Q \\ N_\Delta Q \end{bmatrix} \in \mathcal{J}$$

Using the factorization  $(N - \Delta N, M - \Delta M)$  for  $P_\Delta$  and the fact that  $[\tilde{X}_n \ \tilde{Y}_n] \begin{bmatrix} M \\ N \end{bmatrix} = I$ . the stability condition can be rewritten as:

$$(I - [\tilde{X}_n \ \tilde{Y}_n] \begin{bmatrix} \Delta M \\ \Delta N \end{bmatrix}) \in \mathcal{J}$$

Applying the small gain theorem we have a sufficient condition for stability:

$$\| [\tilde{X}_n \ \tilde{Y}_n] \|_\infty \left\| \begin{bmatrix} \Delta M \\ \Delta N \end{bmatrix} \right\|_\infty < 1$$

Using the fact that  $\| [\tilde{X}_n \ \tilde{Y}_n] \|_\infty = 1$  by definition of normalized left coprimeness, the theorem is proved.  $\square$

**Remark 3.3** The fact that  $[\tilde{X}_n \ \tilde{Y}_n]$  is co-inner implies that the maximum singular value is constant over all frequencies. Thus taking the infinity norm does not introduce conservativeness.

Using the factorizations of Theorem 3.2 the perturbations on the coprime factors of the nominal plant are written as:

$$\begin{bmatrix} \Delta M \\ \Delta N \end{bmatrix} = \begin{bmatrix} M_n \\ N_n \end{bmatrix} \Lambda^{-1} - \begin{bmatrix} M_\Delta \\ N_\Delta \end{bmatrix} Q$$

Now the freedom  $Q$  can be used to determine the smallest upper bound on all allowable perturbations:

$$\left\| \begin{bmatrix} \Delta M \\ \Delta N \end{bmatrix} \right\|_\infty = \inf_{Q \in \mathcal{H}} \left\| \begin{bmatrix} M \\ N \end{bmatrix} \Lambda^{-1} - \begin{bmatrix} M_\Delta \\ N_\Delta \end{bmatrix} Q \right\|_\infty \quad (2)$$

The class  $\mathcal{S}_b$  of plants  $P_\Delta$  stabilized by  $C$  can be rewritten as:

$$\mathcal{S}_b = \{P_\Delta | T(P, C) \in \mathcal{H} \text{ and } \inf_{Q \in \mathcal{H}} \left\| \left( \begin{bmatrix} M_n \\ N_n \end{bmatrix} - \begin{bmatrix} M_\Delta \\ N_\Delta \end{bmatrix} \tilde{Q} \right) \Lambda^{-1} \right\|_\infty < 1\} \quad (3)$$

### Lemma 3.4 (Bongers and Bosgra (1990))

Under the same assumptions of Theorem 3.2 the class  $\mathcal{S}_g$  of all plants  $P_\Delta$  robustly stabilized by  $C$  in the gap-metric can be written as:

$$\mathcal{S}_g = \{P_\Delta | T(P, C) \in \mathcal{H} \text{ and } \inf_{Q \in \mathcal{H}} \left\| \begin{bmatrix} M_n \\ N_n \end{bmatrix} - \begin{bmatrix} M_\Delta \\ N_\Delta \end{bmatrix} Q \right\|_\infty \|T(P, C)\|_\infty < 1\}$$

Because the difference between the gap-bound Lemma 3.4 and the new robustness margin (3) is the factor  $\Lambda$  this margin will be called the  $\Lambda$ -gap.

**Theorem 3.5** The class  $S_b$  is larger or equal to the class  $S_g$

**Proof:** The sufficient condition for stability Theorem 3.2 is:

$$\inf_{\tilde{Q} \in \mathcal{H}} \left\| \left( \begin{bmatrix} M_n \\ N_n \end{bmatrix} - \begin{bmatrix} M_\Delta \\ N_\Delta \end{bmatrix} \tilde{Q} \right) \Lambda^{-1} \right\|_\infty < 1$$

For a specific choice of  $\tilde{Q}_{opt}$  the minimum value of

$$\inf_{\tilde{Q} \in \mathcal{H}} \left\| \begin{bmatrix} M_n \\ N_n \end{bmatrix} - \begin{bmatrix} M_\Delta \\ N_\Delta \end{bmatrix} \tilde{Q} \right\|_\infty$$

is achieved. If we plug in this  $\tilde{Q}_{opt}$  and use the multiplicative properties of the infinity norm a sufficient condition is:

$$\left\| \left( \begin{bmatrix} M_n \\ N_n \end{bmatrix} - \begin{bmatrix} M_\Delta \\ N_\Delta \end{bmatrix} \tilde{Q}_{opt} \right) \right\|_\infty \|\Lambda^{-1}\|_\infty < 1$$

Using the fact that  $\|T(P, C)\|_\infty = \|\Lambda^{-1}\|_\infty$  and  $\|\Lambda^{-1}\|_\infty \geq 1$  this theorem is proved.  $\square$

**Corollary 3.6** The class  $S_b$  equals  $S_g$  if  $\Lambda$  is an  $\alpha I$  matrix, with  $\alpha$  a real number. It can be shown that a specific controller will lead to  $\Lambda = \alpha I$  (Bongers (1992)).

Suppose the real system, for example with some uncertain parameters or uncertain operating condition, can be represented by a set of linear models  $P_i$ . Let a nrcf of  $P_i$  be given by  $(M_n^i, N_n^i)$  and let us chose a nominal model:  $P_o$ . Then according to Lemma 3.4 the nominal plant  $P_o$  determines both the size of the allowable perturbations by  $\|T(P_o, C)\|_\infty$  and the size of the largest perturbation:

$$\max_i \left\{ \inf_{Q_i \in \mathcal{H}} \left\| \begin{bmatrix} M_n^o \\ N_n^o \end{bmatrix} - \begin{bmatrix} M_n^i \\ N_n^i \end{bmatrix} Q_i \right\|_\infty \right\}$$

It is therefore obvious that the choice of a nominal model is important in the controller design, and it is not an trivial choice.

For a given set of models a practical solution is to choose as nominal model that model which generates the smallest gap with the other models.

### Controller synthesis

In view of the previous derived robustness margins we have that for a given nominal model the control objective is then to minimize  $T(P, C)$  over all admissible controllers.

**Theorem 3.7** Let  $(N, M) \in \mathcal{H}$  be a nrcf of  $P(s) \in \mathcal{F}$  and let  $(\tilde{Y}, \tilde{X})$  be a lcf of an admissible controller  $C(s) \in \mathcal{F}$ , then:

$$\|T(P, C)\|_\infty \leq \gamma$$

if and only if:

$$\left\| \begin{bmatrix} M \\ N \end{bmatrix}^* + [\tilde{X} \ \tilde{Y}] \right\|_\infty \leq \sqrt{1 - \gamma^{-2}}$$

**Proof:** The rcf version of Theorem 4.2 in McFarlane and Glover (1989)  $\square$

The controller design procedure implied by this theorem is remarkably simple: solve a one-block Nehari problem as in Theorem 3.7 in order to obtain a controller which stabilizes the closed loop. The minimal achievable value of  $\gamma$  in the one block Nehari problem is well known (Glover (1984)). The minimal achievable  $H_\infty$  bound on the closed loop  $T(P, C)$  can be stated in terms of the Graph Hankel singular values.

**Corollary 3.8** For a given plant  $P \in \mathcal{F}$  with its nrcf  $(N, M) \in \mathcal{H}$ , controlled by a controller  $C \in \mathcal{F}$  such that  $C$  stabilizes  $P$ , the  $H_\infty$  bound on the closed loop transfer function is given by:

$$\|T(P, C)\|_\infty \leq \frac{1}{\sqrt{1 - \sigma_1^2}}$$

with:

$$\sigma_1 = \left\| \begin{bmatrix} M^* & N^* \end{bmatrix} \right\|_H$$

**Remark 3.9** Note that the open loop plant directly determines the maximal achievable closed loop robustness margin.

The controller of Theorem 3.7 has order  $n$  if the plant has order  $n$ . In the next theorem the design of a lower order controller will be presented.

**Theorem 3.10 (Bongers and Bosgra (1990))**  
For a given plant (with distinct  $\sigma_i^G(P)$ )  $P_n \in \mathcal{F}$  of order  $n$  with its nrcf  $(N, M) \in \mathcal{H}$ , controlled by a controller  $C_r \in \mathcal{F}$  of order  $r$ , with  $r < n$ , such that  $C$  stabilizes  $P$ , the  $H_\infty$  bound on the closed loop transfer function is given by:

$$\|T(P_n, C_r)\|_\infty \leq \frac{1}{\sqrt{1 - (\sigma_1 + \sum_{i=r+2}^n \sigma_i)^2}}$$

**Proof:** The low order controller design objective can be formulated as:

$$\begin{aligned} & \inf_{(\tilde{Y}_r, \tilde{X}_r) \in \mathcal{H}} \left\| \begin{bmatrix} M_n \\ N_n \end{bmatrix}^* + [\tilde{X}_r \ \tilde{Y}_r] \right\|_{\infty} \\ &= \inf_{(\tilde{Y}_r, \tilde{X}_r)} \left\| \begin{bmatrix} M_n \\ N_n \end{bmatrix}^* - [\tilde{X} \ \tilde{Y}] + \dots \right. \\ & \quad \left. \dots + [\tilde{X} \ \tilde{Y}] + [\tilde{X}_r \ \tilde{Y}_r] \right\|_{\infty} \end{aligned} \quad (4)$$

The intention of controller design on the nominal plant can be seen in the first two terms (rhs) of (4), controller reduction can be seen in the last two terms (rhs) of (4). Using the triangle inequality (4) leads to:

$$\begin{aligned} & \inf_{(\tilde{Y}_r, \tilde{X}_r) \in \mathcal{H}} \left\| \begin{bmatrix} M_n \\ N_n \end{bmatrix}^* + [\tilde{X}_r \ \tilde{Y}_r] \right\|_{\infty} \quad (5) \\ & \leq \inf_{(\tilde{Y}_{n-1}, \tilde{X}_{n-1}) \in \mathcal{H}} \left\| \begin{bmatrix} M_n \\ N_n \end{bmatrix}^* + [\tilde{X}_{n-1} \ \tilde{Y}_{n-1}] \right\|_{\infty} + \dots \\ & \quad \dots + \inf_{(\tilde{Y}_r, \tilde{X}_r) \in \mathcal{H}} \left\| [\tilde{X}_{n-1} \ \tilde{Y}_{n-1}] - [\tilde{X}_r \ \tilde{Y}_r] \right\|_{\infty} \end{aligned}$$

in which the first term (rhs) is a one-block Nehari problem on the full order model and the second term (rhs) is a Hankel norm model reduction problem on the controller.

The Nehari approximation of an  $n^{\text{th}}$  order plant model results in an  $(n-1)^{\text{th}}$  order controller with a distance of  $\sigma_1^G(P_n)$ . Apply Hankel norm reduction on the rcf of the  $(n-1)^{\text{th}}$  order controller  $C_{n-1}$  to obtain  $r^{\text{th}}$  order rcf of the reduced controller. Using Glover (1984) the Hankel norm model reduction of the  $(n-1)^{\text{th}}$  order model to an  $r^{\text{th}}$  order model induces an  $L_{\infty}$  error bound smaller than  $\sum_{i=r+1}^{n-1} \sigma_i^G(C_{n-1}(s))$ . It is always possible to choose a  $C_{n-1}$  such that  $\sigma_i^G(C_{n-1}) = \sigma_{i+1}^G(P_n)$  and then combining the two errors leads to

$$\|(P_n, C_r)\|_{\infty} < \frac{1}{\sqrt{1 - (\sigma_1 + \sum_{i=r+2}^n \sigma_i)^2}} \quad (6)$$

□

**Remark 3.11** It can be seen Theorem 3.10 that the minimum value of  $\|T(P, C)\|_{\infty}$  is reached for an  $(n-1)^{\text{th}}$  order controller instead of an  $n^{\text{th}}$  order controller from Theorem 3.7

## 4 Control of a wind turbine

In this section we will use the design method of the previous section to design a low order linear controller which will stabilize the wind turbine under full load conditions.

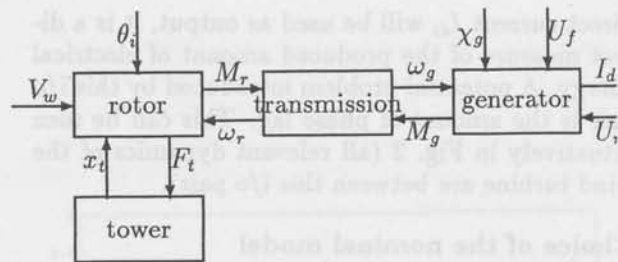


Fig. 2: Block scheme of wind turbine

### Theoretical model

Fig. 2 schematically represents the flexible wind turbine under consideration. The models describing each of the wind turbine parts are mutually connected by interaction variables. Using this interaction variables different submodels of the wind turbine parts can be used easily to describe different wind turbine configurations (Bongers et al. (1990)). Using submodels having the following characteristics:

rotor a two-bladed rotor, each blade having freedom in lag-, flap- and pitch direction of the blades, the pitch angle is controllable. The aerodynamics are described by 2D profile data with 3D correction (Viterna and Corregan (1981)), dynamic inflow (Montgomery and Zdunek (1984)), dynamic stall is described using the ONERA method (Petot (1981)), wind shear is included.

tower is assumed to be flexible, we included the lowest bending mode.

transmission contains the first torsional mode. electrical machine a synchronous generator with field voltage as external input, saturation is included in the model. The generator is connected to the public grid by a rectifier, DC-link and inverter. The delay angle of the rectifier is controllable (Hoeijmakers (1989)).

the interaction of these submodels can be written as a non-linear 13<sup>th</sup> order model.

### Control objectives

The control objectives in full load can be stated as:

- constant amount of produced electrical energy, in order to prevent off-design loads.
- small control effort, fast pitch angle variations are physical impossible.

In this paper we will use only the blade pitch angle  $\theta$  to control the wind turbine. The blade pitch angle has a direct influence upon the conversion efficiency of wind energy into mechanical energy. The

direct current  $I_{dc}$  will be used as output, it is a direct measure of the produced amount of electrical energy. A potential problem introduced by this i/o pair is the amount of phase lag. This can be seen intuitively in Fig. 2 (all relevant dynamics of the wind turbine are between this i/o pair).

### Choice of the nominal model

As stated before the aim is to use one linear controller that will stabilize the non-linear wind turbine model under full load conditions. For that purpose we can derive a set of linear models, each linearized for a specific full load condition. Each full load condition is determined by the average wind speed at hub height. In Fig. 3 and Fig. 4 the characteristics of the transfer function from blade pitch angle  $\theta$  to the direct current  $I_{dc}$  for different wind velocities is given. The desired bandwidth of the blade

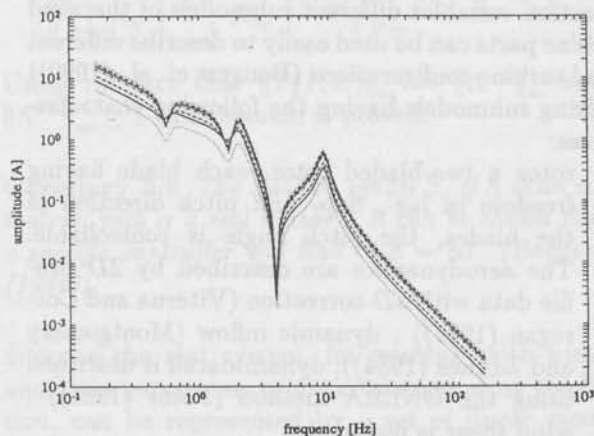


Fig. 3: amplitude characteristic for different wind velocities

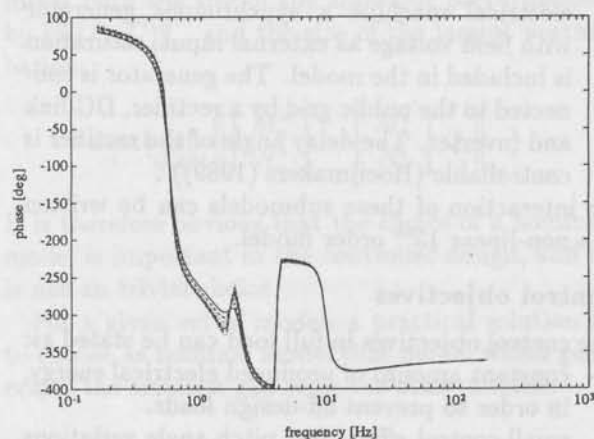


Fig. 4: phase characteristic for different wind velocities

pitch control loop is approximately 1Hz. The first

problem in the control design phase is the choice of the nominal model (the model on which the controller is based). More precisely determine the nominal model such that the distance to the boundary of the model set is minimal. For that reason we search for a nominal model such that for all models in the model set  $(P_{\Delta} = (N_n - \Delta N)(M_n - \Delta M)^{-1})$  with  $N_n M_n^{-1}$  the nominal model)  $\delta_g = \left\| \begin{bmatrix} \Delta M \\ \Delta N \end{bmatrix} \right\|_{\infty}$  is minimal. Hence the desired nominal model will have the smallest gap distance to the boundary of the model set. In Fig. 5 the directed gap (Georgiou (1988)) between different choices of the nominal model and the other models in the model set is calculated. It can be seen that the model for

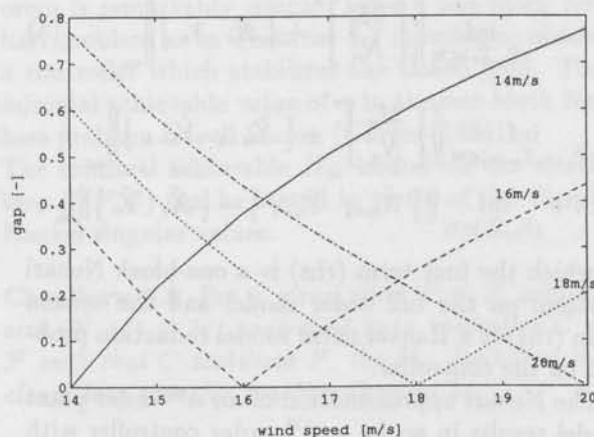


Fig. 5: gap between different models in the model set

16m/s wind velocity is almost in the center of the model set and thus will be used as the nominal model. Hence the controller must robustly stabilize the nominal model with a gap bound of 0.78 (Fig. 5).

### Order of the controller

The graph Hankel singular values of the nominal model are given in Fig. 6. The  $n - 1$  order optimal controller, calculated using the formulas of Section 4, results in a stable closed loop:  $T(P, C) \in \mathcal{H}$  and  $\|T(P, C)\|_{\infty} = 3.43$ .

The gap bound generated by the controller Lemma 3.4 is smaller than the necessary one. Looking at Fig. 5 this controller will stabilize the models with an average wind speed between 14.5m/s and 18.5m/s if the distance is measured in the gap-metric. By Theorem 3.5 the class  $S_b$  is larger than  $S_g$ , therefore it is possible that all plants are in  $S_b$ .

For the nominal plant only, we can inspect the stability margin generated by low order controllers.

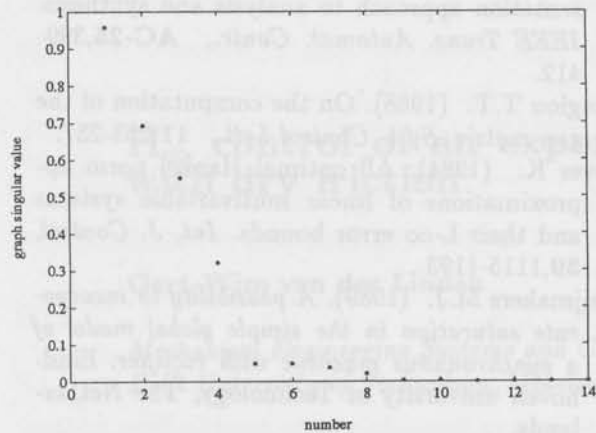


Fig. 6: Graph Hankel singular values

In Fig. 7 the necessary stability bound and the induced bound by the various low order controllers is given for the nominal model. It can be seen that a

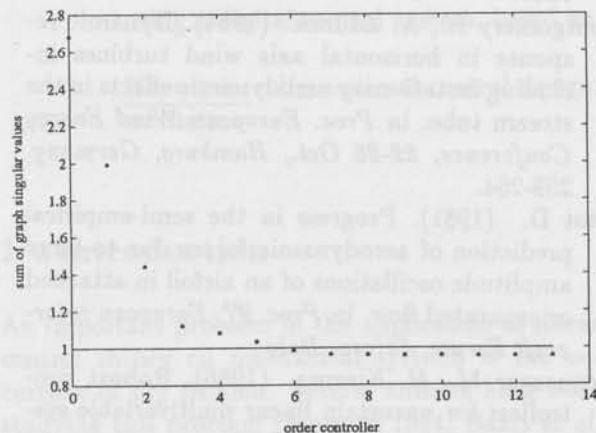


Fig. 7: controller induced stability bounds

6<sup>th</sup> order controller will also stabilize the nominal model with almost the same stability bound. The stability test fails with a 5<sup>th</sup> order controller. Next we will inspect if the 6<sup>th</sup> order controller will stabilize all wind turbine models. For this purpose we calculate the  $\Lambda$ -gap. It can be seen in Fig. 8 that the maximum value is less than one, therefore by Theorem 3.2 all plants are in  $S_b$ .

**Performance**

The requested performance was a bandwidth of about 1 Hz from blade pitch angle  $\theta$  to direct current  $I_{dc}$ . In Fig. 9 the servo behaviour for all plants is given. As can be seen from Fig. 9 the performance requirement is satisfied for the 6<sup>th</sup> order controller. It can be seen in Fig. 4 that the phase lag of the open loop system at the required bandwidth

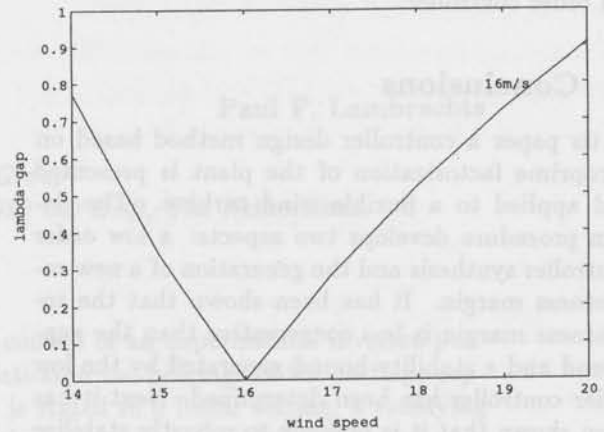


Fig. 8:  $\Lambda$ -gap induced stability bounds

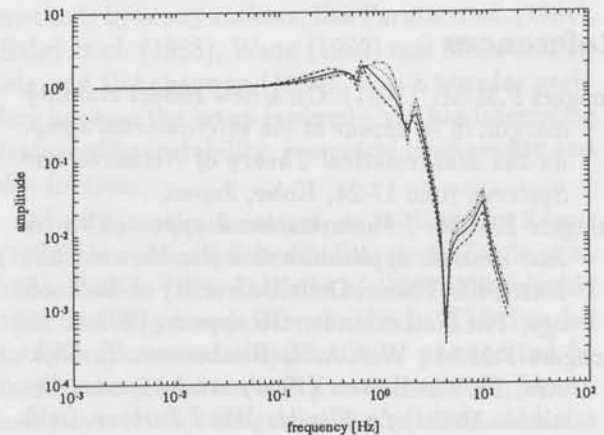


Fig. 9: amplitude characteristics of servo behaviour

is about  $600^\circ$  which means that on physical knowledge we need at least a  $5^{\text{th}}$  order controller to compensate this phase lag without any performance or robustness requirements. The performance of the  $6^{\text{th}}$  order controller is almost the same as for the full order controller.

## 5 Conclusions

In this paper a controller design method based on a coprime factorization of the plant is presented and applied to a flexible wind turbine. The design procedure develops two aspects: a low order controller synthesis and the generation of a new robustness margin. It has been shown that the robustness margin is less conservative than the gap bound and a stability bound generated by the low order controller has been determined. Next it has been shown that it is possible to robustly stabilize the flexible wind turbine model by means of a low order controller. The non-linear model is parameterized by a set of linear models. One model is chosen as nominal model such that the gap distance to the boundary of the model set is minimal. For that reason the deviations of all models from the nominal model are described by coprime factor perturbations. The low order controller has about the same performance as the full order controller. The low order controller does not stabilize the whole model set characterized by the gap distance. Using a less conservative measure it is shown that the low order controller does stabilize the whole model set.

## References

- Bongers P.M.M. (1991). On a new robust stability margin. in *to appear at the international symp. on the Mathematical Theory of Networks and Systems*, June 17-24, Kobe, Japan, .
- Bongers P.M.M. , *Factorizational approach to robust control: application to a flexible wind turbine*. PhD Thesis, Delft University of Technology, The Netherlands, To appear, 1992.
- Bongers P.M.M., W.A.A.M. Bierbooms, S.J. Dijkstra, Th. van Holten (1990). *An Integrated Dynamic Model of a Flexible Wind Turbine*. Delft University of Technology, The Netherlands, .
- Bongers P.M.M., O.H. Bosgra (1990). Low order  $H_\infty$  controller synthesis. in *Proc. 29th Conf. Decision and Control*, Hawaii, USA, 194-199.
- Desoer C.A., W.S. Chan (1975). The feedback interconnection of lumped linear time-invariant systems. *J. Franklin Inst.*, **300**,335-351.
- Desoer C.A., R.W. Liu, J. Murray, R. Sacks (1980). Feedback systems design: the fractional representation approach to analysis and synthesis. *IEEE Trans. Automat. Contr.*, **AC-25**,399-412.
- Georgiou T.T. (1988). On the computation of the gap metric. *Syst. Control Lett.*, **11**,253-257.
- Glover K. (1984). All optimal Hankel norm approximations of linear multivariable systems and their  $L_\infty$  error bounds. *Int. J. Control*, **39**,1115-1193.
- Hoeijmakers M.J. (1989). *A possibility to incorporate saturation in the simple global model of a synchronous machine with rectifier*. Eindhoven university of Technology, The Netherlands, .
- McFarlane D.C., K. Glover (1989). *Robust controller design using normalized coprime factor plant descriptions*. Lecture Notes in Control and Information Sciences, vol.138, Springer Verlag, Berlin, Germany, .
- Meyer D.G. (1988). A fractional approach to model reduction. in *Proc. Amer. Control Conf.*, 1041-1047.
- Montgomery B., A. Zdunek (1984). Dynamic response in horizontal axis wind turbines including instationary aerodynamic effects in the stream tube. in *Proc. European Wind Energy Conference, 22-26 Oct., Hamburg, Germany*, 259-264.
- Petot D. (1981). Progress in the semi-empirical prediction of aerodynamic forces due to large amplitude oscillations of an airfoil in attached or separated flow. in *Proc. 9th European rotorcraft Forum, Stresa, Italy.*, .
- Vidyasagar M., H. Kimura (1986). Robust controllers for uncertain linear multivariable systems. *Automatica*, **22**,85-94.
- Vidyasagar M., H. Schneider, B.A. Francis (1982). Algebraic and topological aspects of feedback stabilization. *IEEE Trans. Automat. Contr.*, **AC-27**,880-893.
- Viterna L., R. Corrigan (1981). Fixed pitch rotor performance of large horizontal axis wind turbines. in *DOE/NASA workshop on large horizontal axis wind turbines, Cleveland, USA.*, .

## $H_\infty$ control of an experimental inverted pendulum with dry friction

Gert-Wim van der Linden

Paul F. Lambrechts

*Mechanical Engineering Systems and Control Group  
Delft University of Technology, Mekelweg 2, 2628 CD Delft, The Netherlands.*

**Abstract.** This paper considers  $H_\infty$  optimal control of an experimental inverted pendulum having a considerable amount of dry friction in the bearings of the carriage supporting the pendulum. Although the problem is stated in a linear setting, a satisfying  $H_\infty$  optimal controller is realized by representing the control problem by means of a linear standard plant, incorporating the essential effect of the nonlinear dry friction phenomenon. The resulting controller is applied successfully on the experimental setup, using a digital control system, based on a TMS320C25 digital signal processor.

**Keywords.**  $H_\infty$  optimal control design; inverted pendulum; dry friction; digital implementation

### 1 Introduction

An important problem in the application of linear control theory on mechanical systems is the occurrence of dry friction. Several authors have been studying this problem (Walrath 1984, Bakri *et al.* 1988 and Brandenburg 1989a/b). This paper will consider the incorporation of dry friction in a standard plant setting and the application of  $H_\infty$  optimal control design to find a controller that is insensitive to dry friction. The approach will be applied to an inverted pendulum setup, to show that this way an important improvement of behaviour can be obtained.

First it will be shown that the application of an  $H_\infty$  optimal controller does not result in a satisfactory behaviour if dry friction is not taken into account and cart position reference error minimization (tracking) is demanded. Next we will consider only the effect of dry friction, leading to a controller that is insensitive to this effect, but has no reference tracking property. Finally a trade-off between the tracking objective and the insensitivity to dry friction is performed, resulting in a controller with good behaviour in both respects. This behaviour

has been validated by means of implementation on a laboratory setup.

The inverted pendulum problem has been considered as a suitable test-case for controller design methods by many authors, like Furuta *et al.* (1984), Bakri *et al.* (1988), Wang (1989) and Meier zu Fawig and Unbehauen (1990). It is a popular problem because the setup is simple, yet has interesting features like instability, geometric nonlinearity and dry friction.

Also  $H_\infty$  optimal control, as initiated by Zames (1981), is well established in literature (Doyle *et al.* 1984, Francis 1987, Doyle *et al.* 1989, Maciejowski 1989 and Boyd and Barratt 1991). This has led to several successful applications, as reported by for instance Limebeer and Kasenally (1986), Morari and Doyle (1986), Skogestad *et al.* (1988) and Balas and Doyle (1989).

We will start by giving some preliminaries on  $H_\infty$  theory in section 2. The experimental setup will then be described in section 3. The dry friction phenomenon is covered separately in section 4, resulting in a linear model, to be used at the control design stage, which is covered in section 5. The results of the implementation of the final controller

on the experimental setup are presented in section 6 and some conclusions are given in section 7.

## 2 Preliminaries

### 2.1 The standard plant configuration

The general framework that we will use in this paper is given in figure (1) (Doyle *et al.* 1984). Any

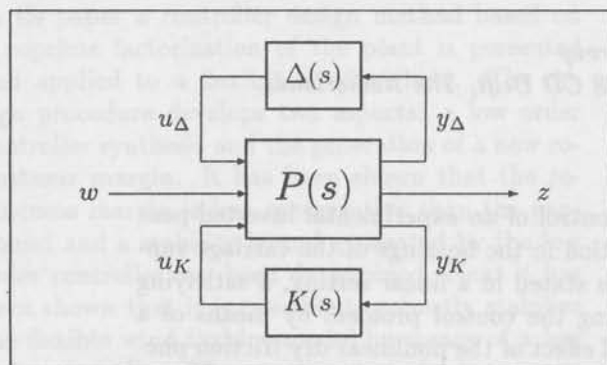


Fig. 1: Standard plant ( $P$ ) with controller ( $K$ ) and uncertainty ( $\Delta$ )

control problem within a linear setting may be written in this form.

The standard plant  $P$  incorporates the plant and provides an interconnection structure, defining the way in which the *uncertainty block*  $\Delta$  and the *controller*  $K$  act on the system.

The inputs to the standard plant are: the output of the uncertainty block  $u_\Delta$ ; the disturbances acting on the standard plant  $w$ , such as reference signals and noise; and finally the controller-output  $u_K$ .

The outputs of the standard plant are: the input to the uncertainty block  $y_\Delta$ ; the control objectives  $z$ , such as tracking error and control effort; and the measurable signals  $y_K$ .

The closed loop transfer function from  $w$  to  $z$  will be denoted as  $T_{wz}(s)$ . The control problem can then be stated as the minimization over all possible controllers  $K(s)$  of  $T_{wz}(s)$  in some given norm. The uncertainty block  $\Delta$  is an arbitrary element of a given set, representing the difference between the linear model and reality.

### 2.2 Norms and function spaces

We will assume that  $\Delta$  is restricted to the function space  $H_\infty$ :

**Definition 2.1** (Francis, 1987)

$H_\infty$  is the Banach space, consisting of all complex

valued functions  $F(s)$ , for which the infinity-norm

$$\|F(s)\|_\infty := \operatorname{ess\,sup}_{s \in \mathbb{C}^+} \sigma_{\max}(F(s)) \quad (1)$$

is bounded.

where  $\sigma_{\max}$  denotes largest singular value and  $\mathbb{C}^+$  denotes the closed right half of the complex plane (including infinity). Furthermore we will assume that:

$$\Delta(s) \in \Delta, \quad (2)$$

$$\Delta := \{\Delta(s) \in H_\infty \mid \|\Delta(s)\|_\infty \leq 1\}. \quad (3)$$

and that appropriate weight functions are incorporated in  $P$ . Note that the combination of  $\Delta$  and  $P$  represents a *set* of systems rather than one particular system.

The restriction of  $H_\infty$  to all its real rational elements is denoted as  $RH_\infty$  and defined as

**Definition 2.2** (Francis, 1987)

$RH_\infty$  is the Banach space, consisting of all functions  $F(s) \in \mathbf{R}(s)$ , for which  $\|F(s)\|_\infty$ , as defined by (1) is bounded.

where  $\mathbf{R}(s)$  denotes the ring of real rational matrices. Since all  $F(s) \in RH_\infty$  must be analytical in  $\mathbb{C}^+$ ,  $RH_\infty$  consists of all proper, real rational asymptotically stable transfer functions.

We will assume that the standard plant  $P$  is real rational and the control problem is well-posed. This implies that a controller  $K$  can be found such that the closed loop system  $T_{wz}(s)$  belongs to  $RH_\infty$ .

### 2.3 $H_\infty$ control design method

To be able to optimize certain design goals, usually performance, under some constraints, like robustness and noise sensitivity reduction, the standard plant (in fact the weight functions reflecting the goals which are to be optimized) may depend on a free parameter  $\gamma \in \mathbb{R}$ .

By defining  $\gamma$  such that the demand with respect to one or more design goals increases when  $\gamma$  increases, we may define the  $H_\infty$  control design problem as finding the largest  $\gamma$  such that there exists a controller  $K(s)$  for which

$$\|T_{wz}(s, \gamma)\|_\infty \leq 1 \quad \forall \Delta(s) \in \Delta \quad (4)$$

If no uncertainty block is present, a direct computational solution is available, based on the solution of two algebraic Riccati equations. This solution has been implemented in the software package PC-MATLAB (1987) using a small adaption of the algorithm given by Glover and Doyle (1988) (see also Doyle *et al.*, 1989).

### 3 Experimental setup

#### 3.1 Description

The inverted pendulum setup can be split into four parts, which will be considered consecutively:

1. Mechanical part (see figure (2))
2. Sensors with accompanying electronics
3. Digital control system
4. Actuator with power amplifier

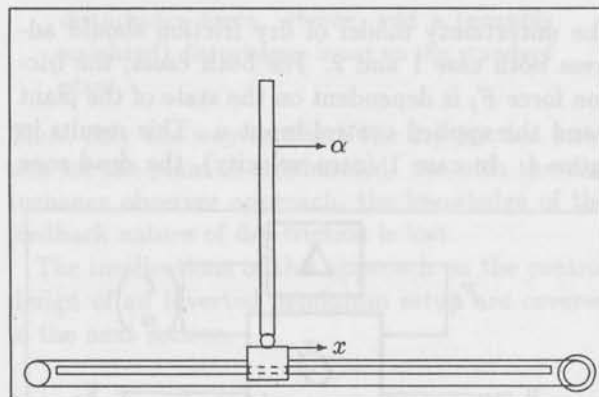


Fig. 2: Inverted pendulum setup; mechanical part

##### 3.1.1 Mechanical part

The mechanical part of the setup consists of a cart, a pendulum and a drive-train. The hollow steel pendulum has a weight of 0.6 kg, and a length of 57cm from the center of rotation to the tip. The pendulum can rotate in the vertical plane by means of low friction roller bearings. The angular deviation is limited to  $\pm 15$  degrees from the vertical.

The aluminium cart can move along steel guiding bars, also using roller bearings. These bearings have a considerable amount of friction (the drive-train also contributes this) and will have to be taken into account at the control design stage.

The drive-train consists of a toothed belt, actuated by an electrical servomotor. The belt is attached to the cart, and combined with a toothed wheel on the motor it provides slip-free traction.

##### 3.1.2 Sensors with electronics

The measurement signals are obtained from three sensors:

1. A magneto-restriction sensor alongside the guiding bars for measuring the linear displacement of the cart.

2. A Rotary Variable Differential Transducer (RVDT) at the rotation point of the pendulum, measuring the angle.
3. A tacho generator on the servomotor, measuring the angular velocity of the motor, which is approximately linear dependent on the cart velocity.

All sensors are sufficiently accurate (less than 1% deviation) and have a high bandwidth (exceeding 100 Hz).

##### 3.1.3 Digital control system

The digital control system is a DSP-based system (dSPACE, 1989a), with a IBM-AT compatible host. High level software (dSPACE, 1989b) provides discretization, scaling (see for instance Hanselmann, 1987) and assembly source code generation almost automatically.

The use of fast A/D and D/A converters in combination with a Texas Instruments TMS320C25 DSP provided adequate computational speed under all circumstances.

##### 3.1.4 Actuator with power amplifier

The actuator is a 400 Watts DC electromotor (Mavilor Iberica mod. 300) connected to a voltage driven power amplifier, supplying up to 10 Ampères. Under normal circumstances the motor with amplifier has a linear behaviour, with a high bandwidth (well above the eigenfrequencies of the mechanical part).

#### 3.2 Mathematical model

Since the dynamics of the sensors and the actuator are relatively fast, we will combine a dynamical model of the mechanical part with static models of all other components. A nonlinear model of cart and pendulum has been derived by means of Kane's method (Kane and Levinson, 1985). This model can simply be linearized manually. In combination with the static models, this results in the following fourth order state space model:

$$G: \begin{cases} \dot{\xi} = A\xi + Bu + Ev \\ y = C\xi + Du + Fv \end{cases} \quad (5)$$

with

$$\xi = (\alpha \quad \dot{\alpha} \quad x \quad \dot{x})^T \quad (6)$$

$$y = (y_\alpha \quad y_x \quad y_{\dot{x}})^T \quad (7)$$

The state  $\xi$  consists respectively of pendulum angle  $\alpha$ , angular velocity  $\dot{\alpha}$ , cart position  $x$  and velocity  $\dot{x}$ . The control input  $u$  equals the controller

output (a voltage on the amplifier) and the disturbance input  $v$  equals the disturbance force on the cart (mainly friction forces). The output  $y$  consists of all measurable variables:  $\alpha$ ,  $x$  and  $\dot{x}$ . For a pictorial representation, see figure 3. Note that

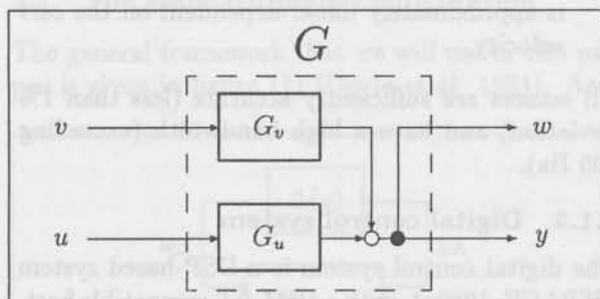


Fig. 3: Linear model of inverted pendulum

$G_u(s)$  is the transfer function from the control input to the measurable outputs, and  $G_v(s)$  from the disturbance input to the measurable outputs. This linear mathematical model will be the central item in the standard plants as considered in section 5.

## 4 Dry friction

To be able to incorporate dry friction in the standard plant setting, a characterization of this phenomenon is necessary. First an attempt is made to construct an appropriate uncertainty model  $\Delta$  in accordance with the theory as presented in section 2. However, it will be shown that this is impossible and an alternative approach will be proposed.

### 4.1 Characterization of dry friction

Generally spoken, a dry friction force occurs at the plane of contact between two bodies. The force acts opposite to the direction of motion, and is highly non linearly dependent on the velocity. Two cases must be distinguished:

1. the relative velocity ( $\dot{x}$ ) of the bodies is zero (*stiction*)
2. the velocity is not equal to zero (*Coulomb friction*)

**Case 1:** If a force is applied on a body at rest, it will not move until the applied force exceeds some limit (stiction or backlash force). This can be modelled as a dead-zone effect.

**Case 2:** When a body (with dry friction) is moving at a certain velocity, a more or less constant Coulomb friction force  $F_C$  will act on it, having the

opposite direction as the direction of motion. Usually the magnitude of this force  $\hat{F}$  is dependent on the velocity, especially at low speeds. Of course it is also dependent on the surface structure and lubrication. To simplify the dry friction model, the magnitude of the Coulomb friction force will be chosen constant (so  $F_C = -\hat{F}\text{sign}(\dot{x})$ ).

For more information on modelling, simulation and compensation of dry friction, see for instance Brandenburg (1989a,1989b), Götzmann and Meyer (1989) and Walrath (1984).

### 4.2 Uncertainty model of dry friction

The uncertainty model of dry friction should address both case 1 and 2. For both cases, the friction force  $F_f$  is dependent on the state of the plant  $\xi$  and the applied control input  $u$ . This results in figure 4. In case 1 (zero velocity), the dead-zone

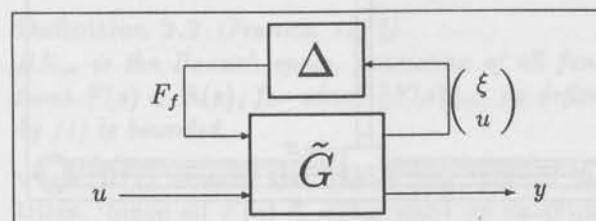


Fig. 4: Model of plant with friction

effect can be modelled quite simple: the magnitude of the friction force will never exceed the applied force, so the dead-zone can be written as an uncertain gain between zero and one.

In case 2 (non-zero velocity) however, we have the problem that at  $\dot{x} = 0$ , the Coulomb friction function is not defined (because of the effect of stiction). This implies that

$$\left. \frac{\partial F}{\partial \dot{x}} \right|_{\dot{x}=0} = \infty \quad (8)$$

Because  $\dot{x} = 0$  is the desired operating point, this results in a non-bounded  $\Delta$  block:

$$\|\Delta_{df}(s)\|_{\infty} = \infty \quad (9)$$

thus no weight functions can be found to normalize  $\|\Delta_{df}\|_{\infty}$  to 1.

### 4.3 Simplified dry friction model

As the uncertainty model is not suitable to incorporate the dry friction effect in a standard plant setting, an alternative solution must be found. The usual approach to the reduction of dry friction influence, is the construction a disturbance observer

(see for example Bakri *et al.* 1988). In that case an extra state is added to the controller to be able to estimate the dry friction force (hence the internal model of dry friction an integrator). The result then resembles the servocompensator approach of Davison (Davison and Goldenberg 1975) for a step-like disturbance input signal, which uses extra dynamics to describe this signal.

To be able to incorporate the dry friction phenomenon in the standard plant setting, but without the necessity of adding dynamics, a similar approach is proposed here:

Model the dry friction force as an external disturbance force. Hence, add a (possibly weighted) disturbance input to the standard plant.

Thus, only the way in which the dry friction force acts on the plant is emphasized. As with the disturbance observer approach, the knowledge of the feedback nature of dry friction is lost.

The implications of this approach on the control design of an inverted pendulum setup are covered in the next section.

## 5 Control design

In order to arrive at a satisfying controller, a few steps have to be made. Each step will consist of the construction of a standard plant, and the calculation of the accompanying  $H_\infty$  optimal controller. The design will be based on a fixed linear model of the setup, since apart from the dry friction, no uncertain effects have to be modeled to obtain sufficient accuracy.

The control of the inverted pendulum setup will have two goals: stabilization of the pendulum, and positioning of the cart. Also, the control energy must be limited, and measurement errors should not be amplified too much. Furthermore, the controller must be insensitive to the effect of dry friction.

The obtained controller will be tested on a nonlinear MATRIX SystemBuild (1986) model, incorporating the nonlinear equations of motion of cart, pendulum, and drive train with dry friction.

### 5.1 Tracking controller

To show that it is necessary to take dry friction into account, first a controller will be designed to meet the tracking objective only. This results in a standard plant as depicted in figure 5. For the objectives and the matching weight functions, see table 1.

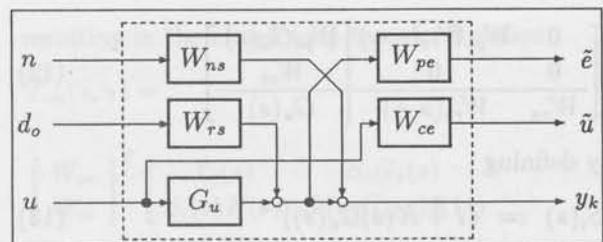


Fig. 5: Tracking standard plant

|                             |   |
|-----------------------------|---|
| Reference signal weight     | $W_{rs}(s, \gamma) = \frac{50}{\gamma^{-1}s+1}$ |
| Control energy limitation   | $W_{cc} = 5$                                    |
| Noise sensitivity reduction | $W_{ns} = 10^{-2}I$                             |
| Position error weight       | $W_{pe} = [0 \ 1 \ 0]$                          |

Table 1: Tracking objective and weight functions

Only the position reference signal weight is chosen to be dynamical, to guarantee a minimal bandwidth of the transfer function from  $d_o$  to  $y_x$ , which will be achieved by minimizing the transfer function from  $d_o$  to  $\tilde{e}$ . The cross-over frequency of  $W_{rs}(s, \gamma)$  can be found by solving

$$\left| \frac{50}{\gamma^{-1}i\omega + 1} \right| = 1 \quad (10)$$

which has the solution

$$\omega = 7\sqrt{51}\gamma \approx 50\gamma \quad (\text{rad/s}) \quad (11)$$

This implies that (given  $W_{pe} = [0 \ 1 \ 0]$ ) the closed loop system has a minimal bandwidth of  $50 \times \gamma$  radians per second. The optimal solution will find the maximal bandwidth, given the other weight functions.

The static position error can be found by evaluating the closed loop transfer function from  $d_o$  to  $\tilde{e}$  at  $\omega = 0$ , resulting in an error of less than  $1/50 = 2\%$ .

Also note that only the *position* error is weighted. Since stability is guaranteed *a priori* if a  $H_\infty$  optimal solution exists, the pendulum angle need not be weighted. To conform to the Glover and Doyle (1988) demands, an external force-input must be added, to prevent a transmission zero at  $s = 0$ . A small weight ( $10^{-3}$ ) will be put on the cart disturbance force, such that this will not influence the result.

The standard plant  $P(s, \gamma)$  (neglecting the cart disturbance force weight) then equals:

$$P(s, \gamma) =$$

$$\left[ \begin{array}{cc|c} 0 & W_{pe}W_{rs}(s, \gamma) & W_{pe}G_u(s) \\ 0 & 0 & W_{ce} \\ \hline W_{ns} & W_{rs}(s, \gamma) & G_u(s) \end{array} \right] \quad (12)$$

By defining

$$S_i(s) := (I + K(s)G_u(s))^{-1} \quad (13)$$

$$S_o(s) := (I + G_u(s)K(s))^{-1} \quad (14)$$

$$T_i(s) := (I + K(s)G_u(s))^{-1}K(s)G_u(s) \quad (15)$$

$$T_o(s) := (I + G_u(s)K(s))^{-1}G_u(s)K(s) \quad (16)$$

the resulting closed loop transfer function is

$$T_{wz}(s, \gamma) = \begin{bmatrix} W_{pe} \\ W_{ce} \end{bmatrix}^T \times$$

$$\begin{bmatrix} T_o(s) & S_o(s) \\ S_i(s)K(s) & S_i(s)K(s) \end{bmatrix} \begin{bmatrix} W_{ns} \\ W_{rs}(s, \gamma) \end{bmatrix} \quad (17)$$

The  $H_\infty$  iteration yields an optimal  $\gamma$  of 0.0334, so the bandwidth must be at least  $50 \times \gamma = 1.5$  rad/s, such that in the time domain a rise time of at most 2 seconds is expected. This is confirmed by the step responses in figure 6. If the controller is ap-

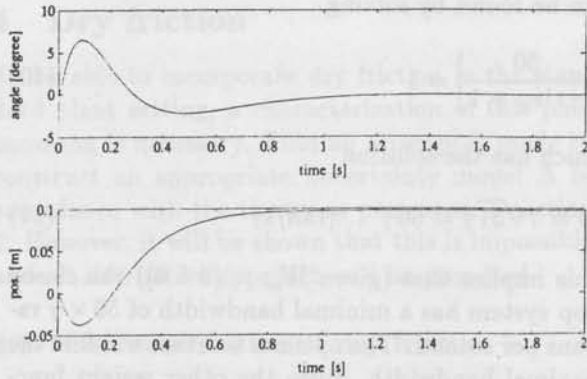


Fig. 6: Step responses tracking case.

plied on the nonlinear simulation model however, the closed loop system has an unsatisfactory behaviour, as shown in figure 7. There is a large limit cycle, due to the combination of dry friction and instability of the plant. Therefore the approach as sketched in section 4.3 will be applied to improve this behaviour.

## 5.2 Disturbance attenuating controller

To find out how much dry friction force influence reduction can be obtained, the tracking objective will be temporarily removed and attention is put on the disturbance force only, see figure 8 and table 2. The standard plant  $P(s, \gamma)$  now appears as:

$$P(s, \gamma) =$$

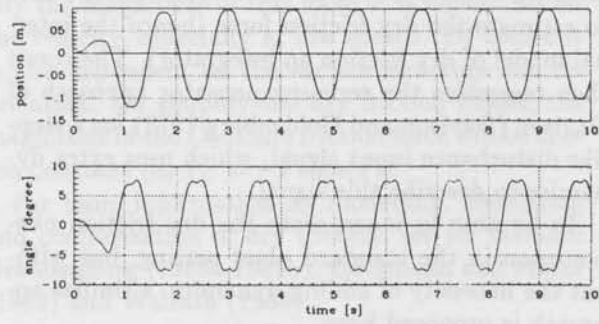


Fig. 7: Limit cycle tracking case.

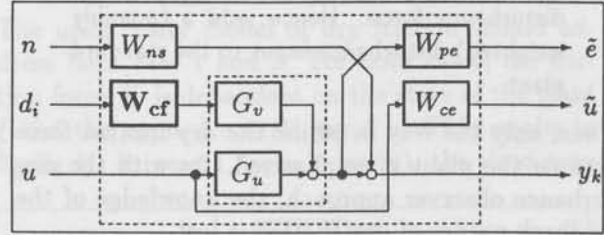


Fig. 8: Disturbance attenuation standard plant

$$\begin{bmatrix} 0 & W_{pe}G_v(s)W_{cf}(\gamma) & W_{pe}G_u(s) \\ 0 & 0 & W_{ce} \\ \hline W_{ns} & G_v(s)W_{cf}(\gamma) & G_u(s) \end{bmatrix} \quad (18)$$

The resulting closed loop transfer function is

$$T_{wz}(s, \gamma) = \begin{bmatrix} W_{pe} \\ W_{ce} \end{bmatrix}^T \times$$

$$\begin{bmatrix} T_o(s) & S_oG_v(s)(s) \\ S_i(s)K(s) & S_i(s)G_v(s)K(s) \end{bmatrix} \begin{bmatrix} W_{ns} \\ W_{cf}(\gamma) \end{bmatrix} \quad (19)$$

$H_\infty$  optimization then results in an optimal  $\gamma$  of 4.11. Note that this  $\gamma$  is the maximum weight on the cart disturbance force, under the restriction that  $\|T_{wz}(s, \gamma)\|_\infty \leq 1$ . If the obtained controller is applied on the nonlinear model, a reasonably good behaviour is found: there is a small drift of the cart, resulting in a slow limit cycle (see figure 9). The initial angular error is quickly recovered, without excessive control effort.

|                             |                           |
|-----------------------------|---------------------------|
| Cart force weight           | $W_{cf}(\gamma) = \gamma$ |
| Control energy limitation   | $W_{ce} = 5$              |
| Noise sensitivity reduction | $W_{ns} = 10^{-2}I$       |
| Position error weight       | $W_{pe} = [0 \ 1 \ 0]$    |

Table 2: Disturbance attenuation objectives and weight functions

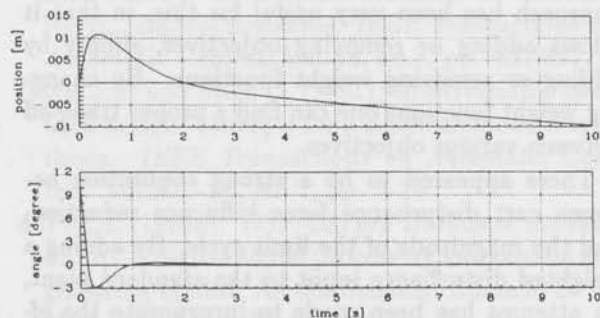


Fig. 9: Limit cycle disturbance attenuation case.

### 5.3 Combined controller

To find a proper trade-off between the tracking objective and insensitivity to dry friction, a combination of the previous two standard plants is made, resulting in figure 10. The matching weights for

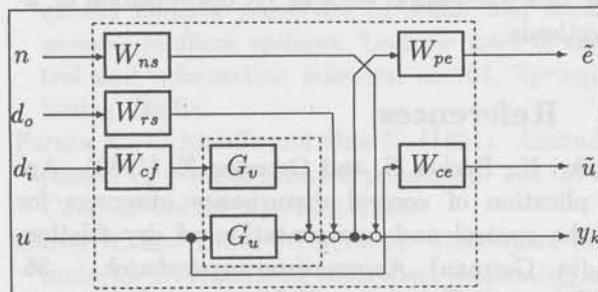


Fig. 10: Combined standard plant

the combination of performance and disturbance attenuation are presented in table 3. An acceptable

|                             |   |
|-----------------------------|---|
| Reference signal weight     | $W_{rs}(s, \gamma) = \frac{50}{\gamma^{-1}s+1}$ |
| Cart force weight           | $W_{cf} = 1$                                    |
| Control energy limitation   | $W_{ce} = 5$                                    |
| Noise sensitivity reduction | $W_{ns} = 10^{-2}I$                             |
| Position error weight       | $W_{pe} = [0 \ 1 \ 0]$                          |

Table 3: Combined objectives and weight functions

trade-off was obtainable with a disturbance force weight of 1. The standard plant for the combined controller then is:

$$P(s, \gamma) = \begin{bmatrix} 0 & W_{pe}W_{rs}(s, \gamma) & W_{pe}G_v(s)W_{cf} & W_{pe}G_u(s) \\ 0 & 0 & 0 & W_{ce} \\ W_{ns} & W_{rs}(s, \gamma) & G_v(s)W_{cf} & G_u(s) \end{bmatrix} \quad (20)$$

resulting in the closed loop transfer function:

$$T_{wz}(s, \gamma) = \begin{bmatrix} W_{pe} \\ W_{ce} \end{bmatrix}^T \begin{bmatrix} T_o(s) & S_oG_v(s) \\ S_i(s)K(s) & S_i(s)G_v(s)K(s) \end{bmatrix} \begin{bmatrix} W_{ns} \\ W_{rs}(s, \gamma) \\ W_{cf} \end{bmatrix} \quad (21)$$

Remarkable is that in this configuration an optimal  $\gamma$  of 0.0329 is obtained: this implies that the bandwidth of the closed loop system is only slightly smaller than in the case of the tracking controller ( $\gamma = 0.0334$ ).

The simulations (see figures 11 and 12) show a promising behaviour; this controller will therefore

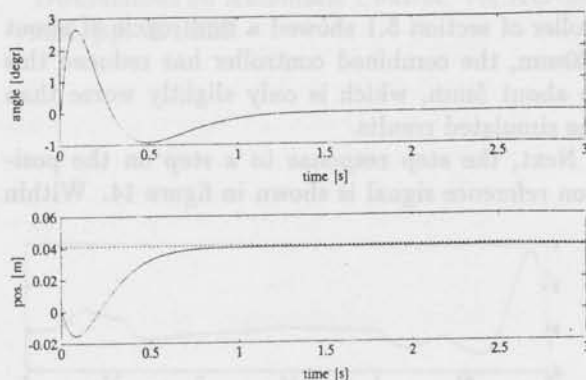


Fig. 11: Step response combined case.

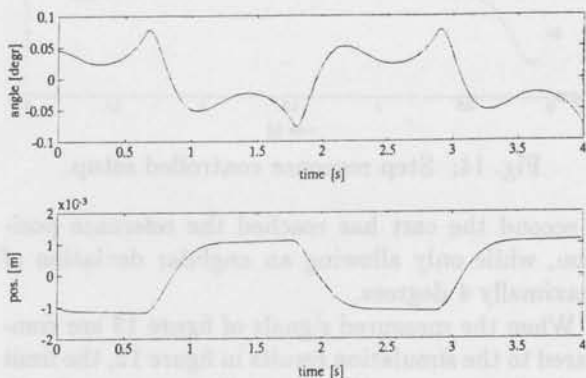


Fig. 12: Limit cycle combined case.

be applied to the experimental setup in the next section.

## 6 Implementation of the controller

The controller as obtained in the previous section is a fourth order, linear, proper continuous time

controller in state-space description which was implemented by means of the digital control system, as described in section 3.

First the resulting limit cycle of the closed loop system is shown in figure 13; while the tracking con-

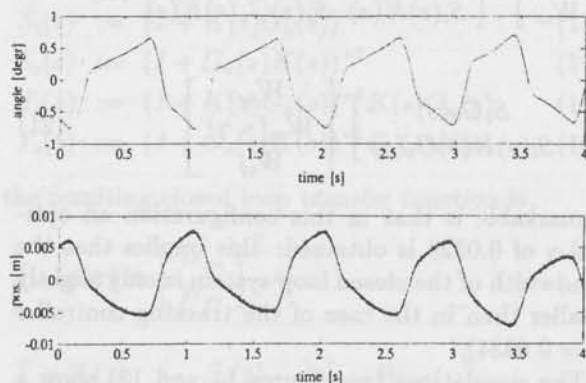


Fig. 13: Limit cycle controlled setup.

troller of section 5.1 showed a limit cycle of about 200mm, the combined controller has reduced this to about 5mm, which is only slightly worse than the simulated results.

Next, the step response to a step on the position reference signal is shown in figure 14. Within

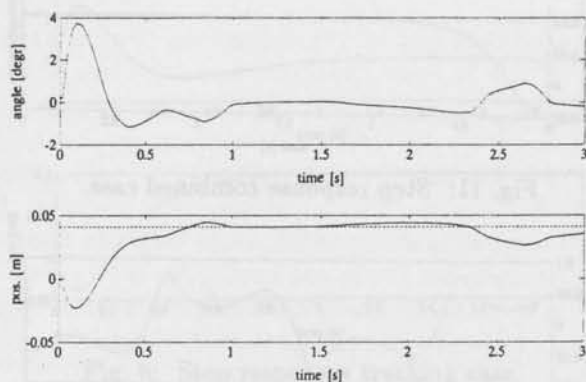


Fig. 14: Step response controlled setup.

1 second the cart has reached the reference position, while only allowing an angular deviation of maximally 4 degrees.

When the measured signals of figure 13 are compared to the simulation results in figure 12, the limit cycle shows some differences. Both the amplitude and shape of the responses are different. This is probably due to other nonlinear effects, such as measurement offset and friction in the pendulum bearings.

## 7 Conclusion

It is shown that the influence of dry friction on a controlled mechanical system can be largely re-

duced, within a linear setting. The standard plant approach has been very useful for this, in that it allows adding or removing objectives, simply by adding or removing weight functions. By changing weight functions one can find a proper trade-off between various objectives.

There appeared to be a strong connection between cart disturbance force influence reduction, and the magnitude of the limit cycle. By adding a weighted disturbance input to the standard plant, an attempt has been made to incorporate the effect of dry friction. Based on this extended standard plant an  $H_\infty$  optimal controller was calculated, which resulted in a satisfying implementation on an experimental inverted pendulum setup.

Since the standard plant setting is not limited to  $H_\infty$  optimization only, the approach to dry friction as presented here, can also be applied in combination with other optimization techniques available for this framework, such as  $H_2$  optimization or  $\mu$ -synthesis.

## 8 References

- Bakri N., Becker N. and Ostertag E. (1988). Application of control disturbance observers for the control and compensation of dry friction. (in German) *Automatisierungstechnik*. 36. Jahrgang, Heft 2, pp. 50-54.
- Balas G.J. and Doyle J.C. (1989) Identification for robust control of flexible structures. *Proc. American Control Conference*. pp. 2566-2571.
- Boyd S.P. and Barratt C.H. (1991). *Linear controller design; limits of performance*. Prentice Hall information and system sciences series.
- Brandenburg G. (1989a). Influence and compensation of backlash and Coulomb friction in a speed- and position-controlled elastic two mass system. Part 1. (in German) *Automatisierungstechnik*. 37. Jahrgang, Heft 1, pp. 23-31.
- Brandenburg G. (1989b). Influence and compensation of backlash and Coulomb friction in a speed- and position-controlled elastic two mass system. Part 2. (in German) *Automatisierungstechnik*. 37. Jahrgang, Heft 3, pp. 111-119 .
- Davison E.J. and Goldenberg A. (1975). Robust control of a general servomechanism problem: The servocompensator. *Automatica*. Vol.11, pp. 461-471.
- Doyle J.C., Chu C.C., Francis B.A., Khargonekar P. and Stein G. (1984). *Advances in multivariable control*. Lecture notes at the ONR/Honywell Workshop, Minneanapolis, MN, Oct 8-10.
- Doyle J.C., Glover K., Khargonekar P. and Francis

- B.A. (1989). State space solutions to standard  $H_2/H_\infty$  control problems. *IEEE Transactions on Automatic Control*. Vol.34, no.8, pp. 831-847.
- Doyle J.C. and Stein G. (1981). Multivariable feedback design: concepts for a classical/modern synthesis. *IEEE Transactions on Automatic Control*. Vol.AC-26, No 1, pp. 4-16.
- dSPACE (1989a). *DSP-CITpro Hardware manual*. dSPACE digital signal processing and control engineering GmbH. An der Schönen Aussicht 2. D-4790 Paderborn, West-Germany.
- dSPACE (1989b). *DSP-CITpro IMPEX manual*. dSPACE digital signal processing and control engineering GmbH. An der Schönen Aussicht 2. D-4790 Paderborn, West-Germany.
- Francis B.A. (1987). A course in  $H_\infty$  control theory. *Lecture notes on control and information sciences*. Vol.88, Springer Verlag, Berlin.
- Freudenberg J.S. and Looze D.P. (1988). *Frequency domain properties of scalar and multivariable feedback systems*. Lecture notes in control and information sciences, no.104, Springer Verlag, Berlin.
- Furuta K., Ochiai T. and Ono N. (1984). Attitude control of a triple inverted pendulum. *Int. J. of Control*. Vol.39, pp. 1351-1365.
- Glover K. and Doyle J.C. (1988). State-space formulae for all stabilizing controllers that satisfy an  $H_\infty$  bound and relations to risk sensitivity. *System and Control Letters*, Vol.11, pp. 167-172.
- Götzmann W.H. and Meyer H. (1989). Zur digitalen Simulation von Übergängen zwischen Gleit und Haftreibung. (in German) *Automatisierungstechnik*. 37. Jahrgang, Heft 10, pp. 399-400.
- Hanselmann H. (1987). Implementation of digital controllers - a survey. *Automatica*. Vol.23, pp. 7-32.
- Kane T.R. and Levinson D.A. (1985). *Dynamics: Theory and Applications*. McGraw-Hill, New York.
- Limebeer D.J.N. and Kasenally E. (1986).  $H_\infty$  optimal control of a synchronous turbo-generator. *Proc. 25th IEEE Conference on Decision and Control*. Vol.32, pp. 23-31.
- Maciejowski J.M. (1989). *Multivariable feedback design*. Addison Wesley, U.K.
- Meier zu Farwig H. and Unbehauen H. (1990). Discrete control of a triple-inverted pendulum. *Optimal Control Appl. & Methods*, Vol.11, pp. 157-171.
- Morari M. and Doyle J.C. (1986). A unifying framework for control system design under uncertainty and its implications for chemical process control. *Proc. CPC III*, Asilomar, CA, pp 5-51.
- PC-MATLAB reference manual. (1987). The MathWorks, Inc., MA.
- Skogestad S., Morari M. and Doyle J.C. (1988). Robust control of ill-conditioned plants: high-purity distillation. *IEEE Transactions on Automatic Control*. Vol.AC-33, no.12. pp.1092-1105.
- Users Guide MATRIXx V6.0 (1986). Integrated Systems Inc., California, USA.
- Walrath C.D. (1984). Adaptive bearing friction compensation based on recent knowledge of dynamic friction. *Automatica*. Vol.20, pp. 717-727.
- Wang J. (1989). Optimally robust output feedback control for SISO nonlinear systems. *Proc. 28th IEEE Conference on Decision and Control*. Vol.35, pp. 2376-2381.
- Zames G. (1981). Feedback and optimal sensitivity: model reference transformations, multiplicative seminorms, and approximate inverses. *IEEE Transactions on Automatic Control*. Vol.AC-26, no.2, pp. 301-320.

The first part of the paper is devoted to a review of the literature on the control of the robot arm. The second part is devoted to the design of the control system. The third part is devoted to the simulation of the control system. The fourth part is devoted to the experimental results. The fifth part is devoted to the conclusions.



Fig. 1. The behavior of the control system.

The control system is designed to control the position of the robot arm. The control system is designed to control the position of the robot arm. The control system is designed to control the position of the robot arm.

### 7. Conclusions

The control system is designed to control the position of the robot arm. The control system is designed to control the position of the robot arm.

The first part of the paper is devoted to a review of the literature on the control of the robot arm. The second part is devoted to the design of the control system. The third part is devoted to the simulation of the control system. The fourth part is devoted to the experimental results. The fifth part is devoted to the conclusions.

## Observability and Controllability Aspects of Continuous Industrial Crystallisers

R.A. Eek, A. Boxman<sup>†</sup>, Sj. Dijkstra

*Laboratory of Measurement and Control  
Dept. of Mechanical Engineering and Marine Technology.  
Mekelweg 2, 2628 CD Delft*

<sup>†</sup> *Dept. of Chemical Process Engineering  
Julianalaan 136, 2628 BL Delft,  
Delft University of Technology, The Netherlands*

**Abstract.** Observability and controllability aspects of a continuous pilot scale crystalliser are discussed. Both are major requirements for control system design. The proposed control system uses the crystal size distributions (CSD), observed by on-line sensors, based on the method of forward light scattering, as inputs, and the rate of withdrawal of fine and large crystals from the crystalliser as outputs. A set of robust process output variables is derived to describe the location and spread of the CSD. A statistical measure to validate the quality of the measurements is also derived which enhances filtering capabilities. Experimental results show good observability and reproducibility of CSD dynamics, and a sufficiently strong correlation of process inputs and outputs to enable process control.

**Keywords.** Chemical industry, Crystallisation, Observability, Controllability, Identification, Control systems design

### Introduction

Crystallisation is a widely used industrial separation and purification technique. Crystals produced in a crystalliser are characterised by the crystal size distribution (CSD). In industrial practice the CSD changes with time caused by instabilities of the process itself and undesired external disturbances. Because marketability and the operation of crystal handling processes like filtration and drying of crystals is considerably affected by the characteristics of the CSD, its control is indispensable. The demand for CSD control also emerges from the need to adapt for supply changes in successive unit operations.

The control problem raised industry can be summarised as the demand for a robust control system which stabilises the CSD and corrects for transients

by applying a reduced set of physically attainable process inputs.

A control system for an industrial crystalliser includes the following items:

- On-line CSD system; a CSD measurement system should be able to observe the CSD dynamics like transients and oscillations with a sufficient level of resolution. The system should be able to validate its measurements in order to prevent the control system from unnecessary upsets.
- Process inputs; controllability of the CSD is established by effective process inputs. Secondly, these inputs should serve requirements invoked by industrial practice.
- Controller; a controller should preserve pro-

cess stability and performance accounting for model uncertainties and constraints on the controller outputs.

Previous work in the field of CSD control was mainly focused on SISO control schemes, (Randolph, 1987 and Rohani, 1987). The performance of these schemes was investigated with limited models. The nucleation rate or closely related variables were used as process outputs. As a process input the fines removal rate was used. The main drawbacks of this approach for CSD control are the lack of a reliable on-line CSD measurement system, the small scale of operation, the use of limited SISO control structures, and the absence of controller input variables which are directly related to the CSD characteristics to be controlled.

In this paper we propose an approach to control system design starting from the derivation of a set of relevant controller outputs. First the inputs of the control system, on-line CSD data, collected at three different sample locations by means of forward light scattering, are presented. Estimated values are derived for the accuracy of the data. Based on experimental results obtained from a 970 litres pilot scale crystalliser equipped with removal systems for fine and product crystals, aspects concerning observability and controllability of industrial crystallisers are discussed.

## CSD Measurements

The method used to measure the crystal size distributions on-line is forward light scattering. The main advantages to implement this technique in a feed back control loop are: speed to perform both measurement and deconvolution, reproducibility, relatively wide size is range covered, error sources are readily detected, and the results have a direct physical meaning. The crystals contained in a flow, representative of either sample location SL1, SL2 or SL3 (Fig. 1), are passed through an optical cell, in which they interact with the light from an incident 2mW He-Ne laser beam. The light scattered in the forward direction is collimated and subsequently focused onto a multi-element detector, yielding an angular intensity distribution. The recorded distribution can be represented by:

$$L = Aq + \epsilon, \quad (1)$$

where  $L$  is the observed vector of the integrated light intensity  $I$  versus scattering angle,  $A$  is a stored scattering model based on the Fraunhofer

diffraction theory,  $q$  is the unknown solution vector representing the  $s$  volume fractions, (denoted by  $f_{v,i}$ , with  $i = 1, \dots, s$ ), of the CSD in each size class and  $\epsilon$  is the random measurement error on  $L$ . The least-squares solution for the estimators of  $q$  is derived by direct inversion of the set of linear equations:

$$q = (A^T A)^{-1} A^T L. \quad (2)$$

Due to the near-singularity of the problem, small errors comprised in  $L$  induce a severely oscillating solution, even accompanied by negative fractions for some elements of  $q$ . We use a method which incorporates the observed intensity fluctuations and successively impose a nonnegativity constraint following the Kuhn-Tucker theorem (Menke, 1984). Including the knowledge about the fluctuations in each intensity determination yields a qualitative improvement of the solution. Also it provides estimated confidence intervals for the volume fractions, and offers a means for model discrimination, e.g. which grid should be selected for the size class boundaries.

A statistical measure used to describe the quality of every measurement is the reduced chi-square:

$$\chi_{red}^2 = \frac{1}{df} \sum_{i=1}^r \left( \frac{L_i - L_{c,i}}{\sigma_i} \right)^2, \quad (3)$$

where  $L_c$  is the calculated pattern which is compared to the measured pattern  $L$ , weighted for the observed standard deviation on each detector element,  $\sigma_i$ , with  $i = 1, \dots, s$ , and corrected for  $df$ , the number of degrees of freedom ( $r - s$ ), with  $r$  the number of detector elements and  $s$  the number of size classes derived. In case of ideal measurements the  $\chi_{red}^2$ -value equals 1, i.e. the prediction error of the deconvolution model equals the measurement noise and therefore the model can be said to describe the observed measurements (Boxman, 1991) correctly.

A separate detector, positioned in the centre of the multi-element detector, measures the obscuration  $obs$  of the incident beam ( $I_0$ ) by the crystals in the cell. A second property inferred from this measurement is the concentration  $c$  of the particles:

$$obs = 1 - \frac{I}{I_0} = 1 - \exp(-Q_{ext}bc) \quad (4)$$

where  $b$  is the optical path length in the cell and  $Q_{ext}$  is the extinction efficiency of the crystals. The concentration of the particles in the sample should be low enough to ensure single scattering. Typically, for proper measurement conditions, the obscuration value ranges from 5 to 30 percent.

A prerequisite for control is the existence of relevant output parameters. In terms of the CSD these parameters should be robust estimators of the location and spread of the distribution. Robustness indicates that in the reduced set of parameters outliers become irrelevant, but the observability of the process dynamics is preserved. Robust parameters fulfilling the above requirements are derived from the quartiles of the size distribution, defined by:

$$\int_{x=0}^{x_k} f_v(x) dx \triangleq \frac{k}{100}, \quad \text{with } k = 25, 50, 75 \text{ and } 100. \quad (5)$$

The median ( $x_{50}$ ), is a descriptor of the CSD which is relatively insensitive to deviations in the wings of the distribution, since it merely points at the location where 50 % of the observed distribution has a smaller size. The robust estimator for spread is the interquartile range, denoted as  $qr$ . It was found that the level of inaccuracy over the whole size range is relatively uniform so the interquartile range is taken on a logarithmic scale, therefore we define:

$$qr \triangleq \ln \frac{x_{75}}{x_{25}}, \quad (6)$$

as a measure for the spread. This has the added advantage of being dimensionless.

## Process Dynamics

The crystalliser studied here is an evaporative isothermal continuous draft-tube baffled crystalliser. The system boundary and the set of inputs and outputs are described in Fig. 1. CSD measurements are performed at the sample locations: SL1, SL2 and SL3. The CSD is characterised in this figure by the population density function  $n(x, t)$ , defined by

$$n(x, t) \triangleq \lim_{\Delta x \rightarrow 0} \frac{\Delta N(x, t)}{\Delta x}, \quad (7)$$

with  $N(x, t)$  the cumulative number function that describes the number of crystals with a size equal or lower than  $x$ .

In order to eliminate undesired disturbances in CSD dynamics process variables have to be locally controlled at a setpoint value. While other process variables are kept constant, a selected set of inputs is deliberately upset to study aspects of controllability. Next by following a step-wise physical modelling procedure these specific variables are considered.

1. The crystalliser volume  $V$  is constant and ideally mixed.

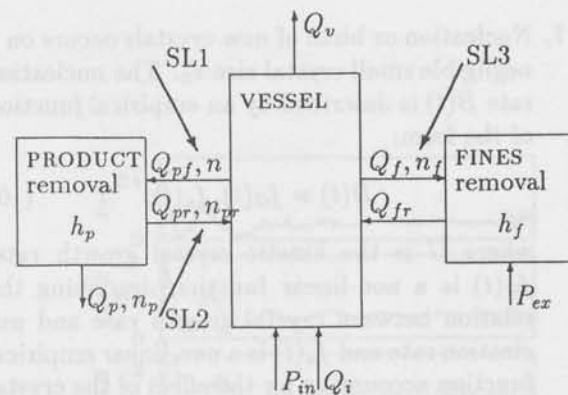


Fig. 1: Schematic drawing of an evaporative crystalliser, equipped with removal systems for fine and product crystals.

2. The feed flow  $Q_i$  has a constant temperature and is free of crystals.
3. All fines are dissolved in the fines removal system and the fines removal efficiency function  $h_f$  is dependent on the fines withdrawal rate  $Q_f$  and the crystal size  $x$ .

$$n_f(x, t) = h_f(Q_f, x, t)n(x, t), \quad (8)$$

with  $n_f(x, t)$  and  $n(x, t)$  the population density functions of the fines and crystals in the vessel.

4. Product is removed from the crystalliser with a product classification system. The return flow from the classifier  $Q_{pr}$  contains small crystals described by the density function  $n_{pr}$ . The return flow is assumed to be returned to the crystalliser in a negligible time and without disturbing the CSD of the crystals contained in this flow. The distribution of product crystals  $n_p$  leaving the classifier is determined by the product removal efficiency function  $h_p$ . The product removal efficiency depends on the size  $x$ , the classifier feed flow  $Q_{pf}$  and the product flow  $Q_p$ :

$$n_p(x, t) = h_p(Q_{pf}, Q_p, x, t)n(x, t). \quad (9)$$

when no classification is present  $h_p$  will be unity.

5. The vapour flow  $Q_v$  contains no solute or crystalline material.
6. The crystalliser is operated at isothermal conditions therefore the specific heat, the crystal density and the saturation concentration can be considered constant in time.

7. Nucleation or birth of new crystals occurs on a negligible small crystal size  $x_0$ . The nucleation rate  $B(t)$  is described by an empirical function of the form:

$$B(t) = f_G(t), f_n(t), \quad (10)$$

where  $G$  is the kinetic crystal growth rate,  $f_G(t)$  is a non-linear function describing the relation between crystal growth rate and nucleation rate and  $f_n(t)$  is a non-linear empirical function accounting for the effect of the crystal population on the birthrate (e.g. attrition of large crystals).

8. The growth rate of crystals obeys the Class II condition which states that the growth rate is directly affected by the crystal mass production rate and no supersaturation build-up occurs.
9. The total heat input  $P_{tot}$  equals the sum of the heat inputs supplied at the internal heat exchanger  $P_{in}$  and the external heat exchanger  $P_{ex}$ .

The CSD dynamics in the crystalliser are modelled with a population balance (as described in (de Wolf (1990)) that is given by:

$$V \frac{\partial n(x, t)}{\partial t} + VG(t) \frac{\partial n(x, t)}{\partial x} + Q_f h_f(Q_f, x, t) n(x, t) + Q_p h_p(Q_p, Q_{pf}, x, t) n(x, t) = 0, \quad (11)$$

with the boundary condition:

$$n(x = x_0, t) = B(t)/G(t). \quad (12)$$

A theoretical crystalliser model consists of a population balance, a heat balance and a set of mass balances for the solution, solvent and crystal concentration in the slurry.

The crystal growth rate  $G$  in equation 11 will mainly depend on the total crystal surface area available for growth, the total heat input and the mean residence time of crystal slurry in the crystalliser. The crystal mass production rate will mainly depend on the total heat input and the mean residence time. Assuming the total heat input and the mean residence time constant, the crystal mass production rate will equal the solution of a linear first order differential equation with a time constant equal to the mean residence time and a zero initial condition. From equations 11 and 12 it can be seen that the CSD dynamic behaviour is influenced by:

- total heat input;
- the fines classification system;
- the product classification system.

Changes in the heat input will affect the crystal mass production rate and the CSD. From an operational point of view it is preferable to keep the crystal mass production rate constant which makes the heat input inappropriate for CSD control. Therefore control of the characteristics of the CSD will be best achieved by manipulating the classification systems for fine and product crystals.

## Experimental setup

Experiments were performed with a continuous evaporative pilot scale (970 litre) draft tube baffled crystalliser operated in accordance with the above stated process model hypotheses. The crystalliser is fed with saturated crystal free liquid. Vapour is extracted at the top of the crystalliser with two condensers. Heat is supplied with an internal heat exchanger positioned in the draft tube.

Classification of fines is established in the annular zone and is based on differences in settling velocities of crystals in the mother liquid. Product classification is performed with a flat bottom hydrocyclone. The overflow of the hydrocyclone is returned to the crystalliser and the underflow is taken as the product flow.

The system is fully automated by a HP-1000 process computer. Local PID controllers are used to control the temperature in the crystalliser, the total heat input, the crystalliser level, the level in the hydrocyclone overflow vessel, the fines flow, the hydrocyclone feed flow and the temperature of the dissolved fines.

CSD measurements are taken at three different locations: the unclassified product flow, which is isokinetically withdrawn from the crystalliser, the overflow of the hydrocyclone system, and the fines flow (see also Fig. 1: SL1, SL2 and SL3 respectively). The scattered light was recorded at 30 detector elements by two Malvern 2600 particle sizers using different collimating lenses. A 300 mm lens was mounted to observe the fine crystals at SL3 and a 1000 mm lens to observe the classifier product and overflow crystals at SL1 and SL2 respectively. In the deconvolution step 20 size classes were calculated based on a logarithmic grid with 23 % resolution. The sampling frequency was kept at a rate of one sample per 2 minutes for all sample

locations. Because the crystal volume in the classifier feed flow is too high for direct measurement, a dilution unit is designed that dilutes slurry samples on-line with saturated mother liquid. This unit also enables automatic background measurements that are necessary to correct for transients due to non constant laser intensity or fouling of the optical cell. The ammoniumsulphate-water system was used as the model material. The crystalliser was operated at a constant level and a constant temperature of 323 K. The total heat input was 120 KW, and the fines were dissolved by increasing the temperature of the fines flow by 10 K. The feed flow to the crystalliser was just saturated at 323 K and the temperature was slightly raised before entering the vessel to ensure a crystal free feed. In case of no product classification the mean residence time of the slurry in the crystalliser was kept constant at 75 minutes. With product classification the hydrocyclone feed flow was 1.0 litres/s which resulted in a product flow of 0.13 litres/s. Slurry circulation in the crystalliser was forced with a marine type impeller which rotated at a speed of 320 rpm.

## Experimental results

Information on the open-loop behaviour of the process was obtained by two different start-up responses of the CSD of the initially unseeded crystalliser (RUN6 and RUN7). In the first experiment (RUN6), a fines flow of 1.0 litres/s and in the second experiment (RUN7) a fines flow of 2.2 litres/s was applied. During these experiments unclassified product was removed.

Figure 2 and 3 show the dynamic behaviour of 4 different relative volume fractions for a period of 40 hours during RUN6 and RUN7 respectively.

In Fig. 4 and 5 the shape of 4 successive relative volume distributions is given corresponding to the trends in Fig. 2 and 3. The fines distribution measured at SL3 (see Fig. 1) remains unaffected during the run. In Fig. 6 the characteristics of the fines distributions, averaged over 50 samples, of RUN6 and RUN7 are depicted. The results are reproducible. It is important to verify that the process behaves in a reproducible manner. In Fig. 7 the start-up response of 3 runs (RUN2, RUN5 and RUN6) under identical conditions is compared. The comparison is based on the derived set of CSD characteristics:  $x_{50}$  as a measure for the location and  $qr$  as a measure for the spread.

In Fig. 8 the effect of different fines flows on  $x_{50}$  and  $qr$  observed during RUN6 and RUN7 is given.

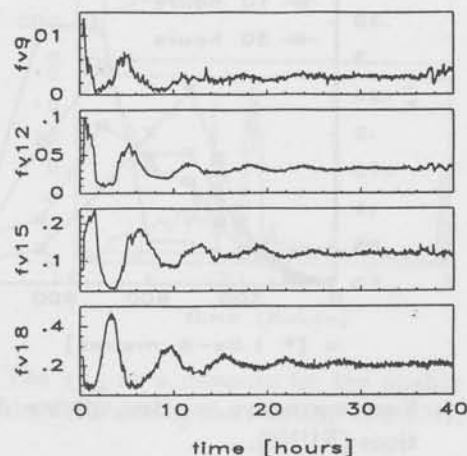


Fig. 2: Start-up response with a fines flow of 1.0 litres/s of 4 product CSD relative volume fractions with:  $f_{v9}$ : 84-106  $\mu m$ ,  $f_{v12}$ : 168-212  $\mu m$ ,  $f_{v15}$ : 353-422  $\mu m$ ,  $f_{v18}$ : 669-843  $\mu m$ , (RUN6).

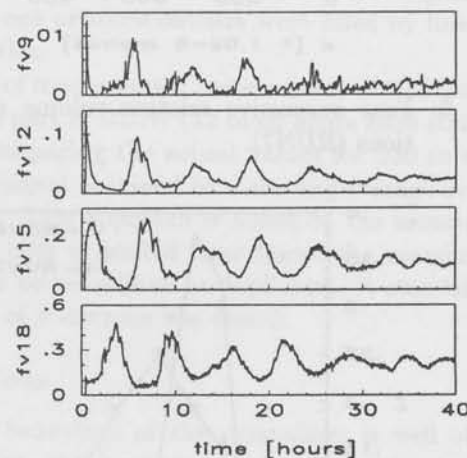


Fig. 3: Start-up response with a fines flow of 2.2 litres/s of 4 product CSD relative volume fractions with:  $f_{v9}$ : 84-106  $\mu m$ ,  $f_{v12}$ : 168-212  $\mu m$ ,  $f_{v15}$ : 353-422  $\mu m$ ,  $f_{v18}$ : 669-843  $\mu m$ , (RUN7).

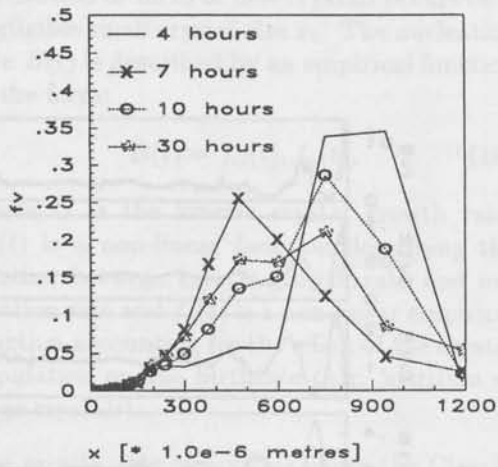


Fig. 4: Four successive relative volume distributions (RUN6).

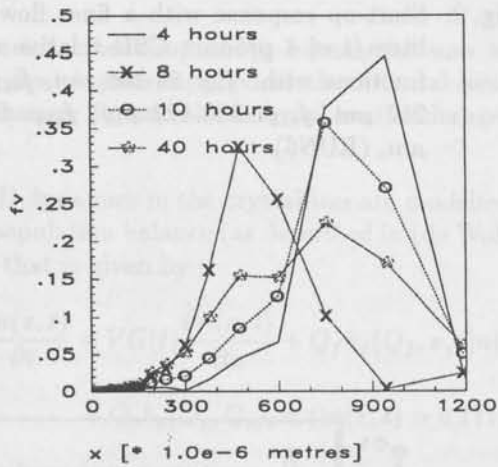


Fig. 5: Four successive relative volume distributions (RUN7).

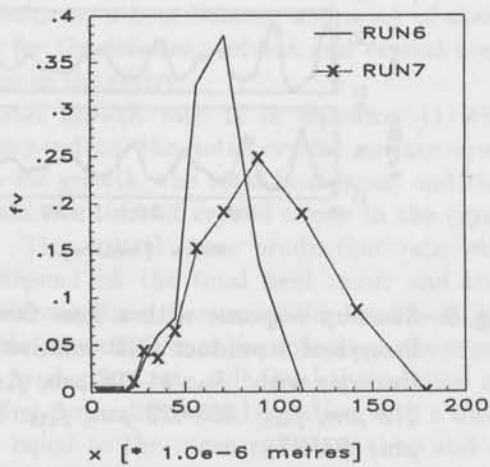


Fig. 6: Two fines distributions measured during RUN6 and RUN7 respectively.

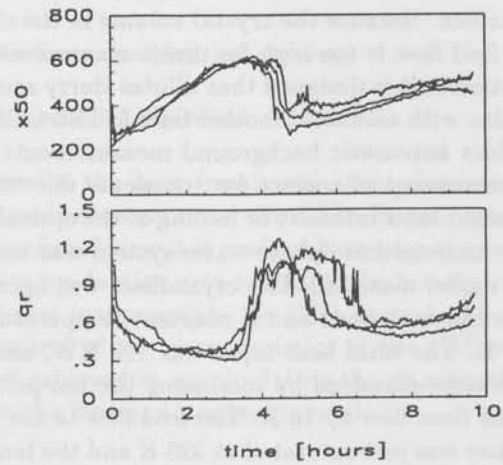


Fig. 7: Comparison of  $x_{50}$  and  $qr$  observed during 3 identical runs (RUN2, RUN5 and RUN6).

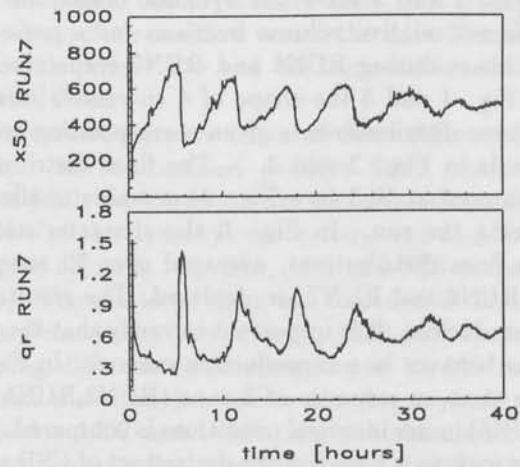
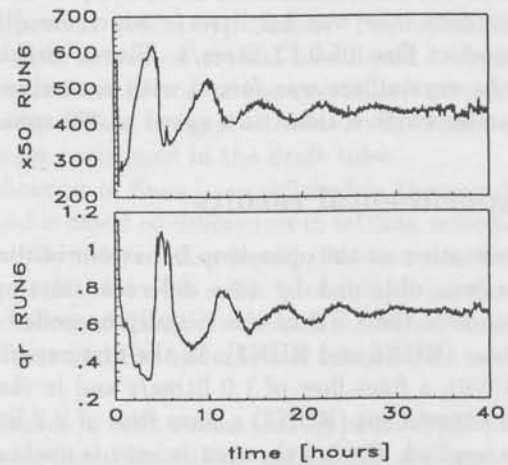


Fig. 8: The influence of different fines flows on the  $x_{50}$  and  $qr$  between RUN6 and RUN7 during 40 hours.

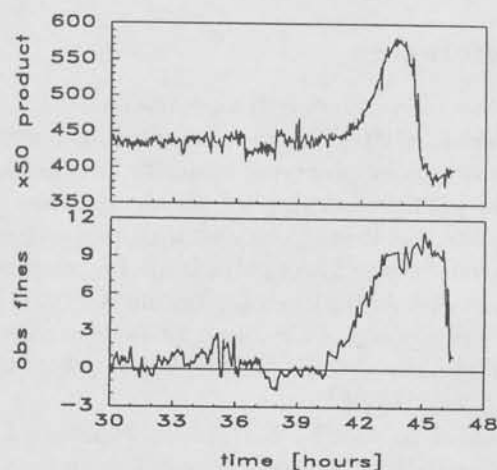


Fig. 9: The relationship between  $x_{50}$  and  $obs_f$  after step change of 1.2 litres/s from steady state in RUN6 at time=40 hours.

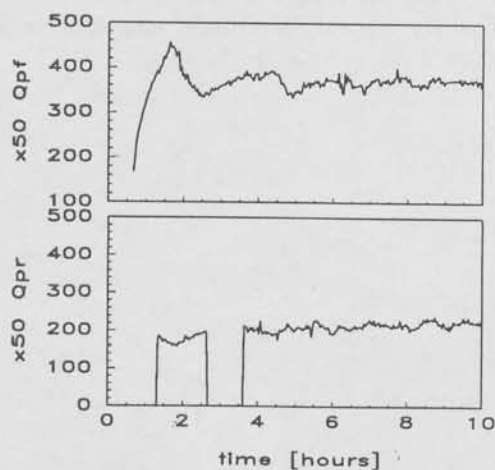


Fig. 10:  $x_{50}$  of the feed and return flow of the classifier.

The effect of changes in the input variables on the CSD is described by the response of the fines obscuration ( $obs_f$ ) and  $x_{50}$  on a step change from 1.0 to 2.2 litres/s on the fines removal rate (Fig. 9). The step change was set at exactly 40 hours after start-up of RUN6 when the CSD was at steady state. The obscuration signal was also applied to locally control the dilution unit.

The effect of product classification on the process was studied by removing product with the classifier during 10 hours after start-up of RUN8. In Fig. 10 the  $x_{50}$  and of both the feed and classifier return flow are shown. A steady state was reached after approximately 10 hours after start-up.

Improvement of the reliability of the CSD measurement system is achieved by using the  $\chi_{red}^2$ -values of the fit when the linear model (1) is applied to the light scattering data. An example of how the

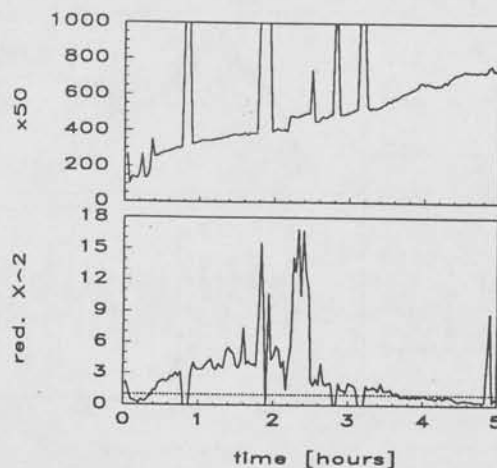


Fig. 11: The  $\chi_{red}^2$  as a measure for the quality of the CSD during the start-up of RUN7.

$\chi_{red}^2$ -signal reports about the quality of unprocessed measurements during the first 5 hours of start-up of RUN7 is depicted in Fig. 11. Clearly, the  $\chi_{red}^2$ -signal serves well as an outlier detector (e.g. at around 0.9, 1.9, 2.8 and 3.2 hours), but can also be used for a more refined method of weighting the relative contributions of successive measurements (e.g. between 2.2 and 2.6 hours). Further, it can be concluded that the deconvolution model is accurate, since the values of the  $\chi_{red}^2$ -signal are close to the ideal value of 1. The above described method for outlier detection was used to filter the raw signals presented in the previous figures. Gaps originating from one or more outliers were filled by linear interpolation.

The level of measurement noise was calculated from a selected part of RUN7 (32 to 40 hours after start-up) by comparing the actual values for  $x_{50}$  to an averaged signal obtained by a moving average over 15 points. This approach is based on the assumption that over a limited time frame the measurements can be considered as duplicates. A standard deviation of 8 microns was found.

## Conclusions

Dynamic behaviour of the crystalliser is well observed with the proposed measurement system. From Fig. 2, 3, 4 and 5 it can be seen how new oscillations originate from the small crystal size region which appear at an approximate size of  $x < 100\mu m$ . Differences in the CSD of the fine crystals for various fines flows are also clearly distinctive (Fig. 6). Since in the case of fines observations the scattering is very weak as compared to measurements in the product flow, adequate background corrections are essential. The proposed reduced set of output pa-

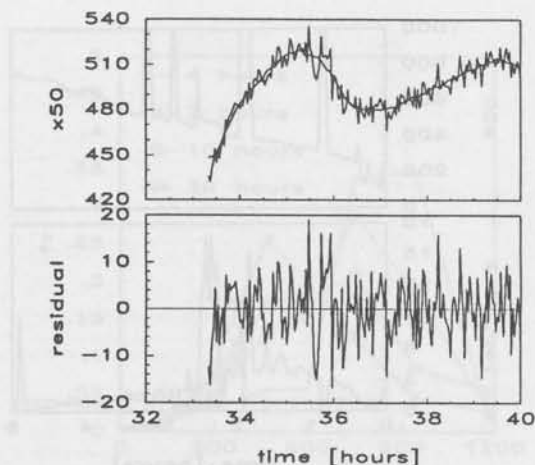


Fig. 12: Unprocessed and filtered trend of the  $x_{50}$  for a selected part of RUN7 (upper) and their residuals (lower).

parameters to describe the CSD consists of a robust estimator for the location, the median ( $x_{50}$ ), and for the spread, the logarithmic quartile ratio ( $qr$ ). The measurements were demonstrated to be highly reproducible in terms of these two variables (Fig. 7). Step changes on the fines removal rate were promptly observed by the measuring system (Fig. 9). The same observability was noticed when the crystalliser was operated permanently at two different fines flows (Fig. 8). The product classification could be identified by comparing the median values of the distributions of the unclassified feed flow and the return flow to the crystalliser (Fig. 10). The  $\chi_{red}^2$  is used as an effective filtering method to weight the measurements. The reliability of the measurements is good. A  $\chi_{red}^2$  close to 1 was observed expressing a legitimate choice of the deconvolution model (Fig. 11). The estimated variability was estimated to be 8 microns (Fig. 12). The measurement system also outputs an indirect measure for CSD dynamic behaviour in terms of an obscuration signal (Fig. 9).

## Acknowledgements

The authors would like to express their gratitude to the Dutch Foundation of Technology (STW), AKZO, DOW Chemicals, DSM, E.I. Dupont de Nemours, Eastman Chemical Company and ICI for their financial support of the UNIAK research program.

## References

- Boxman A., Merkus H.G, Verheijen P.J.T., Scarlett B. (1991). Deconvolution of light-scattering patterns by observing intensity fluctuations. To be published in *Applied Optics November 1991*
- Menke W. (1984) Geophysical Data Analysis: Discrete Inverse Theory *Academic Press, New York.*
- Randolph A. D., Chen L., Tavana A. (1987). Feedback Control of CSD in a KCL Crystalliser with Fines Dissolving. *AIChE Journal, Vol. 33, No. 4, pp. 583-591.*
- Rohani S., Lee K. K. (1987). Feedback Control of a Laboratory scale Potash Crystalliser. *Proc. Int. Symp. on Crystallisation and Precipitation.*
- Wolf S. de. (1990). Modelling, System Identification and Control of an Evaporative Continuous Crystalliser. *PhD thesis, Lab. Measurement and Control, Dept. Mechanical and Marine Techn., Delft University of Technology.*



## CONTENTS Volume 4, March 1992

|  |    |
|--|----|
| Quantification of model uncertainty from data<br><i>D.K. de Vries and P.M.J. Van den Hof</i>                                     | 1  |
| Accurate identification for control: the necessity of an iterative scheme<br><i>R.J.P. Schrama</i>                               | 11 |
| An indirect method for transfer function estimation from closed loop data<br><i>P.M.J. Van den Hof and R.J.P. Schrama</i>        | 17 |
| Control of wind turbine systems for load reduction<br><i>P.M.M. Bongers, T. van Holten and S. Dijkstra</i>                       | 23 |
| Robust control using coprime factorizations, application to a flexible wind turbine<br><i>P.M.M. Bongers</i>                     | 29 |
| $H_\infty$ control of an experimental inverted pendulum with dry friction<br><i>G.W. van der Linden and P.F. Lambrechts</i>      | 37 |
| Observability and controllability aspects of continuous industrial crystallisers<br><i>R.A. Eek, A. Boxman and S.J. Dijkstra</i> | 47 |